Instituto Tecnológico y de Estudios Superiores de Monterrey

Campus Monterrey

Optical spatial soliton propagation through optical lattices with elliptic and circular symmetries

by

Ing. Jesús Adrián Ruelas Urías

Thesis

Presented to the Program of Graduate Studies in Information Technologies and Electronics

In partial fulfillment of the requirements for the degree of

Master of Science

in **Electronic Systems**

May, 2010

.

Instituto Tecnológico y de Estudios Superiores de Monterrey

Campus Monterrey

Division of Information Technologies and Electronics

Program of Graduate Studies

The members of the committee recommend that the present thesis by Jesús Adrián Ruelas Urías be accepted in partial fulfillment of the requirements for the academic degree of **Master of Science**, in:

Electronic Systems

Thesis Committee:

Dr. Julio Cesar Gutiérrez Vega
Thesis Advisor

Dr. Servando López Aguayo
Thesis Reader

Dr. Raúl Ignacio Hernández Aranda
Thesis Reader

Dr. Gerardo Antonio Castañón Ávila
Chair of Graduate Studies of Electronics
at the Division of Information
Technologies

May, 2010

A mis padres Oscar y Manto;
a mis hermanos Oscar, Alex y Miguel

Reconocimientos

Son muchas las personas que contribuyeron favorablemente para el éxito de este trabajo, agradezco a todas ellas por haber sido parte importante de este proyecto, porque lo que hace uno es el reflejo de quien es pero tambien de quienes lo rodean.

Quiero empezar agradeciendo al Dr. Julio César Gutiérrez Vega, por aceptar ser mi asesor; por su tiempo, interés y confianza; por poner los recursos del Centro de Óptica a mi disposición y por sus valiosos comentarios como asesor y amigo. Agradezco también a mis sinodales, al Dr. Servando López Aguayo y al Dr. Raul Hernández Aranda, por tomarse el tiempo necesario para ser partes del comite de revisión de la tésis. Que además, y mucho mas importante, ambos en muchas y no pocas ocasiones estuvieron ahí para aconsejarme y escuchar mis necedades, para ayudarme a crecer y que no doliera tanto la vida; que si bien el mundo no cambia uno se siente mucho mejor al ser escuchado. Gracias Rulo, gracias Vando. También agradezco a toda la pecera por ser parte de este proyecto; a Manuel, a Dorilián, a Toño, a Beto, a Sosa y a Polo; y a los compaeros de las cátedras vecinas, a Juan, a Romo, a Fran, a Robert y Jorge. Agradezco dos veces a Dorilián y a Juan, por ser mis compaeros de casa y entender que todos andamos con prisa y que hay que trabajarle.

Gracias a mi familia por el amor y apoyo que me han brindado, por darme mi espacio para poder trabajar y comprender que ya mi lugar ahora esta aquí, estudiando en Monterrey. Y que aun asi, nunca me he olvidado de ellos. Que puede ser triste, pero aunque los extraño todos los días, mi trabajo y mi carrera me han llevado a vivir aparte de ellos, a buscar un mejor mañana no tan cerca del hogar. Gracias por recibirme los días que se puede como si nunca hubiera partido de casa. Quiero dar muchas gracias a mi padre, por trabajar duramente por su familia desde que tengo memoria, por procurar siempre que no nos falte nada

y estar ahí para ayudarme con lo que pueda, ya sea una maqueta o un consejo. Gracias a mi madre por escucharme y dejar que la escuche tan seguido, por ser tan sensata y amorosa, y por esperar que vuelva cada día con mucha alegría. Me hace desear ser mejor persona. Gracias a mi hermano mayor Oscar, que desde niño lo veía como un modelo a seguir, como una persona muy completa e inteligente. Que el día de hoy trabaja continuamente y se esfuerza a diario de manera honrada y honesta. Quiero dar las gracias a mi hermano Alex, que de niños jugábamos y nos divertíamos a diario. Que aunque ya hemos tomado caminos distintos, recuerdo y extraño muy seguido esos ratos tan amenos y tan sencillos. Espero de todo corazón que pronto estés bien hermano. Doy gracias a mi hermano menor Miguel, que aun es muy joven y de todos nosotros es quien mas vida tiene por delante. De el recuerdo el día que nació, y me ha tocado verlo crecer y convertirse en el joven que es ahora. Espero que si en realidad quiera estudiar fsica que lo logre; que logre eso y mucho mas.

Infinitas gracias le doy a Yaneth, una persona muy especial para mi. Que si bien coincidimos fugazmente en la vida hemos llegado a conocernos y querernos en los últimos meses. Le doy gracias por regalarme su compañia y compartirme su mundo, sus buenos y sus malos ratos, sus secretos y sus verdades, su hermosa persona tal cual es. No importa que la distancia sea larga y que la vida sea difícil. Importa el hoy, que en el presente que vivimos nos queremos sinceramente, que nos apoyamos día a día y que pronto nos habremos de ver. Te quiero mi cielo.

Jesús Adrián Ruelas Urías

Instituto Tecnológico y de Estudios Superiores de Monterrey
Mayo 2010

Optical spatial soliton propagation through optical lattices with elliptic and circular symmetries

Jesús Adrián Ruelas Urías, M.S.

Instituto Tecnológico y de Estudios Superiores de Monterrey, 2010

Thesis Advisor: Dr. Julio Cesar Gutiérrez Vega

This work is devoted to optical spatial soliton propagation through optical lattices induced by nondiffracting beams. The model employed for such was the nonlinear Schrödinger equation, found as a viable and reliable model in this field of study. This last particularity gives the lattice a propagation invariant intensity profile, maximizing control of light and inducing stability on soliton propagations, a major and important issue on this investigation. Propagation on two different families of optical lattices were studied. The results and achievements of this work start with solitons traveling on elliptical photonic lattices, which is a pattern induced by Mathieu helical beams. It depicts an elliptical symmetry and has closed trajectories in the form of elliptic light rings. The dynamics of transverse motion where studied for such lattices when stable propagation was engaged for the soliton. The second family studied was the modulated Bessel lattices, which is induced by a superposition of even and odd type Bessel beams. The power ratio of both parts was fixed such as to ensure that there was no azimuthal modulation induced in the lattice. The transverse motion dynamics where heavily and deeply studied in this case, reaching interesting conclusions such as a model for describing this transverse motion and an explanation for the existence of only two regimes of transverse motion.

Contents

Chapter 1

Introduction

Nonlinear phenomena appear in nature in a variety of ways. Due to computational limitations and high complexity, it developed slowly before the second half of the last century. And yet still it has grown into an important field of study, gathering the attention of a myriad of investigators around the globe. Naturally, nonlinear optics has taken the same course of action and development, nurturing the knowledge of fundamental processes such as second harmonic generation, optical rectification, raman amplification, Pockels effect, etc. This work is devoted to the study of spatial optical solitons, which together with temporal optical solitons constitute the fundamental units of propagation in nonlinear optics. Interests in such particle-wave duals has increased enormously in the last couple of decades due to its fundamental feature: optical solitons, in principle, suffer from no diffraction. This peculiar characteristic can be used in optical communications, as optical solitons could constitute the fundamental unit of information in an all optical communication network. Furthermore, transversal steering an manipulation can be accomplished if the soliton propagates through an electric potential called an optical lattice. This media of propagation offers possibilities that can be greatly taken advantage of if the right technologies are employed. In this chapter we introduce the soliton phenomenon and a description of it, reaching the model we use to describe optical solitons: the Nonlinear Schrödinger equation. Then we present optical lattices and briefly discuss their fundamentals. Lastly, we talk about the phenomena of optical solitons in photonic lattices in a introductory fashion.

1.1 Solitons

There is no clear and universal definition to what a soliton is since the term corresponds to formal mathematical entities and to physical systems obeying distinct differential equations with alike yet slightly different characteristics. A soliton can be defined as a solitary wave which self-reinforces itself and maintains its shape during propagation with constant speed. Furthermore, solitons are fundamentally derived from nonlinear effects; this effects being the cause of the shape invariance. Drazin and Johnson describe solitons to what can be understood as its 3 main properties [1]:
-They are of permanent form.
-They are localized within a region of space.
-They can interact with other solitons, and emerge from the collision unchanged, except for a phase shift. This later characteristic need not hold in the general case, and so can be omitted in a general definition. For practical purposes, we define a soliton to be a nonlinear localized wave that has a propagation invariant intensity pattern.

1.1.1 A historical perspective

The first reported sight and therefore discovery of a solitary wave dates back to 1834. Sir John Scott Russell saw what he described as a smooth, rounded, well defined lump of water traveling through the canal linking Edinburgh and Glasgow for several miles without any important deformation on the shape of the lump. His report, published in 1844, includes the following [2]:

"I was observing the motion of a boat which was rapidly drawn along a narrow channel by a pair of horses, when the boat suddenly stopped not so the mass of water in the channel which it had put in motion; it accumulated round the prow of the vessel in a state of violent agitation, then suddenly leaving it behind, rolled forward with great velocity, assuming the form of a large solitary elevation, a rounded, smooth and well-defined heap of water, which continued its course along the channel apparently without change of form or diminution of speed. I followed it on horseback, and overtook it still rolling on at a rate of some eight or nine miles an hour, preserving its original figure some thirty feet long and a foot to a foot and a half in height. Its height gradually diminished, and after a chase of one or two miles

I lost it in the windings of the channel. Such, in the month of August 1834, was my first chance interview with that singular and beautiful phenomenon which I have called the Wave of Translation".

Scott Russell's report seemed contradictory to Newton's and Bernoulli's theories of hydrodynamics, which could not account for such "Wave of Translation". In 1895 Diederik Korteweg and Gustav de Vries provided what is now known as the Kortewegde Vries equation, which includes solitary wave and periodic conoidal wave solutions [3]. In 1965 Norman Zabusky of Bell Labs and Martin Kruskal of Princeton University demonstrated for the first time soliton behavior in media subject to the Kortewegde Vries (KdV) equation in a computational investigation using a finite difference approach [4]. In 1967 Gardner, Greene, Kruskal and Miura discovered the inverse scattering transform enabling analytical solution of the KdV equation [5]. The work of Peter Lax on Lax pairs and the Lax equation has since extended this to solution of many related soliton-generating systems [6].

1.1.2 Solitons in different physical systems

Solitons are physical entities arising as normal modes to a variety of different physical systems and solutions to a widespread class of weakly nonlinear dispersive partial differential equations. A brief review of soliton and soliton like phenomena is presented.

Rogue waves (also known as freak waves, monster waves, killer waves, and extreme waves) are relatively large and spontaneous ocean surface waves that acquire a considerable height. More precisely, they are waves whose height is more than twice the significant wave height, defined as the mean of the largest third of waves recorded [7]. Rogue waves seem to occur in deep water or where a number of physical factors such as strong winds and fast currents converge. This may have a focusing effect, which can cause a number of waves to join together. Suggested physical mechanism for the formation of rogue waves include diffractive focusing and nonlinear effects. Even though they are not considered formally as solitons, there are common characteristics between both which makes rogue waves related phenomena to solitons.

An oscillon is a soliton like phenomenon that occurs in granular and other dissipative media.

In the later, oscillons are the result from vertically vibrating a plate with a layer of uniform particles placed freely on top. When the sinusoidal vibrations are of the correct amplitude and frequency and the layer of sufficient thickness, a localized wave, referred to as an oscillon, can be formed by locally disturbing the particles. This meta-stable state will remain for a long time (many hundreds of thousands of oscillations) in the absence of further perturbation. An oscillon changes form with each collision of the grain layer and the plate, switching between a peak that projects above the grain layer to a crater like depression with a small rim [8]. Whereas solitons are traveling waves, oscillons can be stationary. Oscillons have been experimentally observed in thin vibrating layers of viscous fluid and colloidal suspensions. Oscillons have been recently associated with Faraday waves because they require similar resonance conditions. Nonlinear electrostatic oscillations on a plasma boundary can also appear in the form of oscillons.

In mathematics, the Kortewegde Vries equation (KdV) is a mathematical model of waves on shallow water surfaces. It is particularly notable as the prototypical example of an exactly solvable model, that is, a non-linear partial differential equation whose solutions can be exactly and precisely specified. The solutions include solitons, which are found by means of the inverse scattering transform. The equation is given by [9]:

$$\frac{\partial \Lambda}{\partial t} + k\Lambda\frac{\partial \Lambda}{\partial x} + \frac{\partial^3 \Lambda}{\partial x^3} = 0, \tag{1.1}$$

where k is a constant. The KdV also describes magnetohydrodynamic waves in plasma, longitudinal dispersive waves in elastic rods and thermally excited phonon packets in low-temperature nonlinear crystals.

The sine-Gordon equation is a nonlinear hyperbolic partial differential equation. Originally considered in the nineteenth century in the course of study of surfaces of constant negative curvature, It has soliton type solutions and is given by [10]:

$$\frac{\partial^2 \Theta}{\partial x^2} - \frac{\partial^2 \Theta}{\partial t^2} = sin(\Theta). \tag{1.2}$$

This equation has been used to describe the Bloch wave motion in magnetic crystals, unitary theory of elementary particles, propagation of light through a crystal dislocation and appears in relativity theories.

Finally, the GrossPitaevskii equation ,named after Eugene P. Gross and Lev Petrovich Pitaevskii, describes the ground state of a quantum system of identical bosons using the HartreeFock approximation and the pseudo-potential interaction model and is given by [11]

$$i\hbar\frac{\partial\Psi}{\partial t} = -\frac{\hbar^2}{2m}\nabla^2\Psi + V(r)\Psi + U_o|\Psi|^2\Psi. \tag{1.3}$$

This equation is a special case of the nonlinear Schrödinger equation, which is used in nonlinear optics and constitutes the core of the model used for the entire work in this thesis.

1.1.3 Optical spatial solitons and the nonlinear Schrödinger equation

As it can be noticed in the past briefing, solitons arise in different physical systems, from hydrodynamics to quantum mechanics. It is possible for a beam of light to suffer nonlinear effects, either when it propagates though a highly nonlinear medium or when the power contained by the beam is noticeable high, enough to shot nonlinear effects in intrinsically linear materials. This gives rise to optical solitons, and optical field with soliton characteristics.

Now, optical solitons are divided in two types: spatial and temporal. The first are those which propagate through a certain spatial coordinate, leaving its intensity pattern fixed in time. They can be though as a laser beam supported by linear effects, in the sense that the pattern left behind by the advancing wavefront of the laser remains as it is. It remains confined and propagates without changing shape.

Optical solitons can be understood as nonlinear waves which vary according to a time dependence while being spatially confined. Furthermore, if optical spatial and temporal solitons are combined certain light pulses known as "light bullets" can be created. They are beams of light spatially confined in all three coordinates that do not irradiate power due to the stability offered by nonlinear effects.

The nonlinear Schrödinger equation is the model employed in spatial optical soliton characterization and propagation, thus providing the starting point and most important fundamental for this whole investigation. As it name indicates it, its the nonlinear version of the quantum Schrödinger equation, but lacking any term containing $\hbar$ or any other quantum fundamental constant. Thus, this equation gives a classical treatment of waves.

In order to derive it, an exhausting yet reachable treatment of optics would have to be carried out. It has provided an excellent frame in the study of optical spatial solitons and has been revised in an extenuated fashion, so making or presenting a treatise on the equation can be redundant or unnecessary, not to consider to that the origins and fundamentals of the equation are out of the scope of this work. However it is important to mention that this equation, carrying nonlinear terms, works well at relatively low amplitudes, while at high powers employed adjustments need to be made. Such analysis are left and here we simply discuss its main characteristics and present the model used in this work, were it is given by

$$i\frac{\partial\Psi}{\partial z} + \nabla_t^2\Psi + \frac{|\Psi|^2}{1+s|\Psi|^2}\Psi + p\Gamma(\mathbf{r}_t)\Psi = 0. \tag{1.4}$$

Ψ stands for our wave function, where $|\Psi|^2$ is the intensity pattern associated with it, the measurable quantity in nature. By definition, Ψ solutions to the equation are normal modes of it and represent soliton patterns.

The first term accounts for evolution in the propagation coordinate, being in this case the spatial z coordinate. That is, our axis of propagation is the z-axis, as in many works involving propagations of optical fields. This spatial first order partial derivative can be understood as an advance operator in our propagation. i the square-root of one, a constant that changes phase for the first term.

The second terms accounts for diffraction of the optical beam, a phenomenon that is inevitable to all light but that can be canceled by other effects, as in our case. Diffraction causes a beam of light to disperse in space, either to focus, de-focus or in general only to change shape in an unordered fashion. ∇_t^2 is the transverse laplacian operator, a second

order differential operator involving the transverse coordinates and dropping the longitudinal z coordinate. In cartesian coordinates it is written as

$$\nabla_t^2 = \frac{\partial^2}{\partial x^2} + \frac{\partial^2}{\partial y^2}. \tag{1.5}$$

The third term involving the intensity pattern of Ψ is called the saturation term. As it names indicates it, it accounts for saturation effects. It is derived from the Kerr nonlinear potential $U(\Psi)_K$, which goes as

$$U(\Psi)_K = |\Psi|^2. \tag{1.6}$$

The Kerr nonlinearity functions as a self-acting index refraction pattern. That is, when propagating, Ψ experiences a refractive index proportional to $|\Psi|^2$; or in other words, the soliton is refracted by itself. The Kerr nonlinearity is the first step towards working with solitons, since it is the simplest and most common nonlinear potential. Even thought it can have more complex and elaborated effects, and it usually does, it can be though as a self-focusing mechanism canceling diffraction effects. So, in the simple picture, nonlinear effects focus light beams and cancel diffraction for solitons.

As said before, it starts acting noticeable at certain used powers. For common materials, it needs extraordinary high powers to be ignited, and thus soliton phenomena is barely seen in nature. But certain materials are more susceptible to linear effects, having a smaller and shorter threshold for shooting nonlinear effects. This material are commonly referred to as nonlinear materials.

Now, the Kerr potential is quite simple and has demonstrated to introduce instabilities in soliton propagating for long distances. Many materials have demonstrated to follow the saturation nonlinearity instead of the Kerr potential. This saturation potential acts as a limiting barrier for the soliton focusing, since it keeps it from suddenly collapsing into one point. In this model, s is known as the saturation parameters, limited to positive values and it has typically values smaller than 1, where $s = 0$ acts as the null saturation Kerr potential limit.

The fourth and final term of our model represents the optical lattice potential contribution.

It holds the key to introducing interesting variations to our model, which can furthermore produce worthy results. $\Gamma(\mathbf{r})$ represents the potential induced by the optical lattice, which is itself a function of space; and p is called the lattice depth, since it is customary to work numerically with a normalized lattice whose peak value is worth p. The next section introduces the concept of optical lattices and how they interact in our model.

This work is devoted to spatial optical solitons, and for convenience and saving notation, in the remaining content of this work they will be referred simply as solitons.

1.2 Optical lattices

Even thought it may seem a bit abstract at a first glance, the concept of optical lattices is quite simple. We go to the purest and most abstract definition of a lattice to understand what it is, being " A regular, periodic configuration of points, particles, or objects throughout an area or a space, especially the arrangement of ions or molecules in a crystalline solid" [12]. So, as it can be seen, it can be understood that a lattice is a periodic arrangement of objects in a region in space. Furthermore, the definition makes it noticeable how the term itself is strongly attached to the nature of crystalline solids. So, we go over the definition of crystal lattice from solid state theory, where they are renamed Bravais lattice [12]: "An infinite set of points generated by a set of discrete translation operations described by:

$$\mathbf{R} = n_1\mathbf{a}_1 + n_2\mathbf{a}_2 + n_3\mathbf{a}_3, \tag{1.7}$$

where n_i are any integers and $\mathbf{a}_i$ are known as the primitive vectors which lie in different planes and span the lattice. For any choice of position vector $\mathbf{R}$, the lattice looks exactly the same. A crystal is made up of one or more atoms (the basis) which is repeated at each lattice point. The crystal then looks the same when viewed from any of the lattice points." For practical purposes, we consider a lattice to be a periodical pattern filling a region in space.

So, the term lattice is strictly associated with a certain high level periodicity. Now, and optical or photonic lattice retains this symmetry nature, but now being with optical intended purposes. It is a refractive index modulation imposed on a region in space. It can be thought

of as a function $n(\mathbf{r})$ of space, the refractive index n associated with the point $\mathbf{r}$. Now, the lattice itself can be fabricated, constructing a material which posses a desirable pattern for n. The advent and availability of suitable materials and fabrication techniques for the generation of optical lattices has been a key ingredient for the advancement of soliton propagation through optical lattices. Some materials used for constructing and manufacturing optical lattices are AlGaAs, fused silica, metal vapors, nematic liquid crystals, LiNbO crystals and SBN crystals [13].

There is even a more extent variety of materials suitable for the exploration of nonlinear wave propagation in periodic media. However, optical induction in suitable materials affords control of the shape, strength and properties of the lattice with an unprecedented flexibility. It allows creation of reconfigurable refractive index landscapes that can be fine-tuned by lattice-creating waves and easily erased, in contrast to permanent, technologically fabricated waveguiding structures. The technique is complicated, but it basically consist in confining a set of standing waves through a photorefractive material, then applying an external static electric field across the crystal a periodic change of the refractive index is induced via the electro-optic effect. As already said, this method opens up the possibilities in optical lattices, since the only problem is reconstructing a desired refractive index modulation pattern with plane waves to be able to imprint it over a nonlinear material.

1.2.1 Solitons in optical lattices

Photonic lattices with specific and useful characteristics can be engineered by applying beam shaping techniques in order to be used in soliton propagation. In principle, the soliton will copy to a certain degree the topology of the section of the lattice it is being propagated on. That is, the soliton can resemble the topology and geometry of the lattice it propagates on.

In order to achieve a maximum control of light in media, the lattice itself must be propagation invariant, and therefore the nondiffracting beams are appropriate to induce a photonic lattice [14]. This limits the photonic lattice Γ to be a function only of the transversal coordinates. That is

$$\Gamma = \Gamma(\mathbf{r}_t), \tag{1.8}$$

and the pattern for Γ repeats itself for each different plane of z.

The simplest case of nondiffracting beams are the plane waves, which are the fundamental solutions to the Helmholtz equation in Cartesian coordinates. Durnin introduced Bessel beams as an exact nondiffracting solution to the scalar wave equation in circular cylindrical coordinates and presented a relatively simple experimental setup to produce them [15]. Over the past few years, more complex nondiffracting beams solutions such as Mathieu beams [16] in elliptic cylindrical coordinates and parabolical beams [17] in parabolic cylindrical coordinates have been both discovered and analyzed.

A soliton in this type of lattices will propagate without suffering diffraction in a stable manner indefinitely, since restricted as it is Γ offers the same refraction index distribution. Still, the interest of this investigation relies on transverse moving solitons along the potential Γ.

When the input laser beams strikes normally into the incidence plane of the lattice, the wave-vector of the soliton points out in the z direction, thus the soliton would respond to the expression

$$\Psi(\mathbf{r}_t) = \psi(\mathbf{r}_t)e^{i\beta z}, \tag{1.9}$$

where the pattern Ψ is propagation invariant as allowed by the longitudinal symmetry of the lattice, eliminating any dependence on z. But if the laser where to be tilted with respect to the incidence plane of the photorefractive crystal, an initial tilt would be imposed on the soliton, meaning the propagation vector of the soliton would initially point in the direction of this tilt. Therefore, the soliton would respond to the expression

$$\Psi(\mathbf{r}) = \psi(\mathbf{r})e^{i(k_z z + k_x x + k_y y)}, \tag{1.10}$$

where as usual,

$$\beta^2 = k_z^2 + k_x^2 + k_y^2, \tag{1.11}$$

and the decomposition of the free space propagation wave vector β follows the initial tilt of the laser. Now, this induces a transverse motion on the soliton profile. As the soliton moves transversally around the photonic lattice it suffers from a different potential at each

different value of z, and thus naturally inducing a smooth auto-transformation on the pattern Ψ in order to fulfil the nonlinear Schrödinger equation. In other words, the soliton continuously transforms itself into other stationary eigenmode, another soliton profiles, as it moves transversally along $\Gamma(\mathbf{r}_t)$. This is way Ψ ends up being a function of z to, of the whole space, and can be a function only of the transverse coordinates if there is no induced tilt on the soliton.

1.2.2 Stationary solitons conversion and the stability criteria

Stationary solitons have their propagation eigenvector along the z axis and do not auto-transform themselves. They have a propagation invariant profile and are the key to propagating transverse moving solitons. This obeys the fact that numerical methods available in literature solve the nonlinear schrodinger equation for a constant phase profile. That is, they assume the solution is of the form

$$\Psi(\mathbf{r}) = \psi(x, y)e^{i\beta z}, \tag{1.12}$$

insert the expression on the original equation, and obtain the profile $\psi(x, y)$ for a given value of β. Obtaining a transverse motion soliton is straight forward after this step, since the symmetry of the nonlinear schrodinger equation allows the modulation of a linear $x - y$ phase. That is, if Ψ is a solution of the equation, the profile

$$\Psi'(\mathbf{r}) = \Psi(\mathbf{r})e^{i(k_x x + k_y y)}, \tag{1.13}$$

is an approximate solution to the nonlinear Schrödinger equation. In the case of an homogenous lattice potential it works as an exact solution, but as the potential surrounding the soliton profile varies it works as a very close solution. As propagation is taken place the soliton auto-transforms itself in order to fit the nonlinear Schrödinger model. This type of solutions are introduced since they constitutes a soliton with a initial induced transverse motion in the direction

$$\hat{u} = \frac{k_x\hat{x} + k_y\hat{y}}{\sqrt{k_x^2 + k_y^2}}, \tag{1.14}$$

thus, producing a transverse moving profile out of a stationary soliton. Furthermore, stationary profiles hold the key to predicting whether the soliton is or not stable in propagation. Being a soliton a beam of light, it transports power, and can be easily deduced from the profile Ψ, this since the squared magnitude $\Psi\tilde{\Psi}$ represents the intensity profile. Thus, integrating the last field in the plane $x-y$ computes the power $\mathscr{P}$ carried by the soliton. Thus, we define

$$\mathscr{P} = \int\int |\Psi(x,y)|^2 dxdy, \tag{1.15}$$

where the integration is carried in the region enclosing the soliton. Now, in order to find out regions of β inducing stable propagation, plots of $\mathscr{P}$ against β are required. The VakhitovKolokolov stability criterion [18] states that if

$$\frac{d\mathscr{P}}{d\beta} > 0, \tag{1.16}$$

then the propagation will be stable.

1.3 Description of the work

In order to study solitons propagation and undertake the research contained in this thesis, a systematic procedure was followed. Initially, the optical lattice to work with must be defined, since it contains a number of variations and soliton propagations change dramatically with different lattices. It can be said as if the lattice itself defines the outcomes of an investigation, being it the most important variable to define. In this work we present research on two different lattices: the elliptical photonic lattice (EPL) and the modulated Bessel lattice (MBL). As it can be inferred for the name, the EPL contains an elliptic symmetry and is induced by a superposition of odd and even Mathieu beams, which are the normal modes of the Helmholtz equation in elliptic cylindrical coordinates. The MBL result form the superposition of cosine and sine Bessel beams, which contain circular symmetry and again are solutions to the Helmholtz equation. Both lattices come from nondiffracting beams, making the lattice propagation invariant.

After having set the lattice and other parameters, such as p and s, a soliton pattern must

be obtained. This is done by solving our nonlinear equation via numerical methods, since the complexity of our models excludes in a natural way analytical solutions. The resulting pattern can be thought as the soliton Ψ at $z = 0$. When obtaining a initial soliton wave-function, the next natural step to take is to propagate it through a certain z distance. Being solitons propagation invariant, they ought to maintain its shape permanently regardless of the propagation distance, making this process to seem unnecessary. But this argument results not valid, because even though a soliton is propagation invariant, not all solitons are stable on propagation. Meaning not that they are not solutions to our model, but that they numerical error associated with our computations can affect seriously the outcome of a propagation. So, even though solutions can be obtained, it does not necessary hold that one can propagate these solitons indefinitely. In the physical world this can be interpreted as a soliton that can propagate only if strictly and ideal conditions are to be preserved. So, a numerically unstable soliton needs perfect and ideal conditions in the lab in order to be constructed and propagated.

As said in the last paragraphs, optical lattices offer interesting and numerous possibilities in soliton control and routing. Even though investigation on the subject has increased greatly in the last couple of years, there is no simple nor clear model that can predict the outcome dynamic of motion when the input are the initial conditions and the lattice employed. This is a major problem, almost limitless due to the numerous possibilities. Still, this work focuses on certain lattices and tries to give a comprehensive explanation of the subject.

1.3.1 Thesis outline

In this first chapter of the thesis the fundamental concepts of the research are defined and stated, giving an introductory explanation to the subject. Even though there are formal and mathematical definitions of what a soliton is, a heuristic and more appropriated to optical systems definition of soliton was given. The mathematical model used for optical solitons, the nonlinear Schrödinger equation, was presented and described. Afterwards, the concept of optical lattice was introduced, being the second fundamental to this work. A brief description of how both a soliton and an optical lattice was given at the end of the chapter.

In the second chapter we focus on numerical methods employed in this investigation. Being

our model nonlinear it admits no analytical solutions, and in order to advance it is necessary to lean on numerical methods. It starts giving a description on the methods used for solving the equation and obtaining initial patterns. Then an explanation is given on the methods used to propagate solitons.

The third chapter deals with soliton propagation in the elliptical photonic lattice, which is a refraction index modulation described by helical Mathieu nondiffracting beam. First the lattice itself is defined from mathematical basis, giving a small description of the topology offered by this lattice. Then, the different soliton topologies found are analyzed, as establishing a region of stability. The chapter ends with transverse moving soliton propagations, and its most important result is how the soliton can engage propagation even though the lattice has an azimuthal modulation.

Soliton propagation in Bessel type lattices is explored in the fourth chapter. A new topology of optical lattices is introduced, the modulated Bessel lattice or MBL. In this chapter the dynamics of transverse motion of the soliton are explored, giving as its final main results that the soliton has a varying rotation rate in non azimuthal modulated lattices and that certain regimes of propagation are found, giving a mechanical explanation for each one.

Chapter 2

Numerical methods and statistical background

Solitons are by nature nonlinear waves, being for our case described by the nonlinear Schrödinger equation. In general, nonlinear partial differential equations have no general method for obtaining exact solutions. Our model is not the exception, since a few analytic solutions are available only in the 1 dimensional case for the Kerr nonlinear potential. And as for numerical solutions, this can be found using either particular but complex numerical methods, specialized in similar differential equations; or employing a more general class of numerical methods which are standard in the field of numerical computations. Still, the first are much better at solving our nonlinear model.

As said before, in order to produce results two individual and separable process must be carried out before. First, the nonlinear Schrödinger equation must be found in order to found what is called a stationary solution. This refers to a soliton profile that has not been propagated in the z coordinate and can be thought of our wavefunction at $z = 0$. Then, what naturally follows is to propagate the soliton and monitor any important observables and quantifiers, such as the position of the centroid and the structure of the solitons, how it is affected by the auto-transformations and if there is any considerable leak of power. We present a brief review of the numerical methods employed and programmed for the research.

2.1 Numerical methods for finding soliton type solutions

Obtaining stationary soliton part gives information concerning the structure of the soliton and the connection it keeps with the symmetry of the lattice, the relation between its power and β and other aspects concerning stability during propagation. Furthermore, the

process of finding stationary solitons is fundamental since the solution needs to be found in order to be propagated. In this section we focus on the numerical methods used for finding stationary solitons.

2.1.1 Petviashvili relaxation method

As said before, numerical computations involving nonlinear waves can be quite complex, involving high level mathematical skills; not to mention that there is no general efficient and robust method of finding answers for the nonlinear Schrödinger equation. Still, there is a standard, well know method for solving this problem. It has different names on the literature, but is commonly known as the petviashvili relaxation method [19]. It involves advanced level mathematics, and its derivation and justification is beyond the scope of this work. Still, a heuristic derivation and its algorithm will be discussed in this section.

In order to start, one must go back to the nonlinear Schrödinger equation

$$i\frac{\partial \Psi}{\partial z} + \nabla_t^2 \Psi + \frac{|\Psi|^2}{1 + s|\Psi|^2}\Psi + p\Gamma(\mathbf{r}_t)\Psi = 0. \tag{2.1}$$

As always, solitons must have propagation invariant intensity patterns, so the usual harmonic dependence on the z coordinate is assumed

$$\Psi(\mathbf{r}) = \phi(\mathbf{r}_t)e^{i\beta z}, \tag{2.2}$$

where β is the longitudinal wave number. The last two terms of the equation represent the nonlinear potential of the equation, so with the notation

$$N(|\Psi|^2) = \frac{|\Psi|^2}{1 + s|\Psi|^2} + p\Gamma(\mathbf{r}_t), \tag{2.3}$$

and inserting the longitudinal symmetry our model equation can be written as

$$\nabla_t^2 \phi + N(|\phi|^2)\phi = \beta\phi. \tag{2.4}$$

The petviashvili relaxation method makes use of the Fourier transform, which is maps the original function f from the configuration space (x, y) to the frequency space (k_x, k_y). Letting

$\mathscr{F}$ be the Fourier transform operator and $F(k_x)$ the Fourier transform of $f(x)$

$$\mathscr{F}\{f(x)\} = \frac{1}{\sqrt{2\pi}} \int_{-\infty}^{\infty} f(x) e^{ixk_x} dx = F(k_x), \tag{2.5}$$

then the following identity holds

$$\mathscr{F}\{\frac{d}{dx} f(x)\} = ik_x F(k_x). \tag{2.6}$$

Applying this identity twice over the entire plane, x and y coordinates, the following identity is obtained

$$\mathscr{F}\{\nabla_t^2 f(x,y)\} = \mathscr{F}\{\frac{d^2}{dx^2} f(x,y) + \frac{d^2}{dy^2} f(x,y)\} = \{-k_x^2 - k_y^2\} F(k_x, k_y) = -k_t^2 F(k_x, k_y). \tag{2.7}$$

The relaxation method begins by applying the Fourier transform to the nonlinear Schrödinger equation with its nonlinear potential representation:

$$\mathscr{F}\Big\{\nabla_t^2 \phi + N(|\phi|^2)\phi\Big\} = \mathscr{F}\Big\{\beta\phi\Big\}, \tag{2.8}$$

where applying the previous statements and identities reduces to

$$-k_t^2 \tilde{\phi} + \mathscr{F}\Big\{N(|\phi|^2)\phi\Big\} = \beta\tilde{\phi}, \tag{2.9}$$

with $\tilde{\phi} = \mathscr{F}\Big\{\phi\Big\}$, the Fourier transform of our soliton profile. Rearranging terms one reaches the identity

$$\phi = \mathscr{F}^{-}\left\{\frac{\mathscr{F}\Big\{N(|\phi|^2)\phi\Big\}}{k_t^2 + \beta}\right\}. \tag{2.10}$$

The petviashvili relaxation method relies on this identity, using it as an iterative formula for calculating a relaxed solution to the equation. Thus,

$$\phi_{i+1} = \mathscr{F}^{-}\left\{\frac{\mathscr{F}\Big\{N(|\phi_i|^2)\phi_i\Big\}}{k_t^2 + \beta}\right\}, \tag{2.11}$$

provides a method for relaxing solutions. Still, the formula as it is does not prove to give expected results. After several iterations ϕ_i either converges to the trivial solution or diverges.

In order to avoid this, a stabilizing factor is inserted as shown below

$$\phi_{i+1} = \mathscr{F}^{-}\left\{ a_i^{\gamma} \, \frac{\mathscr{F}\Big\{ N(|\phi_i|^2)\phi_i \Big\}}{k_t^2 + \beta} \right\}. \tag{2.12}$$

Here a_i is the stabilizing factor and is computed as

$$a_i = \frac{\iint_{\mathscr{V}} \{k_t^2 + \beta\} |\tilde{U}_i|^2 dA}{\iint_{\mathscr{V}} \mathscr{F}\Big\{ N(|U_i|^2)U_i \Big\} \tilde{U}_i dA}, \tag{2.13}$$

where the integral is carried over the region $\mathscr{V}$ of the (x, y) plane containing the soliton and γ is a parameter adjustable to the method. It value can vary from 1 to 2 in order for the method to properly work, but in this investigation it was set to $\gamma = 1.5$. Since this is a relaxation method, it needs an initial estimation of the solution, or ansatz, as an input in order to start working. The final solution acquired can vary depending on the potential surrounding the center of the ansatz, and what determines what possible solutions is computed is the ansatz ϕ_o. A gaussian profile has proved useful in our investigation, being it the standard profile used in the literature. Therefore, we use as a default the profile

$$\phi_o(x, y) = \exp\left[-\Big(\frac{x - x_o}{\sigma_x}\Big)^2 - \Big(\frac{y - y_o}{\sigma_y}\Big)^2 \right], \tag{2.14}$$

where it corresponds to a gaussian bell centered in the coordinates (x_o, y_o) with variances σ_x and σ_y for the x and y parts of the function, respectively.

The Petviashvili relaxation method is quite general since a number of different potentials can be inserted in the form of an operator without changing the structure of the method. Still, it has certain limitations. For an specified nearby potential, it converges only inside an interval of the wave number β, and wether this is due to the limitations of the method or the lack of solutions cannot be answered. Furthermore, this makes close monitoring of the convergence method a need when using it. Stated as the method is and using the ansatz we propose, only finds fundamental type solutions possessing a gaussian like intensity distribution and constant phase can be acquired. In order to obtain more complex solutions one must divert to different methods or use a different ansatz, oriented and thought for the particular

desired profile. Furthermore, this method converges in a few number of iterations when it works properly. So, in conclusion, this method is quite general and robust when obtaining beam like solitons.

2.1.2 Vortex type solution method

To obtain vortex type solitons an alternative approach must be used. Here, we present a standard method for constructing solutions of this type.

To star the concept of optical vortex is limited. In the literature is is defined as a point of null intensity in an optical field with a phase discontinuity. The phase in the field circulates around these points of zero intensity, giving this the name of vortex. A number called the topological charge is associated with each vortex, which indicates how many complete cycles the phase completes around the discontinuity point.

This research is limited to ordinary vortices, excluding the fractional class of vortices. So for this work the topological charge is limited to integer numbers, either positive, negative or zero. The sign indicates the direction of the twist or circulation of the phase and. This twisting behavior traduces physically into a spinning of light around its own axis of propagation. This spinning carries orbital angular momentum with the wave train, and will induce torque on an electric dipole [20]. This orbital angular momentum of light can be observed in the orbiting motion of trapped particles. Interfering an optical vortex with a plane wave of light reveals the spiral phase as concentric spirals. The number of arms in the spiral equals the topological charge.

Limiting ourselves to the simplest type of vortices, the phase varies harmonically around the center of the vortex, where for convenience and without loss of generality we define to be the z axis. Due to the symmetry of this type of vortices, the method for obtaining them starts by constructing an ansatz assuming separation of variables in cylindrical circular coordinates.

$$\Psi = \Psi(\mathbf{r}) = R(r)\Theta(\theta)Z(z). \tag{2.15}$$

The soliton must have a propagation invariant intensity profile, meaning that $|\Psi|^2$ cannot be a function of z. So, as usual, the dependence of Ψ over z is harmonic, as in all propagation invariant cases, that is

$$Z(z) = e^{i\beta z}, \tag{2.16}$$

where β is the transverse propagation constant or wave number. Furthermore, as dealing with vortices, the angular coordinate must account for a circling or twisting phase around a zero or null intensity point. The method restrict solutions to intensity patterns dependent only of r, the radial coordinate, limiting Θ to a variation only in phase. Taking this into account,

$$\Theta(\theta) = e^{im\theta}, \tag{2.17}$$

where m is the topological charge, and integer number. So far, limitations and restrictions have been imposed only on the soliton type solution. The last and strongest restriction, the only real limitation of the method, is that the optical lattice $\Gamma(\mathbf{r}_t)$ must be azimuthally independent. That is,

$$\Gamma = \Gamma(r). \tag{2.18}$$

This restricts the optical lattices that can be used with the method to central potentials. Applying an argument of consistency, it can be found that the radial function $R(r)$ must be real valued. Having set this, the ansatz is

$$\Psi = \Psi(\mathbf{r}) = R(r)\Theta(\theta)Z(z) = R(r)e^{im\theta}e^{im\theta}, \tag{2.19}$$

where $\beta > 0$,m must be an integer and $R(r)$ is our function to find. As the method requires working with the cylindrical circular coordinates (r, θ, z), the laplacian must be expressed in this system,

$$\nabla_t^2\Psi = \frac{\partial^2\Psi}{\partial r^2} + \frac{1}{r}\frac{\partial\Psi}{\partial r} + \frac{1}{r^2}\frac{\partial^2\Psi}{\partial\theta^2}. \tag{2.20}$$

Inserting the ansatz into the partial derivatives and the saturation potential this terms are reduced to

$$\frac{\partial\Psi}{\partial z} = \frac{\partial}{\partial z}\{R(r)\Theta(\theta)Z(z)\} = R\Theta\frac{d}{dz}\{e^{i\beta z}\} = i\beta\Psi, \tag{2.21}$$

$$\frac{\partial^2\Psi}{\partial\theta^2} = \frac{\partial^2}{\partial\theta^2}\{R(r)\Theta(\theta)Z(z)\} = RZ\frac{d^2\Theta}{d\theta^2} = RZ\frac{d^2}{d\theta^2}\{e^i m\theta\} = -m^2RZe^{im\theta} = -m^2\Psi, \tag{2.22}$$

$$\frac{\partial \Psi}{\partial r} = \frac{\partial}{\partial r}\{R(r)\Theta(\theta)Z(z)\} = \Theta Z \frac{dR}{dr}, \tag{2.23}$$

$$\frac{\partial^2 \Psi}{\partial r^2} = \frac{\partial^2}{\partial r^2}\{R(r)\Theta(\theta)Z(z)\} = \Theta Z \frac{d^2R}{dr^2}, \tag{2.24}$$

$$|\Psi|^2 = \Psi\widetilde{\Psi} = \{Re^{im\theta}e^{i\beta z}\}\{Re^{-im\theta}e^{-i\beta z}\} = R^2. \tag{2.25}$$

By applying this simplifications our model equation is reduced to

$$-\beta\Psi + \Theta Z\frac{d^2R}{dr^2} + \frac{\Theta R}{r}\frac{dR}{dr} - \frac{m^2}{r^2}\Psi + \frac{R^2}{1+sR^2}\Psi + p\Gamma(r)\Psi = 0. \tag{2.26}$$

Dividing by the radial part of the solution Θ and the longitudinal harmonic function Z, the equation is reduced solely to a function of the radial coordinate r. Solving for the second order derivative of R ends like

$$\frac{d^2R}{dr^2} = -\frac{1}{r}\frac{dR}{dr} + \beta R + \frac{m^2}{r^2}R - \frac{R^2}{1+sR^2}R - p\Gamma(r)R. \tag{2.27}$$

This equation must be solved numerically since its complexity allows no analytical nor closed form solutions. In order to solve it must be transformed introducing a new parametrization to reach what is called a state space representation. This consists in transforming a n^{th} order ordinary differential equation to n first order coupled differential equations. This technique can be applied to various high order differential equations too via the same method. In the present case, it is needed to introduce a support function, namely $\mu(r)$, which is equal to R's first derivative. This leads to

$$\frac{dR}{dr} = \mu, \tag{2.28}$$

$$\frac{d\mu}{dr} = -\frac{1}{r}\mu + \beta R + \frac{m^2}{r^2}R - \frac{R^2}{1+sR^2}R - p\Gamma(r)R, \tag{2.29}$$

which is a coupled system of two first order ordinary differential equation, thus reaching state space. In order to solve numerically for $R(r)$, s standard algorithm for integrating ordinary differential equations must be employed providing the proper initial conditions. An adaptive step size Runge-Kutta 4th order method has proven to work well with this equation.

The original problem has been reduced to solving two first order ordinary differential equation, which can be solved if either boundary conditions or initial conditions are provided. In

this case, the only information available is that Ψ must have null intensity in the point representing the vortex, which it has been established it is contained along the z axis. Meaning that $R(0) = 0$. The other condition to be met is that as Ψ represents a localized optical field, its intensity must vanish at infinity. Meaning that, as $r \to 0$, R and all of its derivative should be zero valued, the same behavior a gaussian bell has when x tends to infinity. Nevertheless, this brings no information to whatsoever the derivative of R should be at at $r = 0$. Thus, the information available corresponds to a boundary value problem, being that $R(0) = 0$ and that the function R should vanish after a finite value of R.

In order to fill the last gap in this method an algorithm known as the shooting method must be employed. As $\mu(0)$ is unknown, various values must be inserted for solving the system of equations for R. The one's who make R closer to the expected behavior define an interval which contains the right initial condition for making R vanish after a certain r value. This method can be understood as varying slowly the first derivative of R until the expected conditions are reached. Being a nonlinear equation our model, sharp variations are expected, and so a close monitoring is required when using the shooting method.

A final remark must be added, since the equation modeling R as a singularity present at $r = 0$. For the method to properly work the solution $R(r)$ must be calculated starting at a small offset close to zero, that is $r_o > 0$. The method is applied, thus providing a solution $R(r)$ for $r \geq r_o$. The function for $r < r_o$ is simply calculated as $r^{|m|}$, where m is the vortex topological charge. This completely construct the vortex radial profile.

It must be stressed that this method was programmed at the beginning of the research, but was not used after running initial tests. This since the investigation work did not focus on vortex type solitons. Still, it remains as an area of opportunity for the research. Thus, this method is expected to be exhaustively used in the future.

2.2 Numerical methods for propagating solitons

Once a stationary soliton pattern has been obtained what naturally proceeds is to propagate it through the z coordinate. Again, the complexity of the nonlinear schrodinger equation

allows no exact analytical algorithm for doing so and numerical methods have to be necessarily employed. Here are presented the standard methods used to propagate solitons.

2.2.1 Split-step Fourier method

The split step Fourier method [21] relies on the separability of operators assuming that some terms in our nonlinear model can act independently from others. It provides an approximate solution, valid for a small enough value Δz. The natural deviation associated with the numerical method is self-corrected for almost any nonlinear potential associated if the soliton engages stable propagation. To start with, we return to our nonlinear model

$$i\frac{\partial \Psi}{\partial z} + \nabla_t^2 \Psi + N(|\Psi|^2)\Psi = 0, \tag{2.30}$$

where the nonlinear potential notation has been used. First, the diffraction term is discarded, ignoring the transverse laplacian in the equation and leaving

$$i\frac{\partial \Psi}{\partial z} + N(|\Psi|^2)\Psi = 0. \tag{2.31}$$

The next step is to use the essential characteristic of a soliton, its intensity propagation invariance. Mathematically, its means that Ψ is not a function of z. This leaves $N(|\Psi|^2)$ a constant for a fixed value of x and y. Now, in the case of tilted non stationary solitons, the intensity profile $|\Psi|^2$ does vary, but if Δz is small enough, it can be considered again a constant over the range $z + \Delta z$ for fixed (x, y) values. So, $N(|\Psi|^2)$ can be approximately considered a constant for a certain point in the configuration space, leaving our last to solve equation in the form of

$$\frac{df}{dz} + cf = 0, \tag{2.32}$$

where the equation is valid for each individual point on our mesh. Assuming without loss of generality that the soliton pattern has been previously calculated for z_o, where $z_o = 0$ in the case of launching the propagation sequence, the last equation can be solved as

$$\Psi(\mathbf{r}_t, z_o + \frac{\Delta z}{2}) = \exp\left\{iN(|\Psi(\mathbf{r}_t, z_o)|^2)\right\}\Psi(\mathbf{r}_t, z_o). \tag{2.33}$$

Now, it is turn for the nonlinear part to be ignored and for the diffraction operator to act on the wave function. This reduces the nonlinear equation to

$$i\frac{\partial \Psi}{\partial z} + \nabla_t^2 \Psi = 0. \tag{2.34}$$

Taking $\Psi(\mathbf{r}_t, z_o + \frac{\Delta z}{2})$ as an input to the last equation, it can be solved exactly via the Fourier transform. Using an identity shown in the petviashvili section it delivers

$$\Psi(\mathbf{r}_t, z_o + \Delta z) = \mathscr{F}^{-1}\Big\{e^{-ik_t^2 \frac{\Delta t}{2}} \mathscr{F}\{\Psi(\mathbf{r}_t, z_o + \frac{\Delta z}{2})\}\Big\}. \tag{2.35}$$

Thus, fixing the parameter Δz to a small value and having Ψ at a certain value of z, one can propagate indefinitely with this method its solution to obtain the propagation evolution of the soliton. In order to fix Δz one must take in consideration that this method relies on the separability of the diffraction and nonlinear operators, which is approximate only on short intervals. As a check mark, one can propagate the same soliton under the same initial conditions with distinct values of Δz. This interval must be shortened until the outcome results do not vary. Another consideration that must be taken is that Δz should satiety

$$\Delta z \leq \frac{\Delta x \Delta y}{c}, \tag{2.36}$$

where Δx and Δy are the step size used in partitioning the (x, y) plane in order to make it discrete it, and c is a parameters bigger than 1. Usually, $c = 2$ suffices for almost any grid partitioned who faithfully represents an stationary soliton.

There are modifications of the split step Fourier method that improve the results, relying on partitioning the interval in shorter subintervals and combining several nonlinear and diffractive propagation. Nevertheless, this variations produce more complex computations which are not justified by the slight improvement in result. Thus, the original and more simpler approach is used generally, making it simpler to use.

2.2.2 Finite difference method

The finite difference method [22] is an integration technique which relies in the discrete approximate transformation for derivatives. That is, it assumes that a derivative can be represented as a difference among certain short interval, which is entirely true if the variation in the interval is linear. This comes from the concept of derivative, which is defined as

$$\frac{df}{dx}(x = x_o) = lim_{h\to 0}\frac{f(x_o + h) - f(x_o)}{h}. \tag{2.37}$$

A reasonable approximation for the derivative would be

$$\frac{df}{dx}(x = x_o) \approx \frac{f(x_o + \Delta x) - f(x_o)}{\Delta x}, \tag{2.38}$$

for a small value of Δx. This approximation is valid as long as the variation of $f(x)$ in the interval $(x_o, x_o + \Delta x)$ is not sharp or oscillatory, being it linear the exact case where it works. In order to prove how it works in a more formal fashion a derivation from Taylor's polynomial can be carried out. First, it must be assumed that the function to be expanded is well behaved, something that generally holds with functions describing physical quantities. This allows a power series expansion of the function as

$$f(x) = a_o + a_1(x - x_o) + a_2(x - x_o)^2 + a_3(x - x_o)^3 + \cdots = \sum_{n=0}^{\infty} a_n(x - x_o)^n, \tag{2.39}$$

where the expansion coefficients are defined as

$$a_n = \frac{d^n}{dx^n}\{f\}\Big|_{x=x_o}. \tag{2.40}$$

For x close to x_o, the quantity $x - x_o$ is small, and each subsequent term of the series decreases by this factor. So, the last expression can be written as

$$f(x) = f(x_o) + \frac{df}{dx}\Big|_{x_o}(x - x_o) + R(x - x_o), \tag{2.41}$$

where the term $R(x - x_o)$ is small and can be ignored is x is close to x_o, leading to

$$f(x) \approx f(x_o) + \frac{df}{dx}\Big|_{x_o}(x - x_o), \tag{2.42}$$

and solving for the derivative one gets

$$\frac{df}{dx}\Big|_{x_o} = \frac{f(x) - f(x_o)}{x - x_o}, \tag{2.43}$$

then writing x as $x = x_o + \Delta x$, where Δx is small,

$$\frac{df}{dx}\Big|_{x_o} = \frac{f(x_o + \Delta x) - f(x_o)}{\Delta x}. \tag{2.44}$$

This discrete definition of derivative is skewed, in the sense that it uses a forward derivative. In order to correct this arbitrariness, the backward derivative can be combined, to cancel the forward effect,

$$\frac{df}{dx}\Big|_{x_o} = \frac{f(x_o) - f(x_o - \Delta x)}{\Delta x}, \tag{2.45}$$

then calculate the mean of both functions to get

$$\frac{df}{dx}\Big|_{x_o} = \frac{f(x_o + \Delta x) - f(x_o - \Delta x)}{2\Delta x}. \tag{2.46}$$

This corrects the skewness and produces a centralized derivative. This procedure can be applied to second derivatives in order to produce second order discrete derivatives, as

$$\frac{d^2f}{dx^2}\Big|_{x_o} = \frac{f(x_o + \Delta x) - 2f(x_o) + f(x_o - \Delta x)}{2\Delta x^2}. \tag{2.47}$$

Now, in order to use finite differences in the nonlinear Schrödinger equation, the laplacian must be reduced to a discrete second order derivative

$$\nabla_t^2 \Psi(x_o, y_o) = \frac{\partial^2 \Psi}{\partial x^2}(x_o, y_o) + \frac{\partial^2 \Psi}{\partial y^2}(x_o, y_o) = \tag{2.48}$$

$$\frac{\Psi(x_o + \Delta x, y_o) - 2\Psi(x_o, y_o) + \Psi(x_o - \Delta x, y_o)}{\Delta x^2} + \frac{\Psi(x_o, y_o + \Delta y) - 2\Psi(x_o, y_o) + \Psi(x_o, y_o - \Delta y)}{\Delta y^2}. \tag{2.49}$$

It is common to divide the (x, y) plane equally, making Δx equal to Δy. In that case

$$\nabla_t^2 \Psi(x_o, y_o) = \frac{\Psi(x_o + \Delta x, y_o) + \Psi(x_o, y_o + \Delta y) - 4\Psi(x_o, y_o) + \Psi(x_o - \Delta x, y_o) + \Psi(x_o, y_o - \Delta y)}{h^2}, \tag{2.50}$$

where

$$h = \Delta x = \Delta y. \tag{2.51}$$

Applying discrete derivatives to a partial equation reduces the process of integrating the equation to recursive calculations of matrix. Derivatives are replaced by differences, as shown for the laplacian. In the case of the longitudinal z derivative, a forward derivative is used. This because the initial conditions, the stationary soliton pattern, is given only for a initial z_o plane, not for two planes. So,

$$\frac{\partial \Psi}{\partial z}(x_o, y_o)\Big|_{z=z_o} = \frac{\Psi(x_o, y_o)|_{z=z_o+h_z} - \Psi(x_o, y_o)|_{z=z_o}}{h_z}, \tag{2.52}$$

where h_z is the longitudinal step size, the distance between calculated planes of the soliton.

The nonlinear schrodinger equation can be written as

$$\frac{\partial \Psi}{\partial z} = i\nabla_t^2 \Psi + iN(|\Psi|^2)\Psi. \tag{2.53}$$

Combining this with the definitions just presented, the propagation equation is

$$\Psi(x_o, y_o)\Big|_{z=z_o+h_z} = \Psi(x_o, y_o)\Big|_{z=z_o} + ih_z\Big\{\nabla_t^2 \Psi(x_o, y_o) + N(|\Psi(x_o, y_o)|^2)\Psi(x_o, y_o)\Big\}\Big|_{z=z_o}. \tag{2.54}$$

That is, all needed for this method is the initial pattern and defining h_z to propagate the soliton indefinitely. Again, h_z should satisfy

$$h_z \leq \frac{h^2}{2}. \tag{2.55}$$

2.2.3 Comparison of propagation methods

Two methods for numerical propagation of soliton profiles have been presented in this section, while the question remaining is which method is better or must be used for numerical

experiments. Finite differences is a relatively primitive method when compared to the split step propagation method. Besides, the split step method makes uses of the optimized fast fourier transform algorithm. For this and other reasons the split step Fourier method is faster than finite differences. Still, finite differences can be used in order to compare the same propagation, since this method introduces less numerical errors than the split step method, since it makes use of more elaborate and complex calculus. Even though, the split step Fourier method has proven to be accurate and provide good results fast.

2.3 Statistical analysis tools

Since the quantifiers obtained from a propagation consists of a set of ordered points, they can be treated as statistical information. Thus, the need to apply statistical instruments to this work arises naturally.

When obtaining ordered pairs of data a natural question would be whether there exist a linear interdependence between both samples or not, namely X and Y. This falls on the field of linear regression [23], which constructs linear models between two random variables. This whole methodology relies on the curve fitting algorithm of least squares [24]. In short, this method fits a curve to certain given points by minimizing the squares of the errors involved in such approximation. It has proven to be a durable and reliable tool in the field of statistics.

Now, linear regression is used mainly with one of two goals: to forecast a value of the random variable Y for a missing value of X in the original set of points, or two quantify the linear dependence strength between two models, that is two quantify how close the relation to X and Y is from a perfect linear relation $Y \propto X$.

Linear regression gives a compact model for approximating the given data in the form

$$Y = \hat{\beta}_0 + X\hat{\beta}_1, \tag{2.56}$$

where $\hat{\beta}_0$ and $\hat{\beta}_1$ are constructed via least squares. The equations resulting from such method are

$$\hat{\beta}_1 = \frac{S_{XY}}{S_{XX}}, \tag{2.57}$$

$$\hat{\beta}_0 = \overline{Y} - \hat{\beta}_1 \overline{Y}, \tag{2.58}$$

where

$$\overline{Y} = \frac{\sum_{i=1}^{n} y_i}{n}, \tag{2.59}$$

$$\overline{X} = \frac{\sum_{i=1}^{n} x_i}{n}, \tag{2.60}$$

are the mean values of the random variables X and Y and both samples are of size n. The statistics S_{XX} is the variance of X, defined as

$$S_{XX} = \frac{\sum_{i=1} n(x_i - \overline{x})(y_i - \overline{Y})}{n-1}, \tag{2.61}$$

and S_{XY} is called the cross variance, a quantity involving the spread of both random variables. It is defined as

$$S_{XY} = \frac{\sum_{i=1} n(x_i - \overline{x})(y_i - \overline{Y})}{n-1}. \tag{2.62}$$

This gives a quick and easy way of calculating a linear approximation for two given set of points X and Y.

2.3.1 Correlation coefficient

There are diverse methods and quantifiers for testing how valid a linear model is valid for approximating the dependence between two given variables. One such is the linear correlation coefficient, or just correlation coefficient [25]. It is a normalized measure, with values ranging from -1 to 1, of how linear the relation is between two variables. It is defined as

$$r = \frac{S_{XY}}{S_X S_Y}, \tag{2.63}$$

where

$$S_X = \sqrt{S_X}, S_Y = \sqrt{S_Y}. \tag{2.64}$$

A value of $r = 1$ implies a perfect linear relation between X and Y with a positive slope. That is a dependence of the form

$$Y = q + mX, \tag{2.65}$$

with arbitrary q and $m > 0$. If $r = -1$, the same model applies but with $m < 0$; s for in the case of $m = 0$ the statistic r is undefined due to the null-zero variance of Y. When r deviates slightly from 1 or -1, it can be said that the linear model is a good approximation to the real functional dependence of X and Y. Furthermore, numerical issues such as round off errors may introduce a small deviation from the unitary values, so in order to make use of this statistic it should be supported on a clear consideration of the data points. That is, r cannot help to determine by itself whether a dependence is linear or not, but it most be supported on experience and practical considerations.

2.3.2 Statistical hypothesis testing for $\hat{\beta}_1$

Numerical errors can induce unwanted variations in all quantifiers involved, and strike heavily when trying to apply a linear approximation. When a linear model has been considered to correctly describe its inputs, a natural question would be whether the variation introduced by the slope m is considerable or can be ignored. That is, if for practical uses it can be considered that $\hat{\beta}_1 \approx 0$.

In order to answer so, a statistical inference technique must be applied, called hypothesis testing [26]. This method assumes first and hypothesis to be true, and applies numerical quantifiers to either approve it or reject it. There exist a particular hypothesis testing for solving the particular question whether $\hat{\beta}_1$ can be approximated by zero or no. In case it can be done, then the quantifier Y from the linear model can be considered to be a constant.

To start with the method both hypothesis must be established, the null hypothesis

$$H_0 : \hat{\beta}_1 = 0, \tag{2.66}$$

and the alternative hypothesis

$$H_1 : \hat{\beta}_1 \neq 0. \tag{2.67}$$

Afterwards, the evaluation statistic must be computed. This value is obtained from the particular sample of points employed and the nature of such points, being it a number purely drawn from the numerical sample. It is defined as

$$t = \frac{\hat{\beta}_1}{\sqrt{\frac{\hat{\sigma^2}}{S_{XX}}}}, \tag{2.68}$$

where

$$\hat{\sigma^2} = \frac{S_{YY} - \hat{\beta}_1 S_{YY}}{n-2}. \tag{2.69}$$

Then the significance level of the test α must be given a value, where for most cases can be interpreted as the test's probability of incorrectly rejecting the null hypothesis, therefore it may seem convenient to fix α to the lowest value possible. Still, this has repercussions on the test, giving the test a high probability of accepting wrongful results, that is, a false positive. So, a balance must be kept between both factors, and ideally an investigator must be familiar with the test in order to give α a desired, specific value. That is, to accept the null hypothesis with a mild tolerance for false positives. Experience has proved the value of $\alpha = 0.95$ to give good results in a wide range of test and fields. But in the end, this test will be only a hint or tool in taking a decision, based too on observance of the results.

Having discussed the former issue, it can be said that α fixes the critical value of the test to the value $t_{n-2,1-\alpha}$, where

$$F(n-2; t_{n-2,1-\alpha}) = 1 - \alpha, \tag{2.70}$$

and the symbol F represents the t-student cumulative probability function,$n-2$ represents the degrees of freedom associated with the function, an input parameter, and $1-\alpha$ is the argument of the test. Since F is itself a cumulative probability function, it means that the value $F(n-2; t_{n-2,1-\alpha})$ accumulates a probability of $1-\alpha$.

To conclude, the hypothesis test fails if $t > t_{n-2,1-\alpha}$. Thus, the null hypothesis is rejected and it can be concluded that $\hat{\beta}_1 \neq 0$ and that there is a considerable variation involved in the observed process. If the opposite event takes place, $t < t_{n-2,1-\alpha}$, then there is strong statistical evidence pointing that $\hat{\beta}_1 = 0$, concluding that Y can be considered to be a constant.

Chapter 3

Soliton propagation in elliptic photonic lattices

The subject of solitons propagating through optical lattices is a recent and novel topic research in optics. The steering and routing possibilities offered by this media is a theory yet to be developed and under extensive study. As said before, nondiffracting beams are clever options due to their propagation invariant profile, maximizing control of light. The first part of the research corresponds to solitons propagating in the so called elliptical photonic lattice (EPL). It presents a pattern induced by a superposition of Mathieu beams, which contains non circular closed trajectories in the form of elliptic rings azimuthally modulated. This last fact was appealing for the investigation, since closed trajectories allows periodic nonstop motion and there was no precedent for such studies on elliptical trajectories. Since the EPL presents a nonuniform potential over a closed trajectory stability cannot be achieved at all times. This work presents how stable propagation is a possibility on the EPL for certain given parameters.

3.1 The elliptical photonic lattice

As just said, the EPL is induced by a superposition of Mathieu beams. The last are by itself nondiffracting beams, which lead and promote a whole field of study in optics. Here a brief but explanatory description of the EPL and its fundamentals is presented. To start with, must one begin with the model generating all nondiffracting beams, the Helmholtz equation

$$\nabla^2\Phi + k^2\Phi = 0, \tag{3.1}$$

where Φ is the profile describing the nondiffracting beam, k is a constant known as the beam's wave number related to the field's propagation in space and following propagation standards

is taken along the z axis. Since Φ is propagation invariant its intensity cannot be a function of z. Thus, the propagation coordinate amounts only to a phase factor, a common feature of all nondiffracting beams. Therefore Φ is separated as

$$\Phi(\mathbf{r}) = \phi(\mathbf{r}_t)e^{ik_z z}, \tag{3.2}$$

where Φ is a function of space (3 coordinates), ϕ is a function of the transversal coordinates (2 coordinates) and k_z is the longitudinal wave number or propagation constant. This reduces the Helmholtz equation to

$$\nabla_t^2\phi + k_t^2\phi = 0, \tag{3.3}$$

where k_t is the transverse wave number defined as $k_t^2 = k^2 - k_z^2$; and ∇_t^2 is the transverse laplacian, function only of the transverse coordinates. In cartesian coordinates it is written as

$$\nabla_t^2 = \frac{\partial^2}{\partial x^2} + \frac{\partial^2}{\partial y^2}. \tag{3.4}$$

Thus, obtaining the profile for nondiffracting beams is a problem to be solved in two-dimensions, where $\phi(\mathbf{r}_t)$ is known as a normal or stationary mode of propagation. In order to continue, the equation must be properly adjusted to elliptical cylindrical coordinates, the natural coordinate system for Mathieu beams.

3.1.1 Elliptical cylindrical coordinates

This is one of the four orthogonal cylindrical systems in which the Helmholtz equation is separable, thus defining a complete space for representing planar profiles and one of the four unique families of perfectly nondiffracting beams. The transformation from cartesian coordinates $< x, y, z >$ to elliptic cylindrical coordinates $< \xi, \eta, z >$, where as both systems are cylindrical leaves z unaffected, is given by

$$x + iy = f\cosh(\xi + i\eta), \tag{3.5}$$

where f is the semi-focal distance associated to the coordinate system and is related to the ratio of the semi-axis of confocal ellipses. The last transformation can be separated and

expressed for clarity as

$$x = f\cosh(\xi)\cos(\eta), \tag{3.6}$$

$$y = f\sinh(\xi)\sin(\eta). \tag{3.7}$$

Making an analogy to polar coordinates, ξ can be interpreted as a radial coordinates which takes values inside the semi-open interval $[0, \infty)$, that is the nonnegative real numbers. Furthermore, η makes the role of an angular coordinate covering the interval $[0, 2\pi)$. As expected, ellipses should be found in the set of coordinate curves for this system. Ellipses are generated by fixing the elliptic radius ξ to a constant value ξ_o as properly shown in the expression

$$\left[\frac{x}{f\cosh(\xi_o)}\right]^2 + \left[\frac{y}{f\sinh(\xi_o)}\right]^2 = \cos^2(\eta) + \sin^2(\eta) = 1, \tag{3.8}$$

which is the equation for a ellipse with major semi-axis $f\cosh(\xi_o)$ and minor semi-axis $f\sinh(\xi_o)$ having both its principal axes over the x and y axis, respectively. Furthermore, the coordinate curves for ξ is a family of confocal ellipses which collapse in the limiting value $\xi = 0$ to the straight line across the x axis that joins $(x, y) = (\pm f, 0)$ the focal points of this ellipses. The elliptic version of the angular coordinate curves, which are itself straight lines, corresponds to hyperbolas. This can be appreciated by fixing η to η_o in the expression

$$\left[\frac{x}{f\cos(\eta_o)}\right]^2 - \left[\frac{y}{f\sin(\eta_o)}\right]^2 = \cosh^2(\xi) - \sinh^2(\xi) = 1, \tag{3.9}$$

which is an equation for generating a family of hyperbolas by varying the parameter η_o. This conical curves cross the x axis at $\pm f\cos(\eta_o)$ and have straight line asymptotes which cross the origin and have slope $\pm\tan(\eta_o)$. For the values $\eta = 0$ and $\eta = \pi$ the hyperbolas collapse to straight lines on the x axis going from $x = \pm f$ towards $\pm\infty$. As for $\eta = \frac{\pi}{2}$ and $\eta = \frac{3\pi}{2}$, the hyperbolas collapse to the positive y axis and negative y axis, respectively. Coordinate curves for the elliptical cylindrical system are shown in figure 3.1.

As it can be calculated the scale factors of the ξ and η are equal, being them

$$h = h_\xi = h_\eta = \sqrt{\cosh^2(\xi) - \cos^2(\eta)}, \tag{3.10}$$

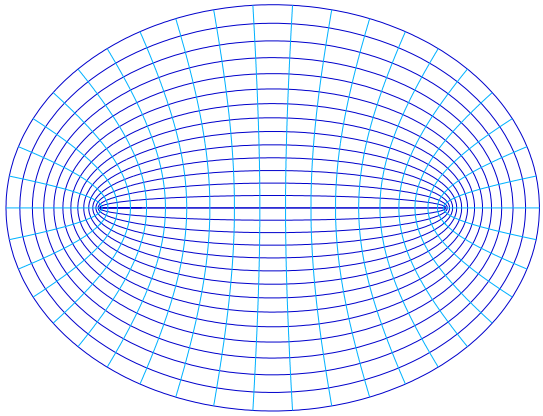

Figure 3.1: A qualitatively sample of coordinate curves in the plane are shown for the elliptic cylindrical coordinates system with $f = 1$. Dark blue curves correspond to constant $\xi = \xi_o$ curves, confocal ellipses. with semi-major and semi-minor axes $\cosh(\xi_o)$ and $\sinh(\xi_o)$, respectively. Light blue curves mark constant $\eta = \eta_o$ curves, hyperbolas with asymptotes $y = \pm\tan(\eta_o)$

and as expected, $h_z = 1$.

3.1.2 Mathieu functions

In order to reach the EPL, the Helmholtz equation must be solved in elliptic cylindrical coordinates. Inserting the proper scale factor in the transversal Helmholtz equation, it is reduced to

$$\frac{1}{f^2\Big[\sinh^2(\xi)+\sin^2(\eta)\Big]}\left[\frac{\partial^2\phi}{\partial\xi^2}+\frac{\partial^2\phi}{\partial\eta^2}\right]+k_t^2\phi=0. \tag{3.11}$$

Applying separation of variables (SOV) technique the following expressions are reached

$$\Big[\frac{d^2}{d\eta^2}-2q\cos(2\eta)+a\Big]\Theta(\eta)=0, \tag{3.12}$$

$$\Big[\frac{d^2}{d\xi^2}+2q\cosh(2\xi)-a\Big]R(\xi)=0, \tag{3.13}$$

where the first equation is know in literature as the Angular Mathieu Equation or Ordinary Mathieu Equation, and the later is the Radial Mathieu Equation or Modified Mathieu

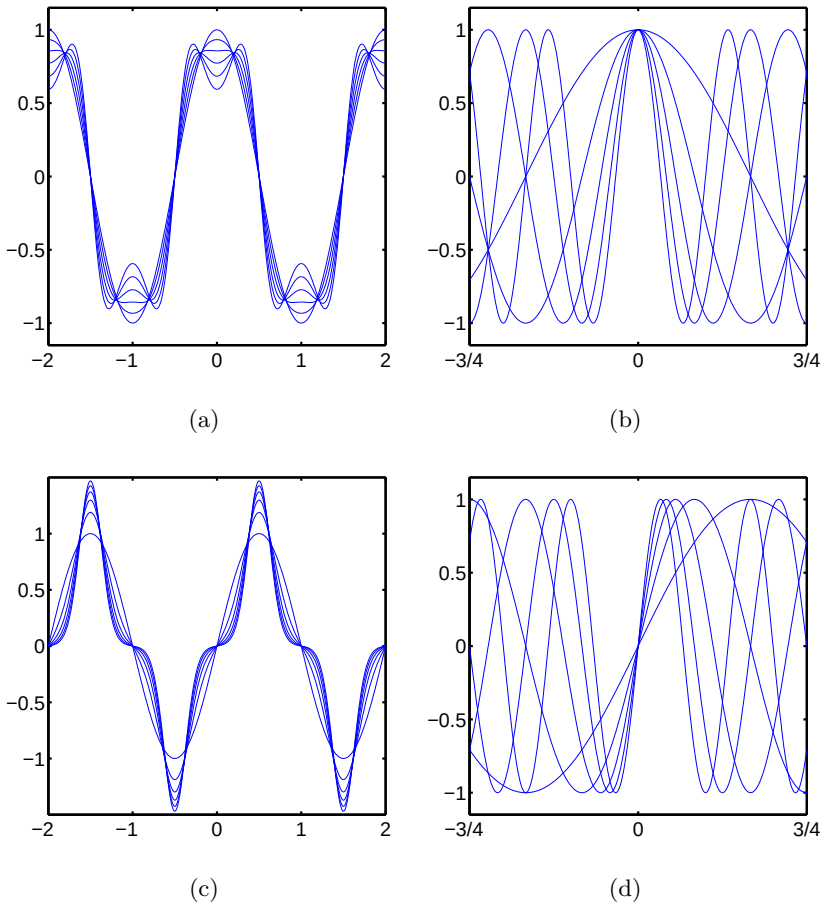

Figure 3.2: Sample plots for the ordinary mathieu functions $ce_m(\eta; q)$ and $se_m(\eta; q)$, their symmetry and periodicity conditions are reflected as being superpositions of cosine and sine functions respectively. In (a) $ce_m(\eta; q)$ is plotted against η for $m = 1$ and $q = \{0, 0.5, 1, 1.5, 2, 2.5\}$. In (b) $ce_m(\eta; q)$ is plotted against η for $q = 0$ and $m = \{1, 2, 3, 4, 5\}$. In (c) $se_m(\eta; q)$ is plotted against η for $m = 1$ and $q = \{0, 2, 4, 6, 8, 10\}$. In (d) $se_m(\eta; q)$ is plotted against η for $q = 0$ and $m = \{1, 2, 3, 4, 5\}$. All x-axis are normalized to π units.

Equation. The parameter a corresponds to the constant of separation in the SOV method, which furthermore corresponds to the eigenvalue of both equations, and q is a dimensionless parameter which stands for

$$q = \frac{f^2}{4} k_t^2. \tag{3.14}$$

In the current notation, the transverse profile of the Mathieu beam would be written as

$$\psi(\mathbf{r}_t) = R(\xi)\Theta(\eta), \tag{3.15}$$

where $\Theta(\eta)$ corresponds to the ordinary Mathieu function and $R(\xi)$ to the modified Mathieu function. Due to the symmetry existent in the Ordinary Mathieu equation, the set of functions corresponding to $\Theta(\eta)$ can be broken in two parts, even type functions and odd type functions, which are commonly labeled as $ce_m(\eta; q)$ and $se_m(\eta; q)$, respectively. The nomenclature comes from the terms elliptic cosine and sine, again making an strong analogy to the circular case. Here m corresponds to the order of the function associated with the particular value of the parameter q chosen, where the order follows and ordering of the eigenvalues a associated with each function. Plots for representative cases of both functions are displayed in figure 3.2.

As for the radial case, the Modified Mathieu functions have been extensively studied as well. The same symmetry in the equation applies for this case, thus allowing the existence of purely even and purely odd functions, in this case labeled as $Je_m(\xi; q)$ and $Jo_m(\xi; q)$, respectively. This time the nomenclature follows the one used for ordinary first time Bessel functions, where $Je_m(\xi; q)$ and $Jo_m(\xi; q)$ resemble in a manner the well know and used Bessel functions.

It must be mentioned that the for either equation more solutions exist in the rigorous mathematical sense, but they are discarded in this brief overview and are excluded as a possibility for constructing the EPL due to their structure, being undefined in the origin as a main problem. So, even though other solutions exists, the research has been taken with the set presented. There exist plenty information concerning Mathieu functions in the literature [27].

3.1.3 Computation of the EPL

Solutions to the transverse Helmholtz equation, the profile $\phi(\mathbf{r}_t)$, correspond to combinations of only even or odd functions, that is either $Je_m(\xi; q)ce_m(\eta; q)$ or $Jo_m(\xi; q)co_m(\eta; q)$. Due to the linearity of the equations used, a more completed solution possessing no preferable symmetry around the origin would be

$$\phi(\mathbf{r}_t) = C_1\ Je_m(\xi; q)ce_m(\eta; q) + C_2\ Jo_m(\xi; q)co_m(\eta; q), \tag{3.16}$$

where this corresponds to one order only, a single value of m, and C_1 and C_2 are simply scaling constant for not loosing generality. Again, considering superposition, multiple and even infinite values of m can be considered to construct a single solution ϕ. For constructing the EPL this was not considering, and restraining to a single value of m was a restriction imposed. So, invoking the last equation, we define

$$\tau(\mathbf{r}_t) = \mathscr{C}_e \; Je_m(\xi; q)ce_m(\eta; q) + \mathscr{C}_o \; Jo_m(\xi; q)co_m(\eta; q), \tag{3.17}$$

where $\tau(\mathbf{r}_t)$ represents the wavefunction of the EPL, $Je_m(\xi; q)ce_m(\eta; q)$ corresponds to the even part of the profile, $Jo_m(\xi; q)co_m(\eta; q)$ represents the odd part of the profile, and $\mathscr{C}_e$ and $\mathscr{C}_o$ are constants for balancing the power contained by each part of the EPL. Moreover, the EPL corresponds to an intensity profile, an observable quantity in nature that corresponds to a index of refraction profile. Thus, the EPL $\Gamma(\mathbf{r}_t)$ is defined as

$$\Gamma(\mathbf{r}_t) = \frac{|\tau(\mathbf{r}_t)|^2}{\max(|\tau(\mathbf{r}_t)|^2)}, \tag{3.18}$$

where the division is carried out in order to assure that the EPL profile is normalized to unity.

Furthermore, there exist another method for computing the EPL via its angular spectrum, which is defined by the angular mathieu functions. The Whittaker integral, presented as follows, reproduces a beam pattern by using as an input the angular spectrum "$A(\eta)$" of the nondiffracting beam,

$$\tau(\mathbf{r}_t) = \int_0^{2\pi} A(\eta) \exp\{ik_t \Big[x\cos(\eta) + y\sin(\eta)\Big]\} d\eta, \tag{3.19}$$

where in the case for an elliptic photonic lattice, the angular spectrum is

$$A(\eta) = \mathscr{D}_e \; ce_m(\eta; q) + \mathscr{D}_o \; co_m(\eta; q). \tag{3.20}$$

Here $\mathscr{D}_e$ and $\mathscr{D}_o$ are the constants used for balancing the power contained by each part of the beam since a different method is used and this constants ought to be different from $\mathscr{C}_e$ and $\mathscr{C}_o$. It is customary to construct a balanced Mathieu beam, that is one which even part and odd part half both 50% of the power of the entire profile. This helps closing the elliptic

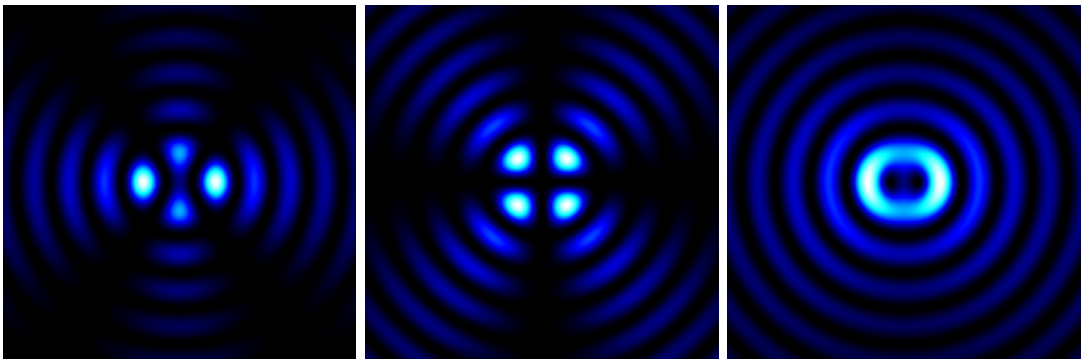

(a) (b) (c)

Figure 3.3: Pure even (a) and odd (b) Mathieu beams do not posses closed elliptic trajectories. The helical Mathieu beam (c) is a superposition of both symmetries, thus closing intensity ellipses and forming light rings azimuthally modulated. Patterns shown are for fixed $m = 1$ and $q = 1$.

trajectories, but still is not a strict rule and small deviations from this power distribution does not alter greatly the continuity trajectories. An example depicting the importance of combining both symmetries is shown in figure 3.3.

3.1.4 General Description of the EPL

The transverse index distribution on the EPL is characterized by a set of confocal elliptic rings whose ellipticity is controlled by f. When $f \to 0$ the EPL reduces to a Bessel lattice characterized by a set circular concentric rings whose intensity is constant along the angular coordinate, presenting only radial variations and a null azimuthal modulation. As f increases , the rings become more and ore elliptical and, after a critical value, they are broken, splitting into a discrete like intensity lattice. When $f \to \infty$, the EPL tends smoothly to a discrete rectangular lattice characterized by cosine functions. It is important to mention that certain cases of the Cartesian and Bessel families of the nondiffracting beams are special cases of the EPL beam, as mentioned above. Representative profiles of the EPL are displayed in figure 3.4.

Unlike balanced Bessel beams, those containing equal power in both its even and odd parts, which have no constant azimuthal modulation, the EPL has a variation in the intensity profile along any of the elliptic rings trajectories, that is varying the angular elliptic coordinate η. Actually, the minimum and maximum intensity points correspond to the major and minor semi-axis, where the correspondence is defined by the balancing constants $\mathscr{C}_e$ and $\mathscr{C}_o$.

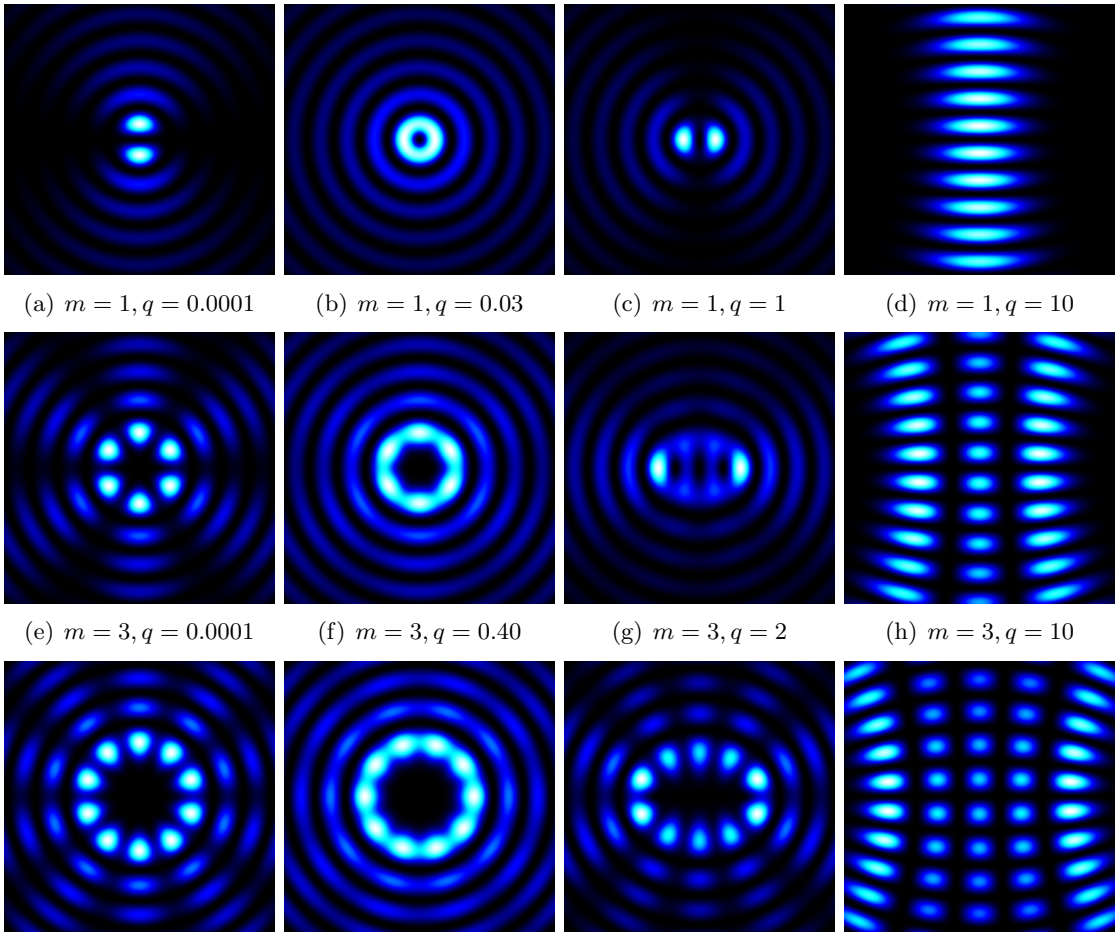

(a) $m = 1, q = 0.0001$ (b) $m = 1, q = 0.03$ (c) $m = 1, q = 1$ (d) $m = 1, q = 10$

(e) $m = 3, q = 0.0001$ (f) $m = 3, q = 0.40$ (g) $m = 3, q = 2$ (h) $m = 3, q = 10$

(i) $m = 5, q = 0.0001$ (j) $m = 5, q = 0.50$ (k) $m = 5, q = 2.65$ (l) $m = 5, q = 10$

Figure 3.4: Helical Mathieu beam intensity profile for balanced power between even and odd parts. Each rows fixes a different value of m, which among other aspects controls the number of maxima and minima around an elliptic ring for the closed trajectories case. For low values of q the profile seems to adjust to a discrete circular symmetric lattice (first column), were critical q values can be found as to produce an approximate Bessel lattice (second column). As q increases the elliptic symmetry arises (third column), which is broken after a critical value and the lattice degenerates into a cartesian like discrete lattice (fourth column).

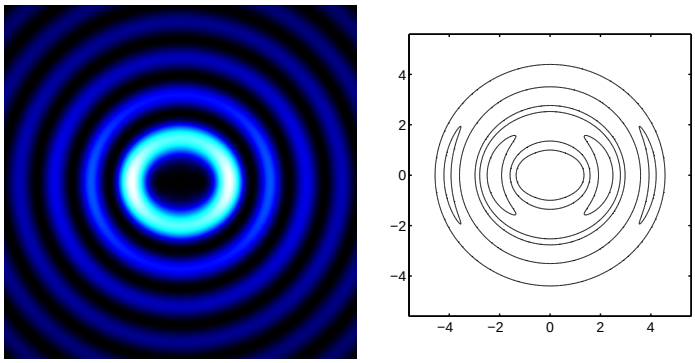

(a) (b)

Figure 3.5: (a) EPL used for the research of soliton propagation, with $m = 3$ and $q = 1$. (b) shows a contourmap of the central region of interest, corresponding to the first and second light rings.

The lattice used for the work in the rest of the section is displayed in figure 3.5.

Having defined the EPL, exposed its computation method and discussed its versatile profile, this works continue with the results found concerning its main theme: propagation of soliton through optical lattices, in this case the EPL.

3.2 Stationary solitons in the EPL

By solving the nonlinear Schrödinger equation stationary solitons are obtained, which have a profile depending on the equation parameters, the ansatz and the precise spot it is centered. By studying this stationary modes

Different profiles can be obtained in the center of the lattice. For small values of p, the soliton retains the bell-shaped pattern from the ansatz and concentrates mostly within the elliptic dark spot of the lattice, where increasing β makes the intensity pattern narrower. if p is increased, the interaction with the EPL becomes stronger and therefore the shape of the lattice is resembled on the obtained solitons. For low values of β, the field distribution covers the central elliptic dark spot and the first bright ring, producing, producing an elliptic ring-shaped stable soliton which is angularly modulated as the EPL, having its maximum along the major semi-axis. As β increases, a symmetry breaking instability is developed, and the soliton concentrates on only one of the maxima of the first elliptic ring. However, for

higher values of β the soliton profiles returns to its bell shaped pattern centered on the lattice.

Stationary solitons can also be trapped in the outer rings of the EPL. If the ansatz is centered at one of the semi-axis maxima, the patterns remains unchanged for small values of β and evolves in the same fashion as if the ansatz centered at the dark elliptic spot, but as the wavelength increases the profile remains at one of the maxima with a narrow bell-shaped. Due to its symmetry, its compact distribution and the localization it holds on the EPL, this type of soliton is the most important for the research. This type of soliton is computed and propagated extensively, since it corresponds to the fundamental modes and is closer to the gaussian distribution of any standard input laser beam. Several profile of stationary solitons are shown in figures 3.6-3.8.

As mentioned in the first section, the power carried by the soliton is calculated as

$$\mathscr{P} = \int\int_{\mathscr{O}} |\phi(\mathbf{r}_t)|^2 dA, \tag{3.21}$$

where as usual, $\phi(\mathbf{r}_t)$ represents the soliton profile and the integral is carried out over the region of the plane $x - y$ that completely encloses the soliton profile. In fig 9. the relation between the power $\mathscr{P}$ and the wavelength β is displayed for solitons in the intensity maximum in the second light ring $(4.05, 0)$ and the intensity minimum in the second light ring $(0, 3.92)$. It was found For both, cases that the Petviashvili relaxation method achieves convergence just when restricted to a finite interval of values that reduces as the lattice depth p increases, as shown in figure 3.9. Applying the Vakhitov-Kolokolov stability criterion described in chapter 1,

$$\frac{d\mathscr{P}}{d\beta} > 0 \longrightarrow \textit{stable propagation for stationary solitons}, \tag{3.22}$$

it was predicted that the solitons contained in the $\beta - p$ regions contained in figure 3.9 were stable. This was confirmed by propagating numerous soliton profiles along hundreds diffraction lengths.

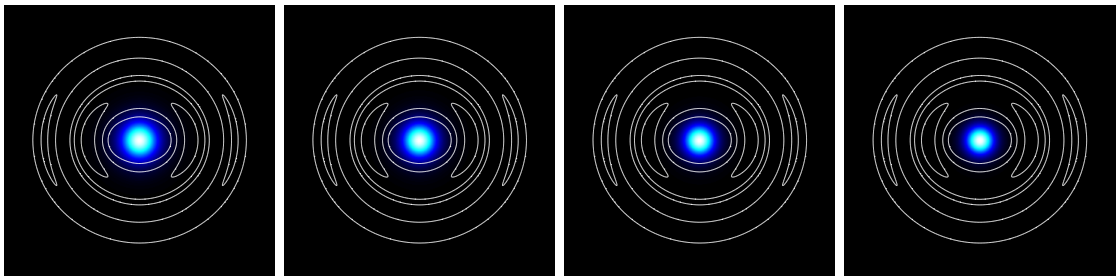

(a) $p = 1, \beta = 1.75$ (b) $p = 1, \beta = 2.00$ (c) $p = 1, \beta = 2.50$ (d) $p = 1, \beta = 3.25$

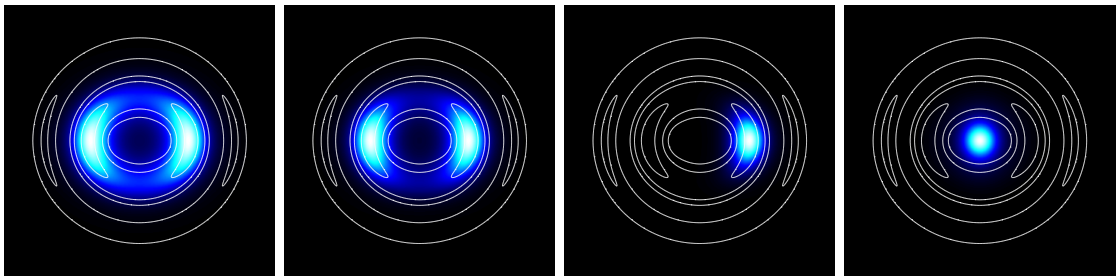

(e) $p = 4, \beta = 1.75$ (f) $p = 4, \beta = 2.00$ (g) $p = 4, \beta = 2.50$ (h) $p = 4, \beta = 3.25$

Figure 3.6: Soliton profiles for the EPL. The ansatz is initially centered at the center of the lattice, coordinates $(0, 0)$ in the $x - y$ plane. The first row of figures corresponds to a fixed lattice depth value of $p = 1$, a relatively low value. With this numerical value the solitons are poorly influenced by the lattice topology and retain the original position of the ansatz and the bell-shaped profile of a fundamental type soliton, while varying the longitudinal wave number β from lower to higher values focuses the soliton into a tighter distribution as can be appreciated from figures (a) to (d). The second row fixes the lattice depth to $p = 4$, a value where the soliton profile is considerably affected by the lattice potential. For low values of β, the soliton profile copies the elliptic symmetry of the center of the lattice as show in (e) and (f). As β increases a symmetry breaking instability is developed, tearing apart the initial profile and concentrating the soliton on only one maxima of the first ring (g). Finally in (h) a value of β is reached as to focus the soliton enough for it to ignore the outer lattice potential and recover a bell shaped pattern.

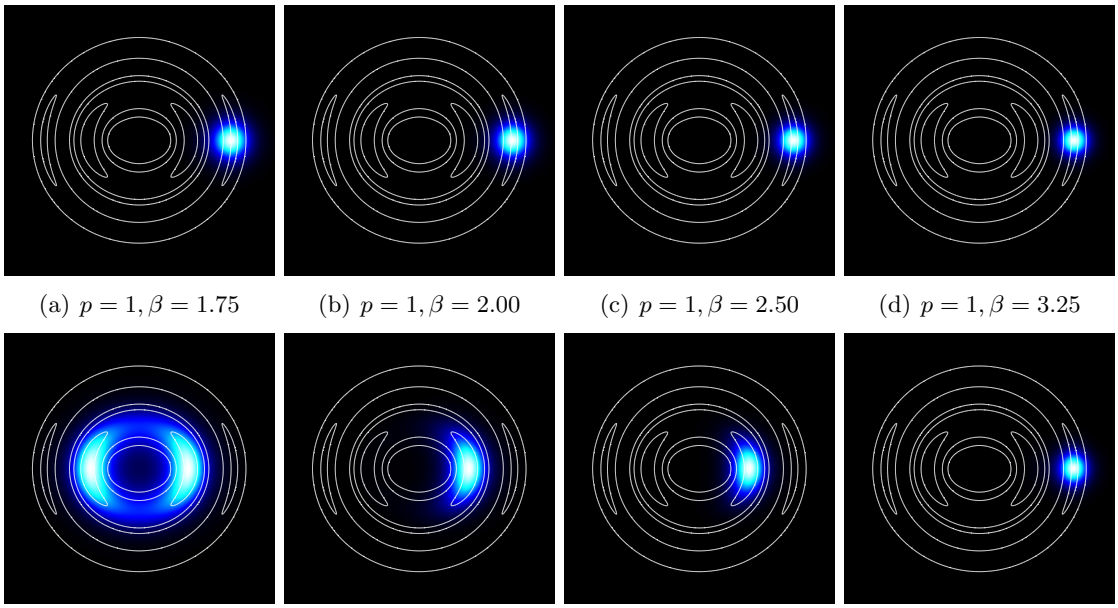

(a) $p = 1, \beta = 1.75$ (b) $p = 1, \beta = 2.00$ (c) $p = 1, \beta = 2.50$ (d) $p = 1, \beta = 3.25$

(e) $p = 4, \beta = 1.75$ (f) $p = 4, \beta = 2.00$ (g) $p = 4, \beta = 2.50$ (h) $p = 4, \beta = 3.25$

Figure 3.7: Soliton profiles for the EPL. The ansatz is initially centered at the intensity maximum of the second light ring,coordinates $(4.05, 0)$ in the $x - y$ plane.The first row of figures corresponds to a fixed lattice depth value of $p = 1$, a relatively low value. With this numerical value the solitons are poorly influenced by the lattice topology and retain the original position of the ansatz and the bell-shaped profile of a fundamental type soliton, while varying the longitudinal wave number β from lower to higher values focuses the soliton into a tighter distribution as can be appreciated from figures (a) to (d). The second row fixes the lattice depth to $p = 4$, a value where the soliton profile is considerably affected by the lattice potential. For small values of β the soliton profile converges to the center of the lattice as if the ansatz was initially positioned at it, shown in (e), (f) and (g). In (h) the soliton retains the position at the second light ring maximum and converges to a fundamental soliton profile.

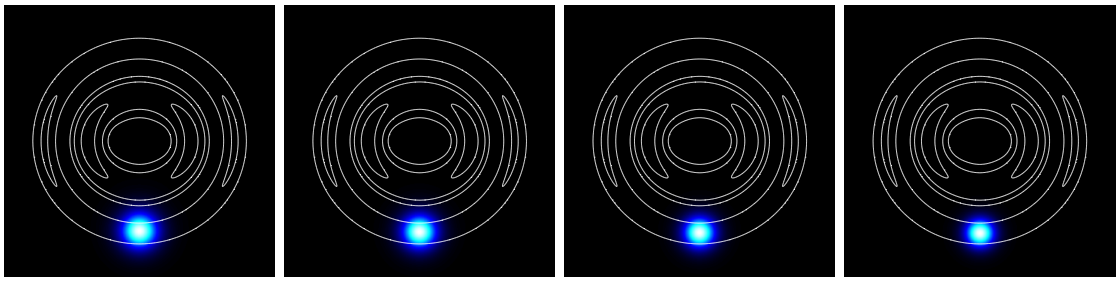

(a) $p = 1, \beta = 1.75$ (b) $p = 1, \beta = 2.00$ (c) $p = 1, \beta = 2.50$ (d) $p = 1, \beta = 3.25$

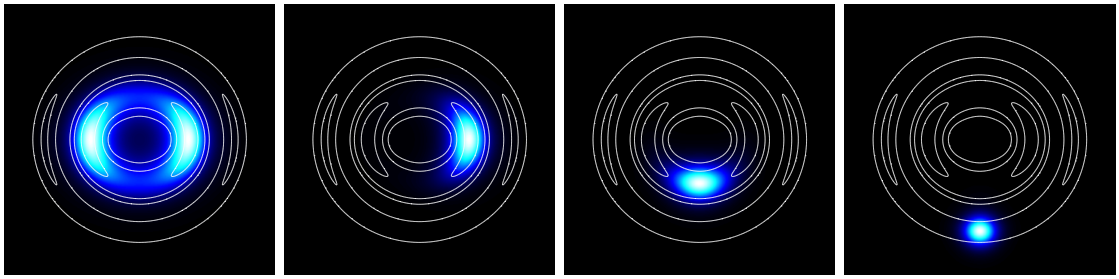

(e) $p = 4, \beta = 1.75$ (f) $p = 4, \beta = 2.00$ (g) $p = 4, \beta = 2.50$ (h) $p = 4, \beta = 3.25$

Figure 3.8: Soliton profiles for the EPL. The ansatz is initially centered at the intensity minimum of the second light ring,coordinates $(0, 3.92)$ in the $x - y$ plane. The first row of figures corresponds to a fixed lattice depth value of $p = 1$, a relatively low value. With this numerical value the solitons are poorly influenced by the lattice topology and retain the original position of the ansatz and the bell-shaped profile of a fundamental type soliton, while varying the longitudinal wave number β from lower to higher values focuses the soliton into a tighter distribution as can be appreciated from figures (a) to (d). The second row fixes the lattice depth to $p = 4$, a value where the soliton profile is considerably affected by the lattice potential. For small values of β the soliton profile converges to the center of the lattice as if the ansatz was initially positioned at it, shown in (e), (f) and (g). In (h) the soliton retains the position at the second light ring minimum and converges to a fundamental soliton profile.

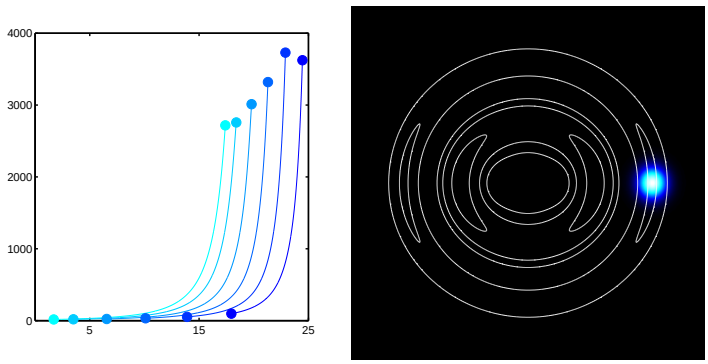

(a) (b)

Figure 3.9: Power $\mathscr{P}$ plotted against β for a soliton centered at the second light ring intensity maximum (a). Each curve corresponds to a different fixed value of the lattice depth, where going from lighter to darker curves p=$\{1,5,10,15,20,25\}$. The location of such solitons in the lattice is depicted in (b).

3.3 Transverse rotating solitons

We now refer to rotating solitons, which move in a transverse fashion while propagating longitudinally. It was found that such can reach a stable condition if trapped in an elliptical ring of the EPL. In order to generate them, the centroid of the gaussian ansatz must be located either at a maximum or a minimum of a bright ring. The following discussion applies to solitons originated from a maximum in the second bright ring, which is what our research in stable rotating solitons covered. To induce rotational motion on the soliton an initial transverse momentum g_{trans} directed along the tangent of the bright ring must be imprinted on the stationary solution; this can be done by imposing a phase twist $exp(ig_{trans}y)$ on the soliton profile as discussed in chapter 1.

For small values of g_{trans} the soliton is still strongly attracted by the local maximum of the elliptic ring and thus oscillates back and forth across this point following an oscillatory trajectory on propagation a shown in Fig. 3.10(a). The rotational motion of the soliton is soliton along the elliptic rings is induced by increasing g_{trans} until a critical value g_{rot}. In this case, the soliton escapes from the intensity maximum vicinity and undergoes elliptic rotation as shown in Figure 3.10(b), where $g_{trans} = 0.628$. The dynamics of the rotating soliton arise from the delicate interplay between the attracting force of the light ring and the initial transverse momentum imprinted to the solitons. An extensive set of simulations were performed under different initial conditions and perturbations.

In order to quantify whether there was any fraction of power radiated from the soliton or not, the power inside a fixed radius circular region centered at the soliton's intensity centroid was calculated along propagation. The radius of the region was set to initially enclose 99% of the total power. Remarkably for stable solitons, the enclosed power oscillates but remains conserved as show in Figure 3.10(d,e). This oscillations for the quantified enclosed power follows the different potential observed by the soliton at each propagation step due to its transverse motion and the elliptic ring azimuthal modulation. The soliton auto-transforms itself continuously along propagation to fit itself to the surrounding potential, causing it to be change its waist and width. Still this oscillations are rather small and way below 0.05%. If the initial momentum g_{trans} exceeds a critical value, namely g_{out}, the soliton leaves the

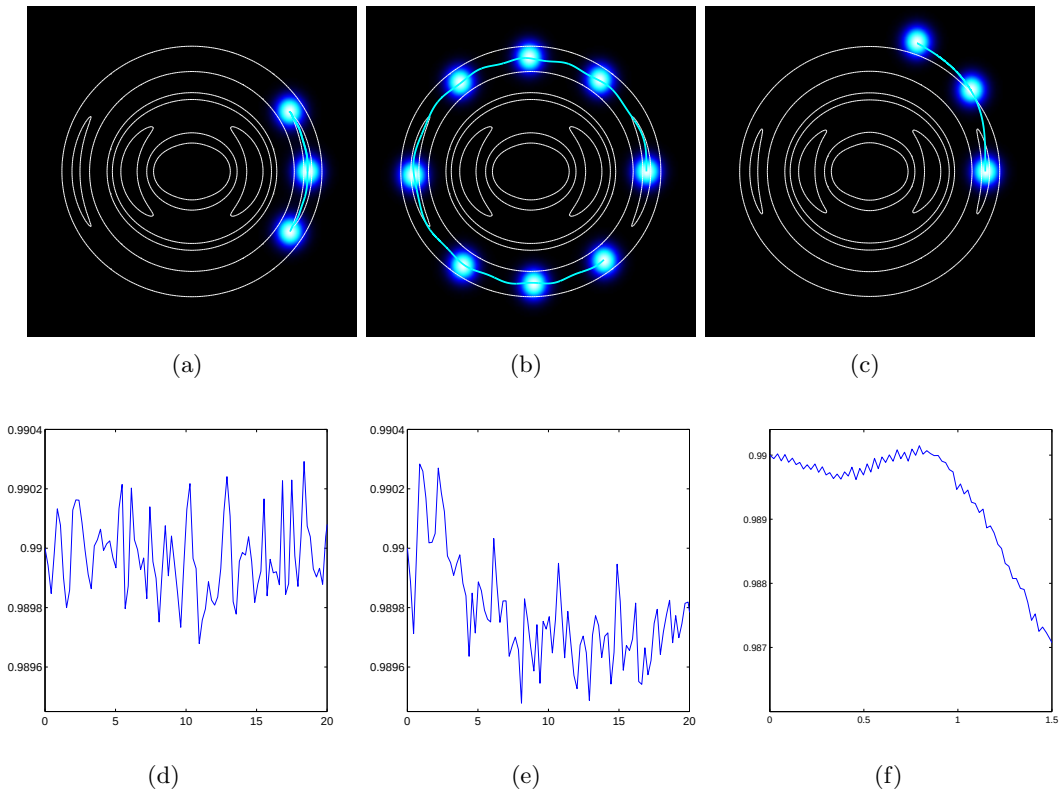

Figure 3.10: Dynamics of motion in the EPL for $m = 3$ and $f = 1$. The propagation parameters are set to $p = 4$, $\beta = 10$ and $q = 0.05$. Three cases were found and are reported: (a) oscillatory motion around and intensity maxima, (b) rotatory stable motion and (c) unbounded-escaping motion. The second row corresponds to a plot of power $\mathscr{P}$ enclosed by the soliton against propagation distance, where values are calculated inside a waist centered at the soliton centroid which initially enclosed 99% of the total power. Power is found to be enclosed by the soliton for the first two cases, while in the last the soliton irradiates power rapidly.

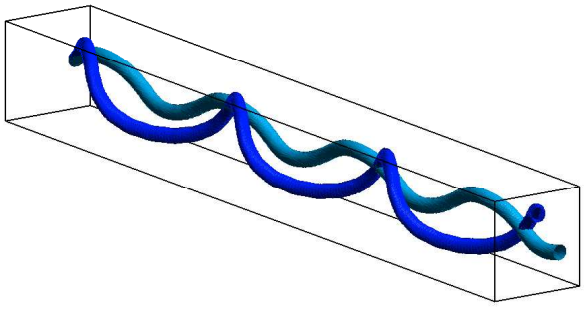

Figure 3.11: Three dimensional display of soliton propagation for both oscillatory (light blue) and rotatory (dark blue) motion.

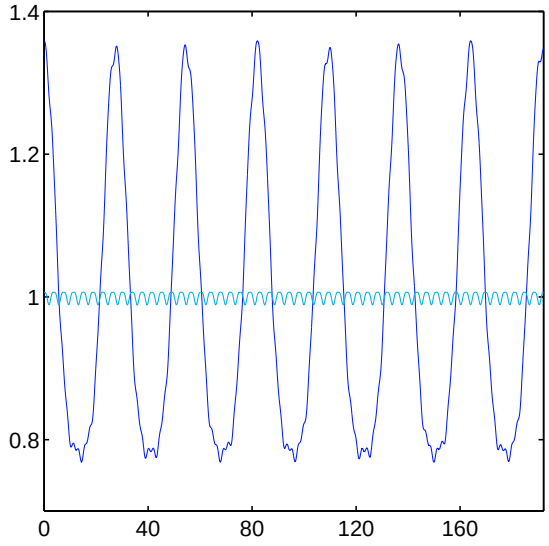

Figure 3.12: Plot of rotation rate γ against propagation distance z for a soliton propagating on an EPL and a Bessel lattice. The former is displayed as a darker line (blue online) and the latter in a brighter color. For comparison purposes, we normalized both rotation rates to its mean value.

ring with where it was initially launched as depicted in figure 3.10(c), and its power decays rapidly as shown in figure 3.10(f).

Since the refraction index along the rings of the EPL is not azimuthally symmetric, solitons trapped within the elliptic rings increase (decrease) their angular speed as they approach intensity maxima (minima). In Fig. 3.12 the varying rotation rate of solitons trapped in the EPL allows a varying rate of the solitons in the Bessel lattice, being the latter result of the particular modulation of the EPL.The appearing constant rotation rate of the Bessel lattice is one of the main themes from the next chapter. For this work purposes, the rotation rate was defined as

$$\gamma = \frac{|\Delta \mathbf{r}_t|}{\Delta z}, \tag{3.23}$$

where $\mathbf{r}_t$ stands for the coordinate vector in the transverse (x, y) plane. Being defined as it is, γ represents the displacement made by the soliton along the transverse plane per unit length traveled in the z axis. It can be thought of as a generalized speed, where instead of taking derivatives with respect to a time coordinate, differentiation is carried with respect to the propagation coordinate z. The later is done since z accounts for the independent variable for

all quantifiers involved with the propagation. In order to appropriately compare both motion properly, both γ quantifiers were normalized to its mean value, and what is important from both quantifiers is their degree of variation and spread, not its actual values.

3.4 Concluding remarks on soliton propagation through the EPL

The main result of this chapter is the existence of stable soliton propagation through the EPL. There was no previous report to this research of such phenomena, since the EPL contains an azimuthal modulation which was thought to impede such stable propagation. Therefore, this part of the thesis demonstrates how it is possible for solitons to propagate through elliptic light rings azimuthally modulated through hundreds of diffraction lengths. Furthermore, two cases of stable propagation were found, and a third one involving unbounded motion. The existence of these three regimes of propagation are lead by this azimuthal modulation, since an oscillatory like motion is created for particular initial conditions. Furthermore, it was appreciated how the soliton changes its rotation rate along the elliptic light ring, heavily influenced by the azimuthal modulation. Thus, this family of lattices offer generous possibilities in nonlinear propagations, and further characterizations of such are yet to be explored more deeply.

Chapter 4

Soliton propagation and the modulated Bessel lattice

This chapter constitutes the core of this work, since more time employed in the research presented here was dedicated to the solitons propagating through Bessel type lattices rather than through the EPL. This obeys to the complexity of the azimuthal modulation imposed naturally in elliptical symmetries, where in circular coordinates a simple sinusoidal pattern arises. The modulated Bessel lattice (MBL) is introduced in this chapter, being it a natural solution to the Helmholtz equation in circular cylindrical coordinates and introducing a control parameter to the angular modulation. Preceding a brief and sufficient description of the MBL comes the characterization of soliton propagation through this lattice. Not only does expected dynamics of propagation appears, such as oscillatory motion around an intensity maxima or escapin/unbounded motion. Interesting phenomena arose in the course of studying solitons propagating through the MBL, such as unstable periodic motion. This dynamic of motion appears when solitons initially engage periodic stable motion and experiment instabilities after several complete cycles. These phenomena does not occur due to numerical errors and is consequently a natural part of this research subject. Proper numerical experiments were carried out in order to establish so. Furthermore, a model for correctly explaining this phenomena is currently being developed, being this model tightly bound to the theory of dynamical billiards.

4.1 The modulated Bessel lattice

The MBL is constructed via Bessel beams, which are by nature nondiffracting optical fields and solutions to the Helmholtz equation

$$\nabla_t^2 \phi + k_t^2 \phi = 0, \tag{4.1}$$

where k_t is the transverse wave number, the nondiffracting beam transverse pattern ϕ is a function of two transverse coordinates and the usual an required harmonic dependence $e^{ik_z z}$ has been inserted. This time the symmetry of the beam indicates that calculations must be carried out in circular cylindrical coordinates, or polar coordinates in short. This coordinate system is well know in the literature, and the corresponding transformations are

$$x = r\cos(\theta), \tag{4.2}$$

$$y = r\sin(\theta), \tag{4.3}$$

where r is the radial coordinate, indicating the distance from a point to the origin, and θ is the usual polar angle, measured counterclockwise in radians starting from the x axis. The transverse laplacian operator transforms in this coordinate system to

$$\nabla_t^2 = \frac{\partial^2}{\partial r^2} + \frac{1}{r}\frac{\partial}{\partial r} + \frac{1}{r^2}\frac{\partial^2}{\partial \theta^2}. \tag{4.4}$$

In order to find such family of beams the last expression must be inserted in the reduced transverse Helmholtz equation, and since this equation is separable in polar coordinates the technique of separation of variables is applied. The trial solution

$$\phi(r,\theta) = R(r)\Theta(\theta), \tag{4.5}$$

must be inserted in the equation, being R a function purely of r and Θ a function only of θ. After carrying out algebraic manipulations two equations coupled by a single constant are reached, where the equation corresponding to the angular coordinate is

$$\frac{1}{\Theta}\frac{d^2\Theta}{d\theta^2} = -\alpha, \tag{4.6}$$

and the equation for the radial coordinate is

$$\frac{r^2}{R}\frac{d^2R}{dr^2} + \frac{r}{R}\frac{dR}{dr} + r^2k_t^2 = \alpha, \tag{4.7}$$

where α is the separation constant introduced in the method. What naturally proceeds is to find families of solutions to this last equations, which can be narrowed by introducing physical considerations into the assumptions made.

4.1.1 General solution to the Helmholtz equation in circular cylindrical coordinates

It is preferable to start with the equation for θ, which can be rewritten as

$$\frac{d^2\Theta}{d\theta^2} + \alpha\Theta = 0. \tag{4.8}$$

Periodic functions are required as solutions since polar transformations are multiple valued for the coordinate θ. That is, $< r_o, \theta_o >$ and $< r_o, \theta_o + 2\pi n >$ make reference to the same point in space for any integer value of n. Thus, functions having a period equal to 2π should be natural solutions of the equation. This restriction is fulfilled since the equation has as general solutions sines and cosines. Furthermore, to fully comply with the periodicity condition, $\sqrt{\alpha}$ should be an integer number. This imposes an important and necessary restriction on the general solution, and without loosing generality α can be defined by

$$\alpha = m^2, \tag{4.9}$$

where m is a positive integer, commonly refereed to as the order of the solution. In the end, the angular solution can be written in its most general form as

$$\Theta(\theta) = A\cos(m\theta) + B\sin(m\theta), \tag{4.10}$$

where A and B are integration constants yet to be defined. The α restriction falls on the equation for R as well, which after making certain arrangements can be written as

$$r^2\frac{d^2R}{dr^2} + r\frac{dR}{dr} + (k_t^2r^2 - m^2)R = 0. \tag{4.11}$$

In order to properly adjust this equation to well mathematical expressions a change of variable

is required, corresponding to a simple scale of the form

$$s = k_t r, \tag{4.12}$$

leaving the radial equation as

$$s^2 \frac{d^2 R}{ds^2} + s\frac{dR}{ds} + (s^2 - m^2)R = 0, \tag{4.13}$$

which perfectly fits the form of the Bessel equation. Since m is restricted to positive integer values,the solutions in turn avoid certain complexities and difficulties that would naturally arise in the case of having m arbitrary values. Carrying on, the Bessel equations has general solutions of the form

$$R(s) = CJ_m(s) + DY_m(s), \tag{4.14}$$

where $J_m(s)$ corresponds to the mth-order Bessel function of the first kind and $Y_m(s)$ represents the mth-order Bessel function of the second kind. As our solution must in the end represent a physical quantity, in this case the field of a nondiffracting beam, it should be rid of singularities and any other badly behaved phenomena. Furthermore, the Bessel functions of the second kind are singular at the origin, regardless of the order of the solution. Thus, our physical solutions should not include this functions, naturally imposing that $D = 0$ narrowing the possibilities but respecting physical principles. After regrouping constants and returning to the original physical variables, the expression for the transverse profile of a Bessel beam in its most general form is solved to

$$\phi(r, \theta) = J_m(k_t r)\Big[A\cos(m\theta) + B\sin(m\theta)\Big], \tag{4.15}$$

where again, A and B are constants yet to be defined.

4.1.2 Construction and description of the MBL

The MBL is a novel topology of optical lattice offering interesting possibilities and options. It posses a well defined circular symmetry and is described by the transverse intensity pattern of a subset of the family of Bessel beams, where a control parameter is introduced in the form of an angle α in generalized space. The constants A and B form a set of parameters

that over determines the shape of the Bessel beam. More precisely, by increasing or decreasing both A and B in a fashion as to fix its ratio the spatial distribution of the beam remains invariant. What actually changes is the total power contained by a single transverse cut and can be simply understood as a uniform scaling of the complete profile. As a consequence and without loss of generality, the power of the beam can be fixed to a certain value introducing a shape-controlling parameter which is labeled as α; letting $A = \cos(\alpha)$ and $B = i\sin(\alpha)$. This way the intensity integral is independent of the parameter α. This leads to the expression

$$\phi(r,\theta) = J_m(k_t r)\Big[\cos(\alpha)\cos(m\theta) + i\sin(\alpha)\sin(m\theta)\Big], \tag{4.16}$$

where the constant i in the second term can be understood as a dephasing between optical fields. The intensity pattern $|\phi(r,\theta)|^2$ describes the profile of the MBL $\Gamma(r,\theta)$, which after algebraic manipulations is reduced to

$$\Gamma(r,\theta) = J_m^2(k_t r)\Big[\frac{1}{2} + \frac{\cos(2\alpha)\cos(2m\theta)}{2}\Big]. \tag{4.17}$$

The term $\cos(2\alpha)$ has a period over the parameter α of π. Furthermore, the function $\cos(x)$ replicates all values twice while covering a complete period. Thus, in principle it suffices to consider α values in the interval $[0, \frac{\pi}{2})$. Moreover, this interval can be reduced since both $\frac{\pi}{4} - \alpha_o$ and $\frac{\pi}{4} + \alpha_o$ account for a rotation of $\frac{\pi}{2}$ radians around the origin for the same profile whenever both values are in the reduced interval. So, without loss of generality, the value of α is restricted o the interval $[0, \frac{\pi}{4}]$, which will be enough to cover all the possible profiles of the MBL.

Since the MBL was constructed via separation of variables, its profile can be analyzed separately for each coordinate. As in the case of the radial coordinate r, the profile varies as

$$\rho(r)_{m,k_t} = J_m^2(k_t r). \tag{4.18}$$

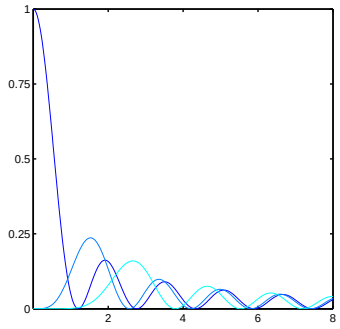

Figure 4.1: Radial modulation of the modulated Bessel lattice plotted against the radial coordinate r. The profile corresponds to the function $J_m^2(k_t r)$, where k_t accounts for an expansion or shrinking of the modulation as has been set equal to 2 for this figure. The order m is varied, and it can be appreciated how it changes dramatically the profile. Still, a damped oscillatory behavior is depicted as r increases.

This radial modulation changes dramatically near the origin depending on the value of m, where it changes dramatically near the origin depending on the value of m. For positive integer values, $\rho(0) =$, and since the profile slope increases till reaching the global maximum of the function, the origin accounts for a depression in the MBL. Now, for $m = 0$, the global and first maximum is actually localized at the origin, thus creating a single centered lump for the profile. Therefore, the origin can either project an intensity lump on the lattice or a depression on the pattern depending on the order m employed.

In both cases, as r continues increasing more maxima appears, corresponding to lumps in the radial pattern that flatten and decrease in its peak value. This can be understood as an oscillatory behavior, periodically reaching a depression in the pattern followed by a peak. This peaks form the so called light rings when the angular and radial variations are inserted in the plane. It is worth mentioning that for $m = 0$ the first centered maxima is far superior from its subsequent maxima by a factor of approximately 3; where in all other cases consecutive maxima differ by a more moderate factor. This behavior is depicted in fig. 4.1.

The angular variation of the MBL is what introduces the richness to the investigation of this family of optical lattices, this since the research is devoted mainly to studying solitons around closed trajectories, which in this case suffer from the azimuthal modulation intrinsic

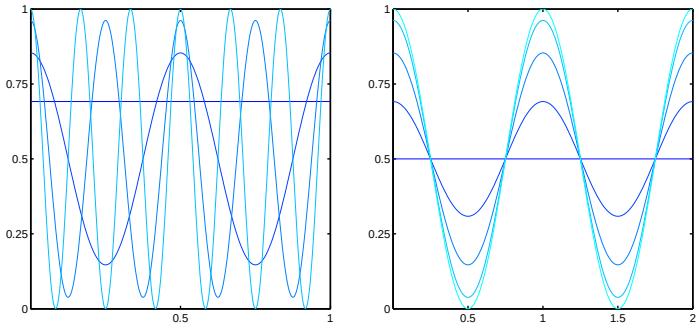

Figure 4.2: Profiles for the angular modulation ω for the modulated Bessel lattice. Figure (a) contains profiles for different various of the order m while fixing the modulation parameter α, while in figure b α varies for each curve and the order m is fixed.

to the MBL represented as

$$\omega(\theta)_{\alpha,m} = \frac{1}{2}\Big[1 + \cos(2\alpha)\cos(2m\theta)\Big], \tag{4.19}$$

and as mentioned before, α is the lattice shape parameter and m the order of the MBL. This angular modulation varies as a cosine with tunable period and an amplitude depending on α, Furthermore, this sinusoidal variation is mounted over a constant value, admitting only positive values as an outcome. The $\frac{1}{2}$ factor can be understood as a normalization constant ensuring ω peak value to 1.

The parameter for tuning the periodicity of the modulation is m. For the case of $m = 0$ there is no variation in the lattice introduced by the polar angle, and ω is simply a constant equal to $\frac{1+\cos(2\alpha)}{2}$. For m a positive integer, the period of ω is defined as $\frac{\pi}{m}$. Incrementing m makes the period shorter and introduces a steeper variation in the azimuthal modulation. The number of maxima across the range of ω equals the number of minima, in this case being equal to $2m$. The variation of ω according to m is graphically displayed in fig 4.2a.

The shape parameter α defines the amplitude of the sinusoidal variation for ω. For the case of $\alpha = \frac{\pi}{4}$, the amplitude $\cos(2\alpha)$ is equal to 0 and the azimuthal modulation is null, thus recovering a perfectly balanced Bessel lattice with no deformation along the angle coordinate. As α decreases away from $\frac{\pi}{4}$ towards 0, the amplitude of the cosine modulation is incremented,

thus introducing a wider variation in the azimuthal modulation ω. This makes the difference between maxima and minima bigger, creating a steeper gradient in intensity along a circular light ring path. Finally when $\alpha = 0$ the amplitude $\cos(2\alpha)$ reaches its maximum value and the function $\omega(\theta)$ reaches its extreme values of 0 and 1. This case accounts for the biggest variation possible around a circular light ring path, having null intensity points in the MBL profile. Thus, $\alpha = \frac{\pi}{4}$ represents the null azimuthal modulation case and $\alpha = 0$ introduces the strongest modulation possible, while intermediate values account for a transition in a cosine like fashion. Examples of ω for different α values are shown in fig 4.2b.

Combining both modulation the MBL pattern is recovered. The simplest patter available corresponds to either $m = 0$ or $\alpha = \frac{\pi}{4}$. The resulting pattern results in a set of concentric light rings, which have a radial distribution according to the order m of the lattice. Many combinations are available by adjusting m and α to distinct values. Plenty of work has bee done on the general family of modulated Bessel lattices, and there is still more work programmed. Still, due to time issues and consistency of presented results, the rest of the work is devoted to balanced Bessel lattices, that is, fixing α to $\frac{\pi}{4}$.

An extensive research has been undertaken for propagations in the general modulated Bessel lattice. Interesting results have been produced, as the existence of periodically unstable regimes of transverse motion. That is, solitons engage transverse periodic rotatory motion for a number of cycles and end up escaping after so. This is due to the modulation of the lattice and the non-periodic transverse motion of the lattice. Still, time is limited and those studies are still under preliminary stages of research. This work presents results limiting ourselves to the simples case, the non modulated Bessel latice. This since this results are simpler and will represent the basis for constructing the general theory of transverse motion. Thus, the general case for modulated Bessel lattices is a next step to take.

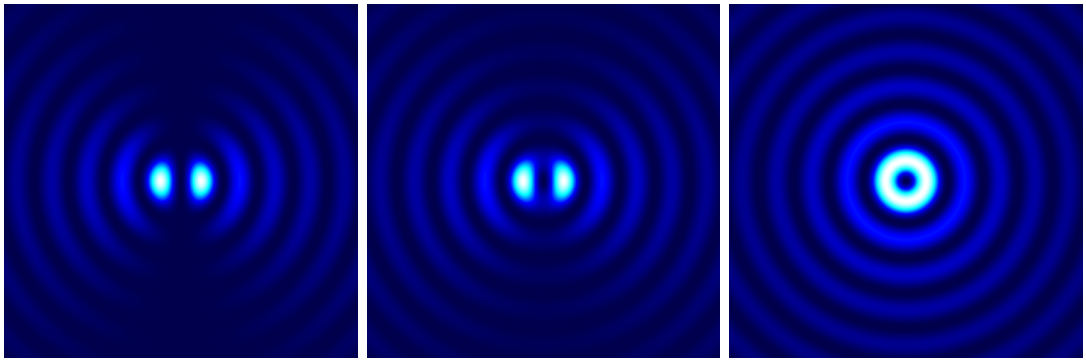

(a) $m = 1, \alpha = 0$ (b) $m = 1, \alpha = \frac{\pi}{8}$ (c) $m = 1, \alpha = \frac{\pi}{4}$

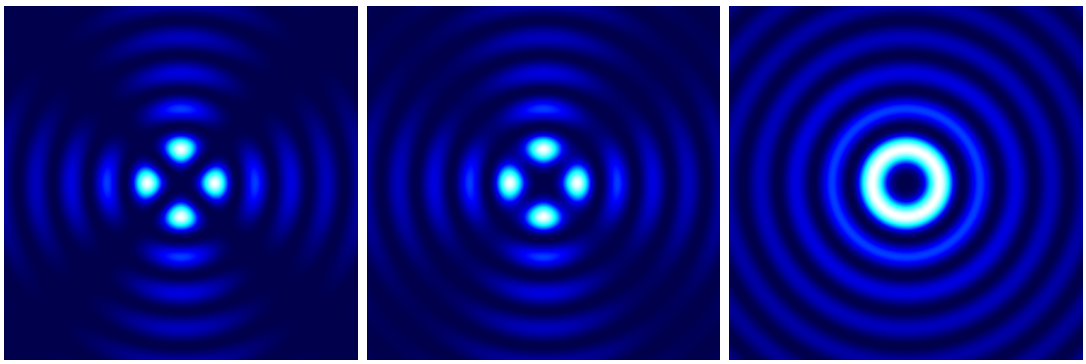

(d) $m = 2, \alpha = 0$ (e) $m = 2, \alpha = \frac{\pi}{8}$ (f) $m = 2, \alpha = \frac{\pi}{4}$

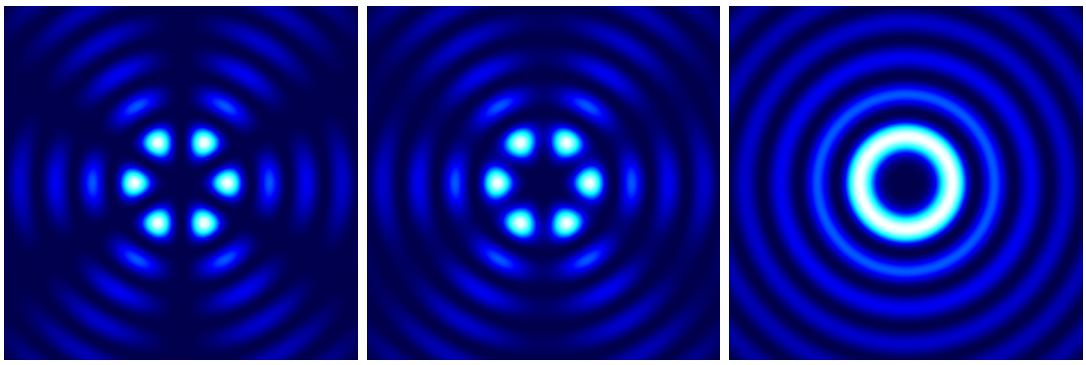

(g) $m = 3, \alpha = 0$ (h) $m = 3, \alpha = \frac{\pi}{8}$ (i) $m = 3, \alpha = \frac{\pi}{4}$

Figure 4.3: Representative profiles of the modulated Bessel lattice family for various values of m and α. It can be seen how m controls the number of maxima and minima distributed along a circular light ring, while $x\alpha$ controls how close these values for maxima and minima are, modulating the intensity of the lattice.

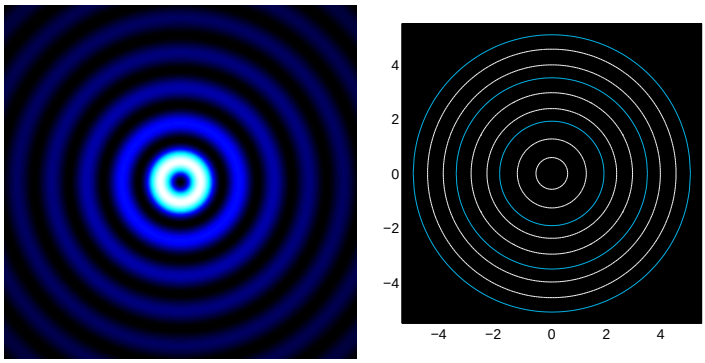

Figure 4.4: Balanced Bessel lattice used for the research in this section. lattice parameters are set to $\alpha = \frac{\pi}{4}$,$m = 1$ and $k_t = 2$. Figure 1.a is an image-colored plot of the lattice, while 1.b is a contour plot of the lattice's central region of interest. Bright blue lines mark the division between adjacent light rings, and white lines represent constant intensity curves for a value of 0.5.

4.2 The balanced Bessel lattice and induced dynamics of motion

Soliton propagation in optical lattices is a multiple variable problem, and dealing with the general problem can become an overwhelming task. Specific cases must be solved separately to reach knowledge in the area, thus solving a jigsaw piece by piece as an analogy. The rest of this document deals with the simplest case in order to study soliton propagation on the MBL: the balanced Bessel lattice. This fixes α to $\frac{\pi}{4}$, directly balancing the power to both even-cosine and odd-sine parts of the lattice, giving each one 50% of the total power. This produces a lattice with null azimuthal modulation and constant intensity light rings regardless of the lattice order m. Thus, the only variation in the intensity profile is radial dependent via Bessel functions. If an analogy between soliton propagation on this lattice and classical mechanics where to be made, it can be thought of as a central force problem of a semi-rigid body. Now, even though m and k_t do not change the azimuthal modulation, it does affect the radial intensity profile. So, for this case m was fix to 1 and k_t to 2, thus producing a first order balanced Bessel lattice, shown in fig. 4.4.

In the beginning, certain parameters where fixed at a certain value, since α is one of many variables in this problem. The lattice depth and the saturation parameter were fixed respectively to $p = 4$ and $q = 0.05$. Furthermore, the initial launch angle of the soliton was $\phi = \frac{pi}{2}$

for all simulations involved in the study of solitons in MBL lattices. This means that initially solitons had a transverse rotation rate in an azimuthal direction with respect to the symmetry of the lattice. By doing so, two variables are left for experimenting: the longitudinal wavelength p_θ and the magnitude of the tilt initially imposed p_θ. This will be the control variables used for this whole section, and all results concern the variations of this parameters. Having said so, the propagation parameters are left as follows

-lattice depth $p = 4$
-saturation parameter $q = 0.05$
-launch angle $\phi = \frac{\pi}{2}$
-modulation parameter $\alpha = \frac{\pi}{4}$
-lattice order $m = 1$
lattice transverse wavenumber $k_t = 2$
-longitudinal wavenumber -β subject to change, control variable
-initial tilt imposed magnitude p_θ subject to change, control variable

Furthermore, another issue to deal with is the initial position of the ansatz, where the solution will converge to a soliton profile ready to be propagated. A rotatory motion around a light ring was desired for studying soliton propagations, thus the second light ring was chosen for propagation. This choice was made since the first ring is really close to the central maxima peaks, which tend to focus the soliton around it, draining power attached original to the soliton profile. Furthermore, outer rings posses relatively low intensity values, which can cause the soliton to escape in most cases.

To start the research a sample set of propagations was carried out in order to identify parameters for stable propagations and limit this study to a certain subset of the control variables. It can be understood as both control variables, β and p_θ, group and classify the outcome of all propagations done in what is called a parametric space, which is nothing but a coordinate system whose axis correspond to this control variables. This allows another way of visualizing results and observing how increments or decrements in β, p_θ or both affect directly the quantifiers involved with the propagation. In this case, the x axis corresponds to p_θ, and goes

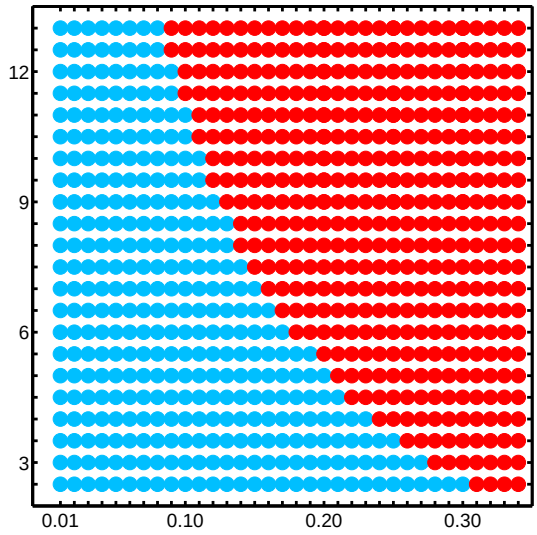

Figure 4.5: Parametric diagram for the propagation regimes in this research, where the parametric variables are β for the y axis and p_θ for the x axis. Blue brighter dots represent periodic rotatory motion, while red darker dots resemble escape-unbounded motion.

from $p_\theta = 0.010$ to $p_\theta = 0.300$, with increments between successive points of $\Delta p_\theta = 0.01$. The y axis corresponds to the longitudinal wave number, where it goes from $\beta = 2.5$ to $p_\theta = 13$, with increments between successive points of $\Delta p_\theta = 0.5$. This gives a total of $22 \times 30 = 660$ points in the parametric βp_θ space.

Initially, all points inside the parametric space compose the sample set of propagations to work with. Still, all points can be divided in to one of two general categories, which are defined by the outcome of the propagation dynamics of the soliton. First, they are those which produce solitons that indefinitely propagate contained by the second light ring, which are labeled as periodic rotational dynamics, or just rotational motion. There are other in which the soliton escapes initially from the lattice by fleing away. This are labeled as unbounded-escape dynamics of motion, or simple escape motion. Such results are grouped and presented in fig. 4.5.

Representative examples of soliton propagation around the lattice are shown in figure 4.6. where it can be noticed how the soliton motion tends to deviate from a perfect circular ring. This can be pictured as the soliton bouncing inside the boundaries of the second light ring.

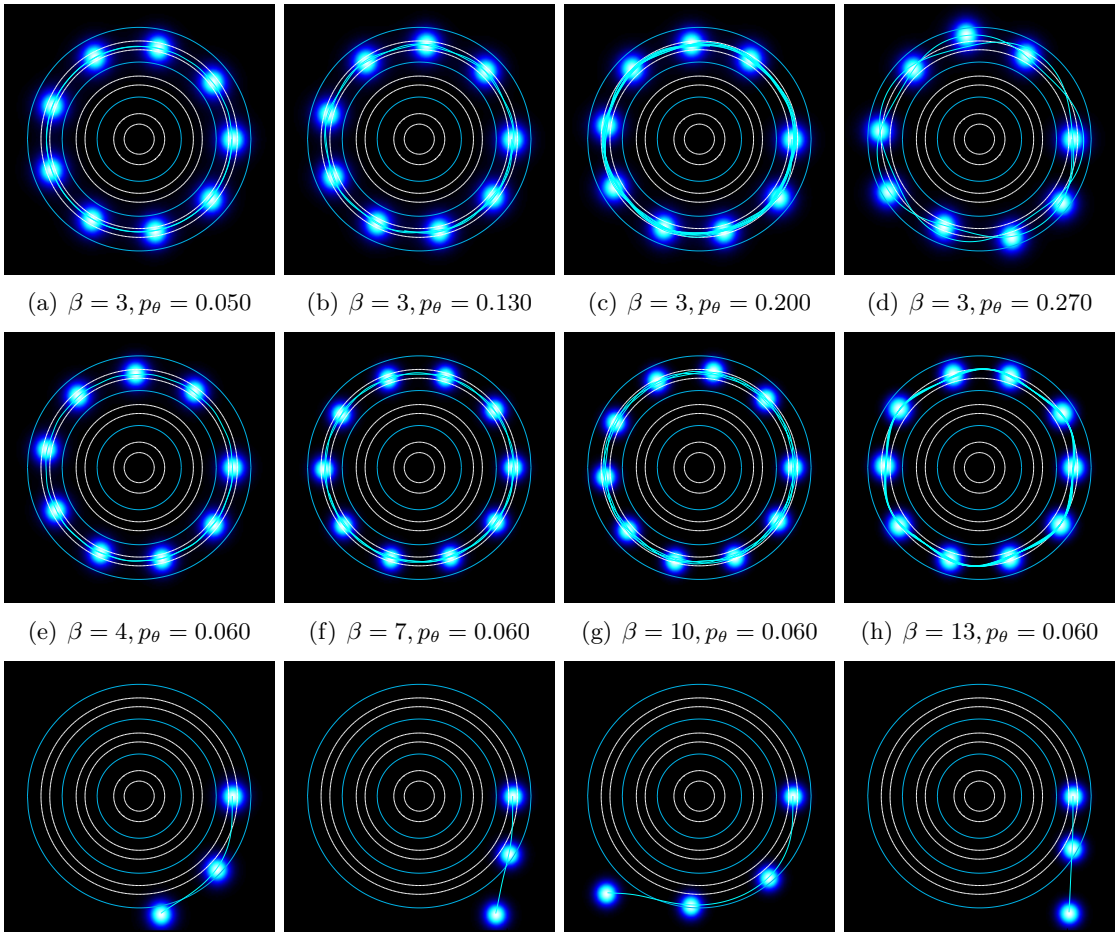

(a) $\beta = 3, p_\theta = 0.050$ (b) $\beta = 3, p_\theta = 0.130$ (c) $\beta = 3, p_\theta = 0.200$ (d) $\beta = 3, p_\theta = 0.270$

(e) $\beta = 4, p_\theta = 0.060$ (f) $\beta = 7, p_\theta = 0.060$ (g) $\beta = 10, p_\theta = 0.060$ (h) $\beta = 13, p_\theta = 0.060$

(i) $\beta = 4, p_\theta = 0.240$ (j) $\beta = 6, p_\theta = 0.250$ (k) $\beta = 8, p_\theta = 0.140$ (l) $\beta = 10, p_\theta = 0.300$

Figure 4.6: Transverse motion dynamics for solitons propagating through a balanced Bessel lattice. The first row fixes the value of β and varies p_θ, and the second row fixes p_θ to a constant while varying β. Dynamics from (a) to (h) depict rotatory motion, while the rest present escape-unbounded motion.

And as in the case of escape-unbounded motion, this can be produced in several ways. But still, what is constant to all this unbounded motion is the fact that soliton do not recoil from the inner light ring walls.

4.3 Stability and enclosed power

Stability is a major issue in this work since in principle a soliton should propagate indefinitely when no initial tilt is imposed. Thus, wether a transverse moving soliton will propagate in a stable manner is an open question, subject to physical mechanisms and the finite preci-

sion managed by computers.

The power $\mathscr{P}$ carried by the soliton is the feature considered to evaluate stability. Power is itself a conserved quantity and it must be quantified inside the vicinity of the soliton, since the soliton may engage unstable propagation, lose its original shape and decay into a diffuse pattern; but still the power will be conserved along propagation planes. Thus, power should be monitored inside an effective area representing the region of space occupied by the soliton. The strategy for doing so is as follows: first, a coordinate system centered at the soliton's centroid at $z = 0$ is created, where its radial coordinate is labeled as r_c. Afterwards, through bisections a numerical value r_o is calculated that encloses a certain fraction of the total power in the region $r_c \leq r_o$. That is, on the plane $z = 0$ a circle centered on the soliton's centroid with radius r_o should enclose a fixed amount of fractional power of the complete soliton profile. High values of fractional power should be used in order to account for a region covering the soliton almost completely. For this research, a fraction of 0.99 was used.

In order to continue, propagation must be carried out. At each desired step of monitoring, the coordinates of the soliton centroid must be calculated, in order to locate its center. Afterwards, the power contained in a circle with origin on the soliton centroid and radius r_o is quantified as a measure of the stability of the soliton. This enclosed fractional power is labeled as $\mathscr{P}_w$, and it can be thought as the power inside the region which initially comprehended the soliton. Nevertheless, numerical errors may introduce slight variations to this quantifiers, and so will the discreteness of the lattice.

This numerical issue introduces errors to all quantifiers extracted from a propagation. Still, the split step Fourier method has proven to give good results, as solitons would not propagate for thousands of propagation steps if accuracy in computation was poor or round off errors were to change dramatically the propagation. And furthermore, the potential involved with the nonlinear Schrödinger equation tends to self correct the wave function ψ associated to the soliton. So, the method uses is self-correctable, even though it naturally introduces numerical errors. Since $\mathscr{P}_w$, the power enclosed inside the solitons waist, ought to remain constant as the propagation takes place, the variation introduced by numerical computations ought to

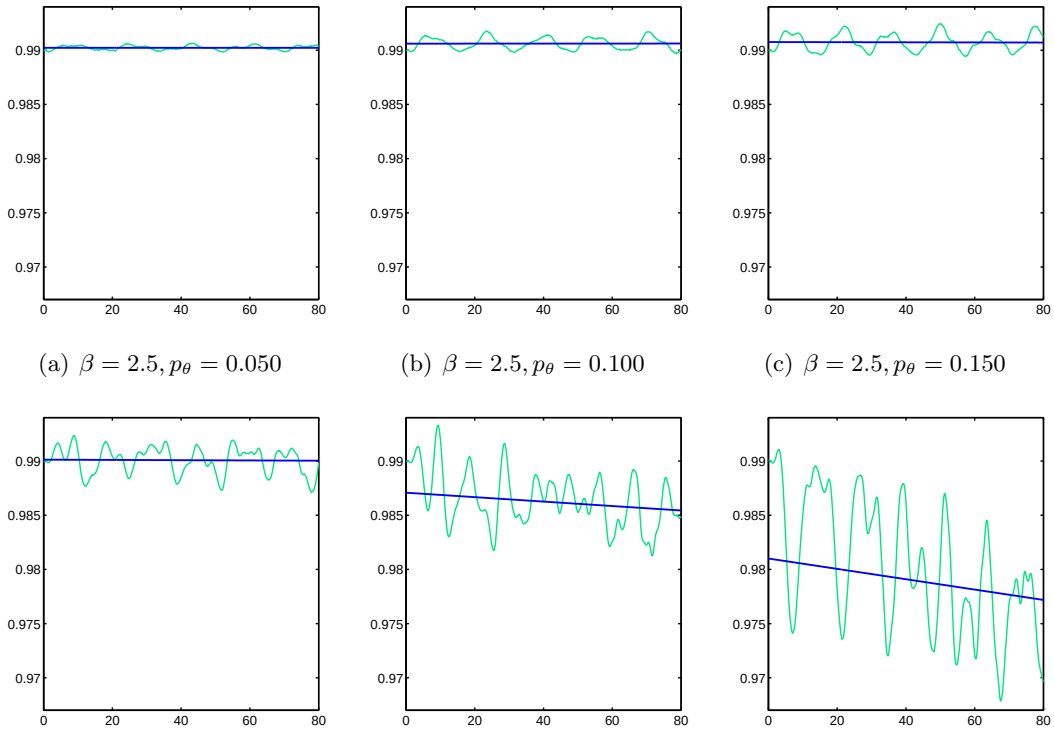

(a) $\beta = 2.5, p_\theta = 0.050$ (b) $\beta = 2.5, p_\theta = 0.100$ (c) $\beta = 2.5, p_\theta = 0.150$

(d) $\beta = 2.5, p_\theta = 0.200$ (e) $\beta = 2.5, p_\theta = 0.250$ (f) $\beta = 2.5, p_\theta = 0.300$

Figure 4.7: Plots of soliton's enclosed fractional power $\mathscr{P}_w$ against propagation distance z for a fixed value of β and a varying initial tilt p_θ. For tilts higher than $p_\theta = 0.200$ the soliton irradiates a small yet finite amount of radiation as shown in the plots. Still, for the maximum propagation distance used, the radiation diminishes as less than 2%.

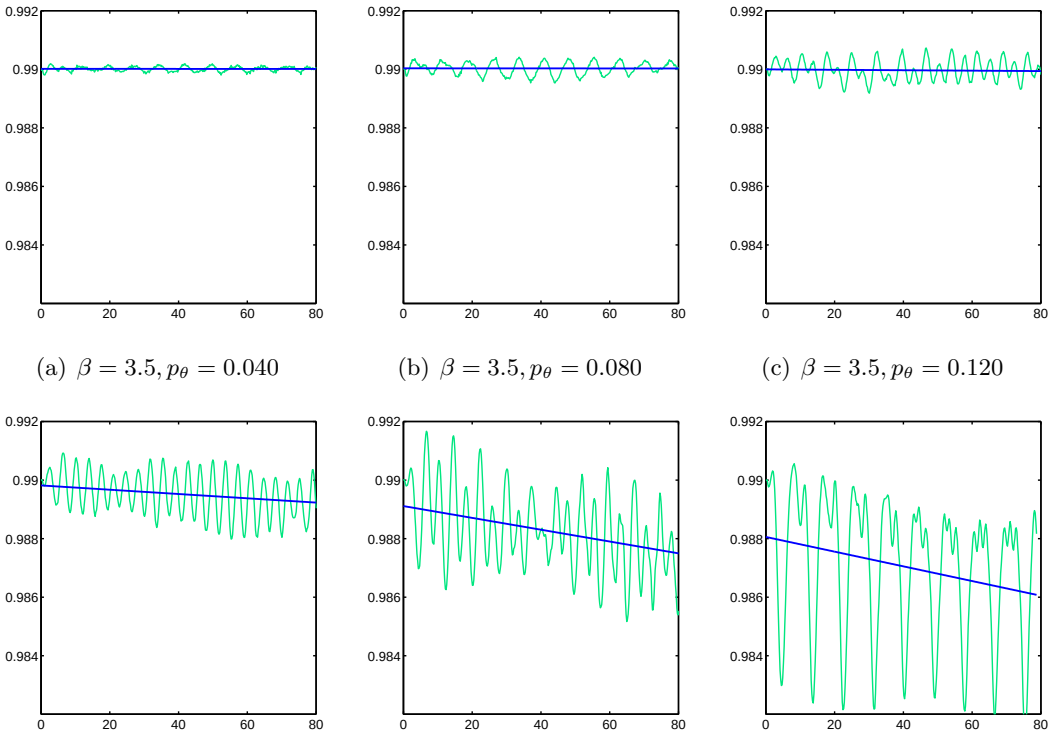

(a) $\beta = 3.5, p_\theta = 0.040$ (b) $\beta = 3.5, p_\theta = 0.080$ (c) $\beta = 3.5, p_\theta = 0.120$

(d) $\beta = 3.5, p_\theta = 0.160$ (e) $\beta = 3.5, p_\theta = 0.200$ (f) $\beta = 3.5, p_\theta = 0.240$

Figure 4.8: Plots of soliton's enclosed fractional power $\mathscr{P}_w$ against propagation distance z for a fixed value of β and a varying initial tilt p_θ. For tilts higher than $p_\theta = 0.200$ the soliton irradiates a small yet finite amount of radiation as shown in the plots. Furthermore, there is a small yet nonzero power irradiation at $p_\theta = 0.160$. The soliton radiates less power in nearby values of the escaping tilt at $\beta = 3.5$ when compared to $\beta = 2.5$, as can be appreciated in the plots.

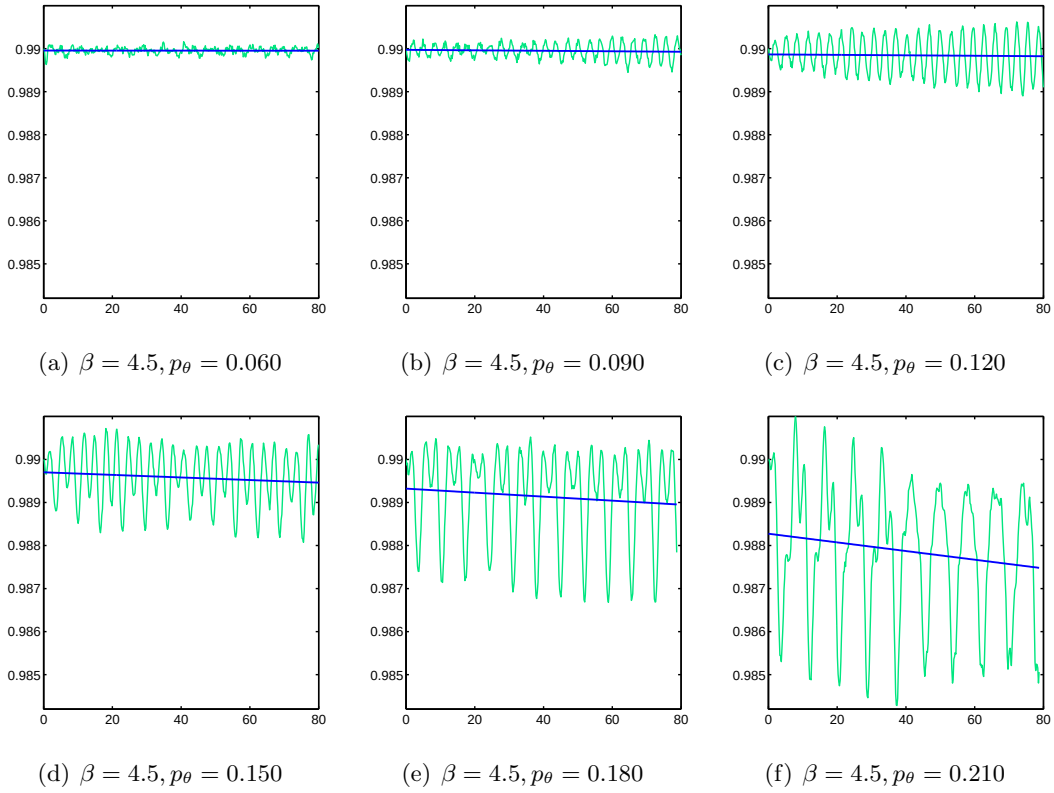

(a) $\beta = 4.5, p_\theta = 0.060$ (b) $\beta = 4.5, p_\theta = 0.090$ (c) $\beta = 4.5, p_\theta = 0.120$

(d) $\beta = 4.5, p_\theta = 0.150$ (e) $\beta = 4.5, p_\theta = 0.180$ (f) $\beta = 4.5, p_\theta = 0.210$

Figure 4.9: Plots of soliton's enclosed fractional power $\mathscr{P}_w$ against propagation distance z for a fixed value of β and a varying initial tilt p_θ. The total percent of power radiated by the soliton diminishes as β grows to 4.5 when compared to smaller values. Furthermore, a certain periodic behavior starts to appear as the tilt takes high values.

strike harder than on any other quantifier that may vary along the propagation.

An important feature to consider is the soliton position in the light ring. While traveling through the same potential the soliton suffers in theory from no diffraction whatsoever. But as the refraction index in its vicinity changes, so does the soliton profile. It must reconfigure itself and auto-transform in the corresponding eigenmode of the new potential. This alters the width of the soliton mostly, since fundamental type solitons tend to retain their bell-shaped configuration. So, as seen in the last section propagations, solitons can't be restrained to a particular value of the radius. Moreover, they tend to bounce inside the light ring, and since the photonic lattice has a radial dependence, this bounces traduce in a variation of the enclosed power P_w. As bounces are periodic phenomena in these soliton propagation, so does $\mathscr{P}_w$ inherits this periodic behavior, which is better exhibited for values of $\beta \geq 6.00$. Plots of

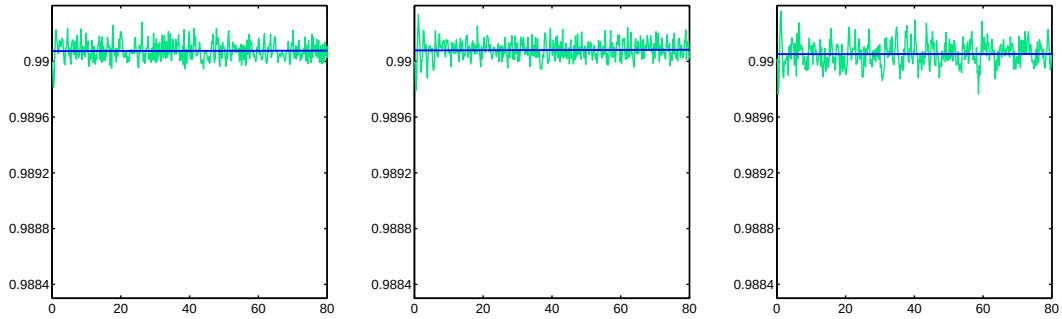

(a) $\beta = 7.5, p_\theta = 0.040$ (b) $\beta = 7.5, p_\theta = 0.060$ (c) $\beta = 7.5, p_\theta = 0.080$

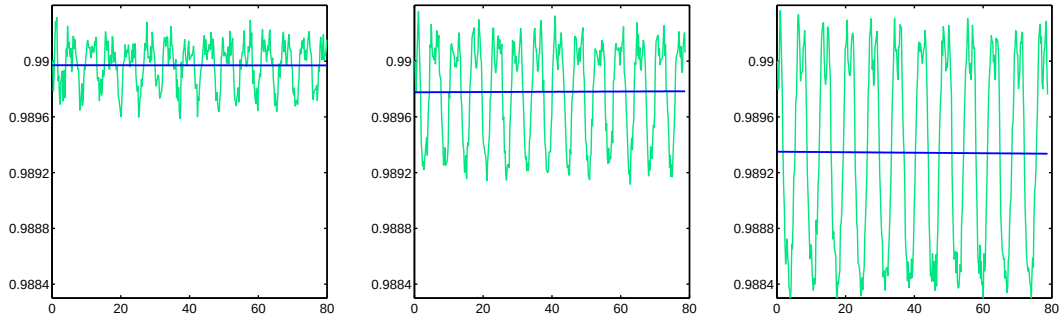

(d) $\beta = 7.5, p_\theta = 0.100$ (e) $\beta = 7.5, p_\theta = 0.120$ (f) $\beta = 7.5, p_\theta = 0.140$

Figure 4.10: Plots of soliton's enclosed fractional power $\mathscr{P}_w$ against propagation distance z for a fixed value of β and a varying initial tilt p_θ. Finally the soliton's radiated power becomes null or undetectable to the statistical methods used. Furthermore, the periodic behavior of the soliton power is fully displayed for tilts higher than $p_\theta = 0.100$. This behavior consists of reaching maximums and minimums systematically with a sharp transition between. Where again, this consist the power enclosed by a fixed size window over the soliton, not the complete power of the soliton. This result can be interpreted as the soliton contracting and expanding periodically over propagation.

$\mathscr{P}_w$ against z are exhibited for various combinations of β and θ are shown in figures 4.7-4.12. In order to quantify true physical power radiation and filter out numerical error noise a hypothesis test was applied in the following way. First, a linear regression was calculated for $\mathscr{P}_w$ in function of z. AS it is, it gives a linear model in the form

$$\mathscr{P}_w = \tilde{\beta}_0 + \tilde{\beta}_1 z. \tag{4.20}$$

Now, the round off errors inherent to numerical calculations do introduce a nonzero random variation in quantifiers related to soliton propagation, so even though in a small degree, $\mathscr{P}_w$ and other quantifiers can be though of having a random variable like variation. Thus, $\tilde{\beta}_1$ can

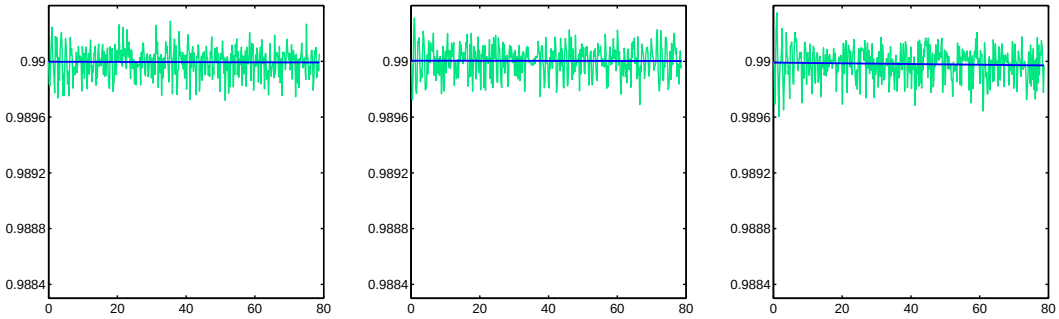

(a) $\beta = 9.5, p_\theta = 0.020$ (b) $\beta = 9.5, p_\theta = 0.040$ (c) $\beta = 9.5, p_\theta = 0.060$

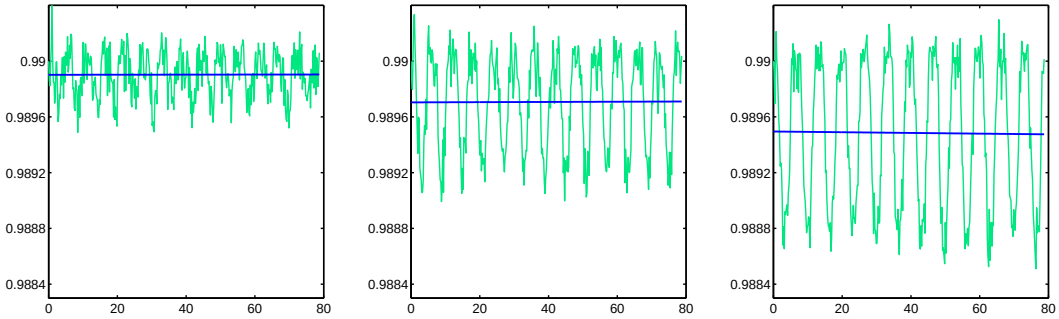

(d) $\beta = 9.5, p_\theta = 0.080$ (e) $\beta = 9.5, p_\theta = 0.100$ (f) $\beta = 9.5, p_\theta = 0.110$

Figure 4.11: Plots of soliton's enclosed fractional power $\mathscr{P}_w$ against propagation distance z for a fixed value of β and a varying initial tilt p_θ. Finally the soliton's radiated power becomes null or undetectable to the statistical methods used. Furthermore, the periodic behavior of the soliton power is fully displayed for tilts higher than $p_\theta = 0.080$. This behavior consists of reaching maximums and minimums systematically with a sharp transition between. Where again, this consist the power enclosed by a fixed size window over the soliton, not the complete power of the soliton. This result can be interpreted as the soliton contracting and expanding periodically over propagation.

be in a way be analyzed as a random variable, letting statistical analysis and tools be valid when applied to it. The linear regression model itself gives a small yet nonzero value for $\tilde{\beta}_1$, and a question that naturally arises is whether this variation is due to numerical errors, that is, can be ignored and will sum up to 0 as the propagation tends to an infinite distance, or whether this is actually a considerable value in the scale used for $\mathscr{P}_w$, having an abstract mathematical consideration which traduces in a physical variation of the enclosed power. That is, if $\mathscr{P}_w$ remains constant or if there is any power radiated.

To quantify this, a hypothesis test is applied to the statistic β_1, in order to find out if $\beta_1 = 0$

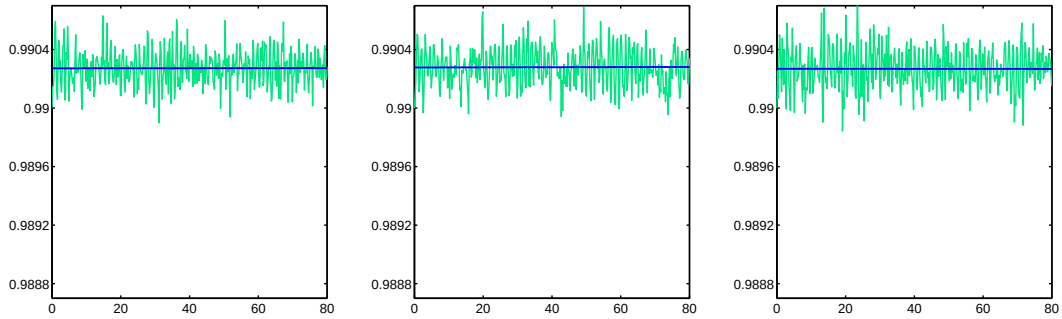

(a) $\beta = 11.5, p_\theta = 0.010$ (b) $\beta = 11.5, p_\theta = 0.030$ (c) $\beta = 11.5, p_\theta = 0.050$

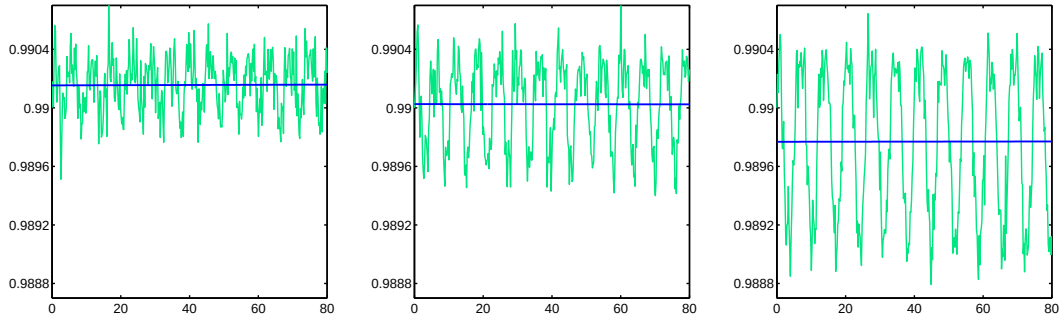

(d) $\beta = 11.5, p_\theta = 0.070$ (e) $\beta = 11.5, p_\theta = 0.080$ (f) $\beta = 11.5, p_\theta = 0.090$

Figure 4.12: Plots of soliton power $\mathscr{P}_w$ against propagation distance z for a fixed value of β and a varying initial tilt p_θ. Finally the soliton's radiated power becomes null or undetectable to the statistical methods used. Furthermore, the periodic behavior of the soliton power is fully displayed for tilts higher than $p_\theta = 0.080$. This behavior consists of reaching maximums and minimums systematically with a sharp transition between. Where again, this consist the power enclosed by a fixed size window over the soliton, not the complete power of the soliton. This result can be interpreted as the soliton contracting and expanding periodically over propagation.

or $\beta_1 \neq 0$. Results are shown in figure 4.13 for a wide variety of points in the parametric $\beta - p_\theta$ diagram.

As a conclusion, it was found that solitons engage unstable propagation at low values of β for high values of p_θ, loosing a small yet considerable proportion of their enclosed power as shown in fig 5. This behavior disappears for high values of β inside the parametric (β, p_θ) space. As an hypothesis yet to be proven, it is proposed that this obeys the soliton's width dependence on β. That is, as β increases the pattern focuses and its width becomes smaller, this for fundamental type solitons. Still, there is a wide region in the parametric space for

which soliton do not radiate power.

4.4 Angular coordinate dynamics

Exploiting symmetries and invariance is the key to constructing models and obtaining answers for any physical system. As in this case, the Bessel lattice presents null modulation at $\alpha = \frac{\pi}{4}$, the problem presented in this section. Thus, the mathematical model, the nonlinear Schrödinger equation, lacks any dependence to the angular coordinate θ, making it a cyclic coordinate and suggesting it might be a good point to deal with.

To start with, it should be stressed that the soliton is itself a spatial distribution, a extended profile in space. It is not a point particle, and thus its analytical and mathematical modeling requires the full scope of the original model. Furthermore, it is a nonlinear entity, meaning that linear principles and laws need not hold with it. Nevertheless, it was found that the θ polar coordinate of the soliton's intensity centroid acts in quite a simple way. From now on, when talking about to the θ coordinate, it will be refereed to as the coordinate of the soliton's intensity centroid. And since z is the propagation coordinate, the independent coordinate, all quantifiers can be thought in a first instance as functions of z, such that θ is itself a function of z. Plots spanning the region occupied by our parametric β, p_θ of $\theta(z)$ versus z are shown in figures 4.14-4.17.

At a first glance θ appears to be a linear function of z. Still, this suspicion needs to be confirmed by mathematical analytical methods. The natural step is to evaluate the derivative of $\theta(z)$. Being it a constant function would be a clear and sufficient condition for $\theta(z)$ to be a linear function. Nevertheless, this does not hold, as can be appreciated in the figures. There are nonlinear variations in $\theta(z)$ reflecting as a nonconstant derivative. This variations are introduced since the propagation is evaluated on a discrete, finite grid and the numerical system involves a finite accuracy in calculations. Naturally, this numerical errors can't be eliminated.

Furthermore, as the soliton bounces back and forth radially inside the light ring the variation of the refraction index a variation is is naturally introduced in all quantifiers involving

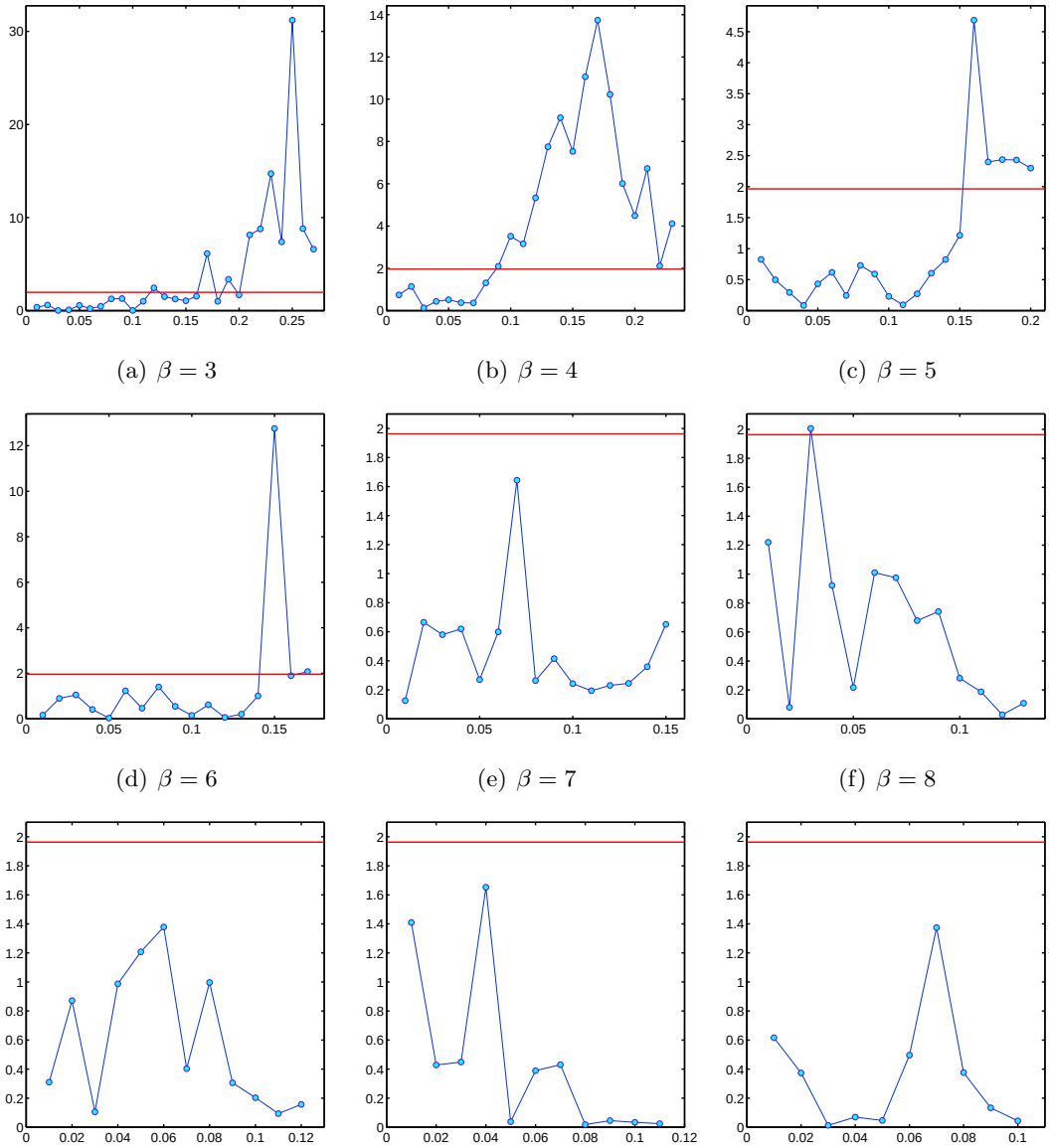

(a) $\beta = 3$ (b) $\beta = 4$ (c) $\beta = 5$

(d) $\beta = 6$ (e) $\beta = 7$ (f) $\beta = 8$

(g) $\beta = 9$ (h) $\beta = 10$ (i) $\beta = 11$

Figure 4.13: Hypothesis testing for evaluating the variation of the enclosed power $\mathscr{P}_w$. Results can be interpreted as followed: if a point of the parametric space (circular markers) falls below the critical value (straight null slope line) the variation in $\mathscr{P}_w$ can be interpreted as null, leaving a non-radiating power soliton. If the blue dot overcomes the critical value, a closer look at the respective plot must be taken. Generally, it can be said that solitons with high values of β do not radiate power for any value of the initial tilt, while as for solitons with β values lower than 6, power is radiated at high values of p_θ.

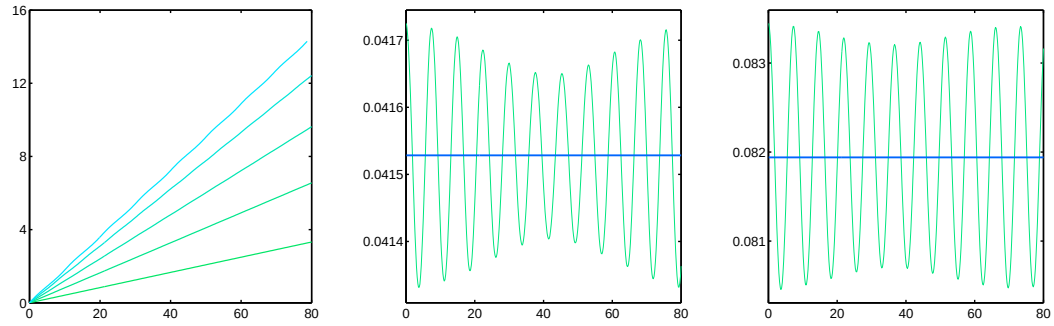

(a) $\beta = 3.5, p_\theta = \{0.050 \ldots 0.250\}$ (b) $\beta = 3.5, p_\theta = 0.050$ (c) $\beta = 3.5, p_\theta = 0.100$

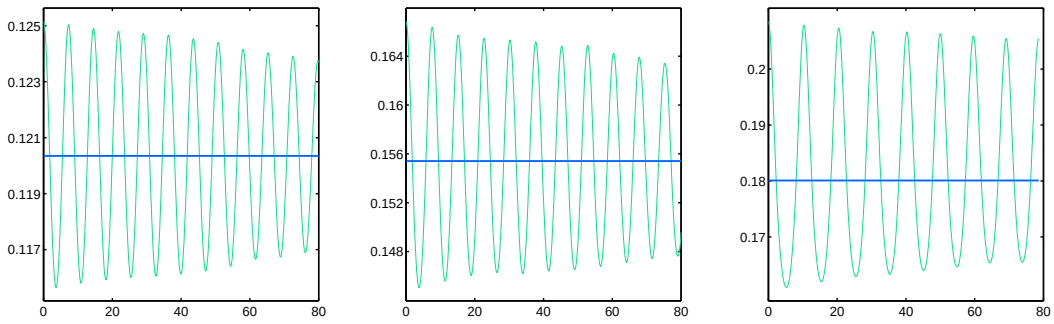

(d) $\beta = 3.5, p_\theta = 0.150$ (e) $\beta = 3.5, p_\theta = 0.200$ (f) $\beta = 3.5, p_\theta = 0.250$

Figure 4.14: The first plot exhibits curves of θ, the angular coordinate position of the intensity centroid of the soliton, against the propagation distance z, where all curves share the same value of β and have different initial tilts p_θ. The set of last five figures plot the derivative of θ against z, where as it can be seen, each curve has small oscillations which form around a constant value.

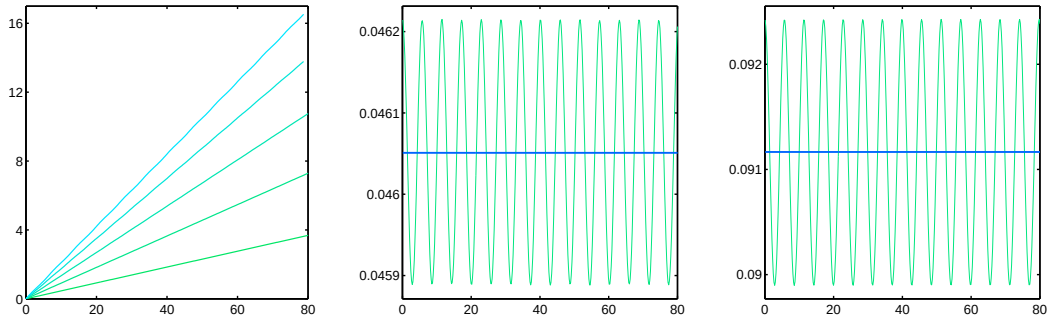

(a) $\beta = 6.5, p_\theta = \{0.030 \ldots 0.150\}$ (b) $\beta = 6.5, p_\theta = 0.030$ (c) $\beta = 6.5, p_\theta = 0.060$

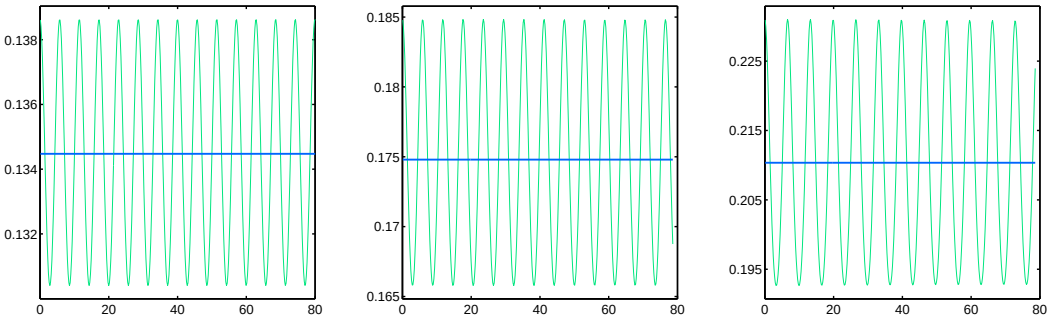

(d) $\beta = 6.5, p_\theta = 0.090$ (e) $\beta = 6.5, p_\theta = 0.120$ (f) $\beta = 6.5, p_\theta = 0.150$

Figure 4.15: The first plot exhibits curves of θ, the angular coordinate position of the intensity centroid of the soliton, against the propagation distance z, where all curves share the same value of β and have different initial tilts p_θ. The set of last five figures plot the derivative of θ against z, where as it can be seen, each curve has small oscillations which form around a constant value.

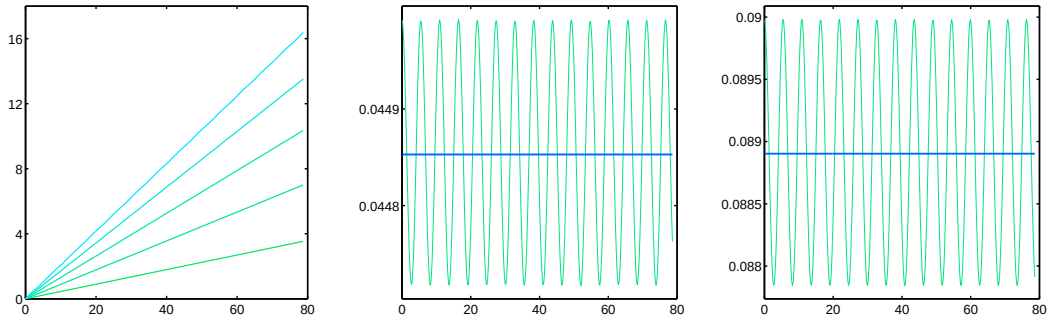

(a) $\beta = 9.5, p_\theta = \{0.020 \ldots 0.100\}$ (b) $\beta = 9.5, p_\theta = 0.020$ (c) $\beta = 9.5, p_\theta = 0.040$

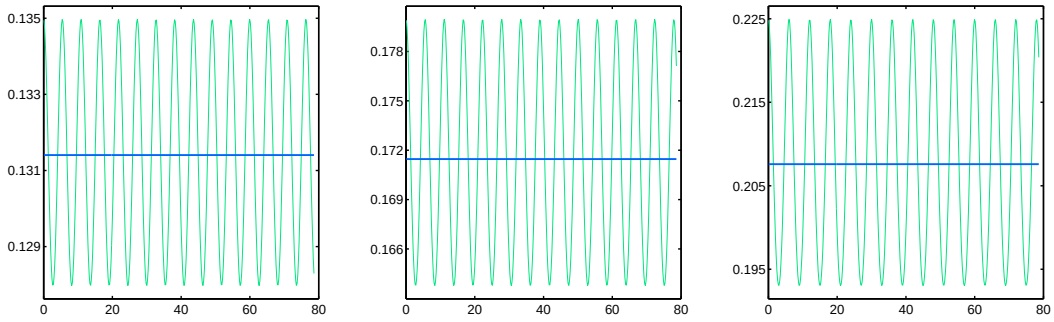

(d) $\beta = 9.5, p_\theta = 0.060$ (e) $\beta = 9.5, p_\theta = 0.080$ (f) $\beta = 9.5, p_\theta = 0.100$

Figure 4.16: The first plot exhibits curves of θ, the angular coordinate position of the intensity centroid of the soliton, against the propagation distance z, where all curves share the same value of β and have different initial tilts p_θ. The set of last five figures plot the derivative of θ against z, where as it can be seen, each curve has small oscillations which form around a constant value.

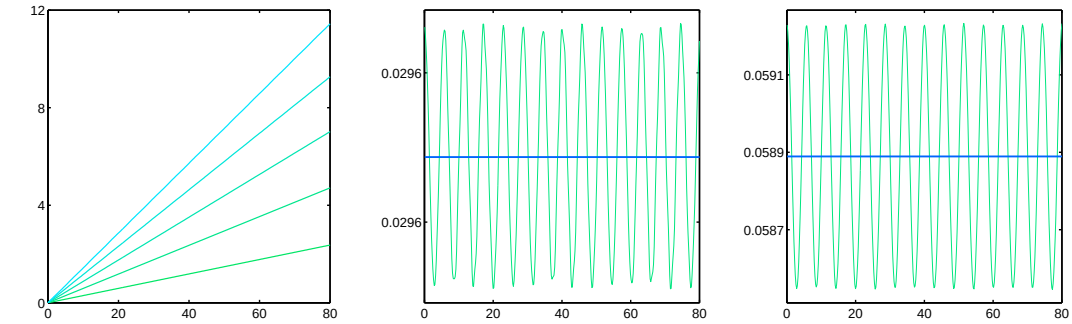

(a) $\beta = 12.5, p_\theta = \{0.050 \ldots 0.250\}$ (b) $\beta = 12.5, p_\theta = 0.010$ (c) $\beta = 12.5, p_\theta = 0.020$

(d) $\beta = 12.5, p_\theta = 0.030$ (e) $\beta = 12.5, p_\theta = 0.040$ (f) $\beta = 12.5, p_\theta = 0.040$

Figure 4.17: The first plot exhibits curves of θ, the angular coordinate position of the intensity centroid of the soliton, against the propagation distance z, where all curves share the same value of β and have different initial tilts p_θ. The set of last five figures plot the derivative of θ against z, where as it can be seen, each curve has small oscillations which form around a constant value.

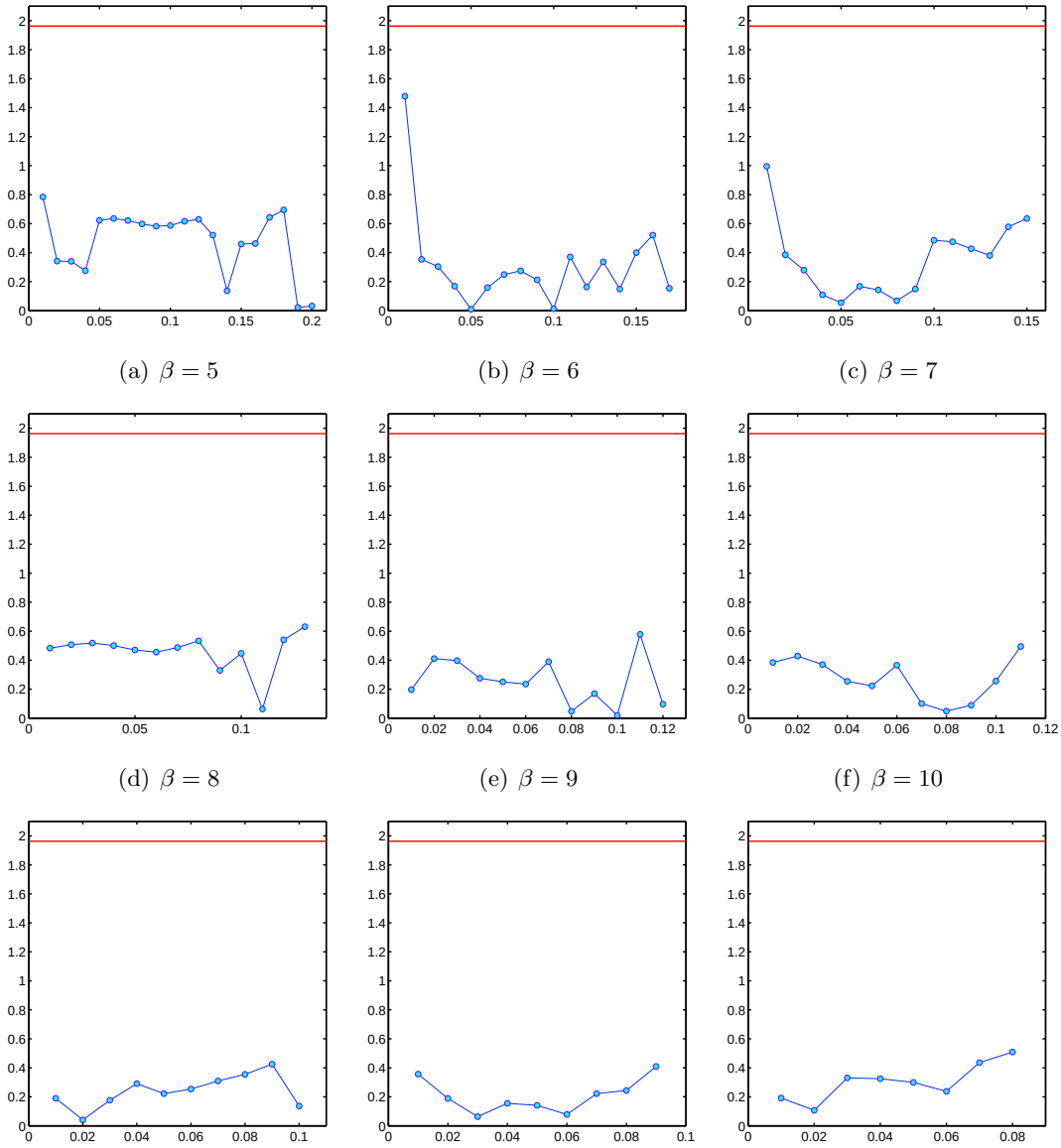

(a) $\beta = 5$ (b) $\beta = 6$ (c) $\beta = 7$

(d) $\beta = 8$ (e) $\beta = 9$ (f) $\beta = 10$

(g) $\beta = 11$ (h) $\beta = 12$ (i) $\beta = 13$

Figure 4.18: Hypothesis testing for evaluating the variation of the function $\theta(z)$. Results can be interpreted as followed: if a point of the parametric space (circular markers) falls below the critical value (straight null slope line) the variation in $\theta(z)$ can be interpreted as null, leaving a non-radiating power soliton. If the blue dot overcomes the critical value, a closer look at the respective plot must be taken. It can be concluded that for all values inside the parametric space $\theta(z)$ behaves as a linear function.

the soliton. This occurs as the system is nonlinear and so the variation induced by the radial variation can't be quantified in an exact fashion this periodic behavior being present to in the quantifier $\mathscr{P}_w$ of last section.

Nevertheless, both variations (radial and numerical) may represent a small percent of the total derivative, since $\theta(z)$ appears to be a linear function. In order to find so, a linear interpolation was carried out for every simulation. After so, the same hypothesis test as the one used in the last section was employed for determining whether this variation was relevant to the function itself, or if rather it could be ignored. All test carried (fig. 4.18) seemed to point to the second option, that is the variation is irrelevant.

So, for concluding this section, it was found that $\theta(z)$ is a linear function of z for all other parameters fixed, that is

$$\theta(z) = Qz, \tag{4.21}$$

where Q is a constant of propagation yet to be related to other parameters.

4.5 Radial coordinate dynamics

Exploring the dynamics of the radial coordinate r is the next natural step after clarifying and investigating the z depends of the polar angle coordinate θ. This time the model proposed is not so simple, since the lattice itself has a radial dependence following a squared Bessel function. Again, z is our independent variable, the propagation coordinate, so all functions of the soliton profile can be thought as functions of z To start exploring this subproblem, plots of $r(z)$ versus z are presented in figure 4.19, where again, $r(z)$ is a coordinate taken with respect to the soliton's intensity centroid.

The main feature of $r(z)$ that strikes view at a first glance is that it is a semi-periodic function, where the term semi enters as that the function itself approximately reproduces itself after each complete period for low values of β, but for almost all the parametric space βt_θ it is a periodic functions. Furthermore, for a fixed value of β the minimum radius for each propagation remains constant and the maximum radius increases as p_θ does so. This issue is

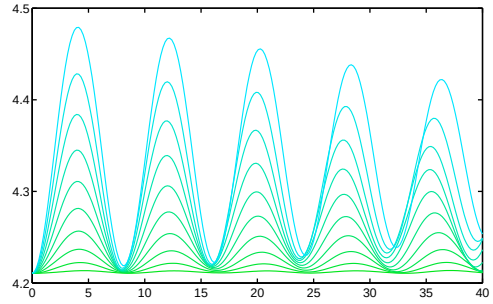

(a) $\beta = 3, p_\theta = \{0.02, 0.04, 0.06 \ldots, 0.18, 0.20\}$

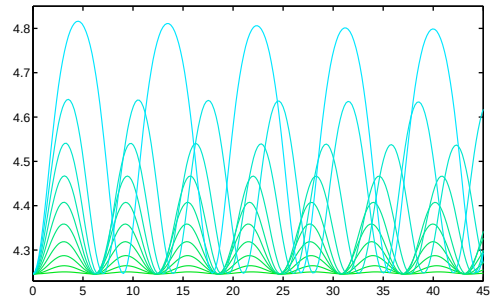

(b) $\beta = 5, p_\theta = \{0.02, 0.04, 0.06 \ldots, 0.18, 0.20\}$

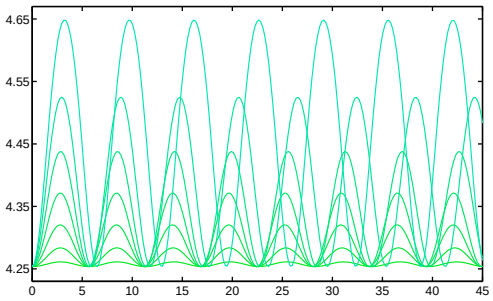

(c) $\beta = 7, p_\theta = \{0.02, 0.04, 0.06 \ldots, 0.12, 0.14\}$

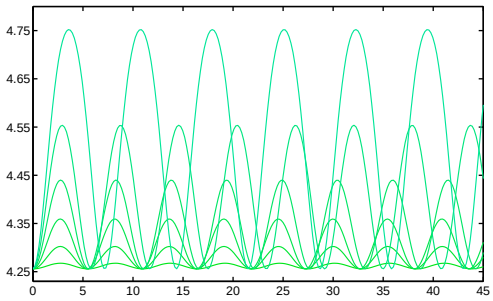

(d) $\beta = 9, p_\theta = \{0.02, 0.04, 0.06, 0.08, 0.10, 0.12\}$

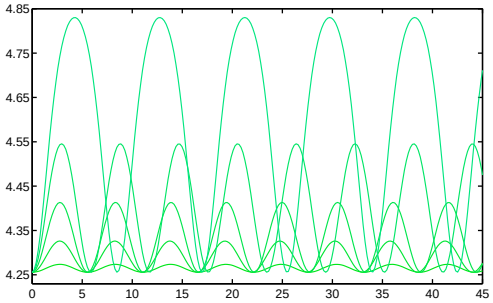

(e) $\beta = 11, p_\theta = \{0.02, 0.04, 0.06, 0.08, 0.10\}$

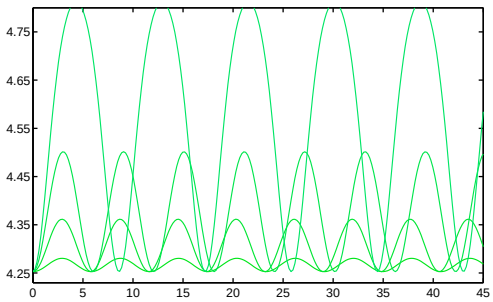

(f) $\beta = 13, p_\theta = \{0.02, 0.04, 0.06, 0.08\}$

Figure 4.19: Plots of the $r(z)$, the radial coordinate of the soliton intensity centroid, against z, the propagation independent coordinate. All single figures fixes β to a value, where each different curve corresponds to a value of p_θ. Functions exhibit a periodic behavior, where in some cases the amplitude is slightly modulated. A constant to all curves is the minimum value acquired, which is a constant along propagation. Furthermore, for a fixed value of β, the minimum radius is independent of the initial tilt p_θ as shown. It can be shown how for small values of z all plots seem to be in phase with respect to its period, but as z increases distinct sections of the periodic function start overlapping, resulting in a dephasing.

dealt and exposed clearly in the following figure 4.20.

After qualitatively exploring the dynamics of $r(z)$, it is time to propose an approximate model for it. Following the strategy for angular dynamics the model starts from the idea that the lattice itself acts as an external force on the soliton, where more precisely, the refraction index of the lattice is a conservative potential for the dynamic function $r(z)$. Newton's second law goes as

$$\mathbf{F} = m\mathbf{a}, \tag{4.22}$$

where $\mathbf{F}$ is a force acting on an object with mass m and acceleration $\mathbf{a}$. Now, following the hypothesis that the motion dynamics can be separated when used the natural coordinates for the symmetry, in this case r and θ, Newton's second law can be rewritten as

$$F_r = ma_r, \tag{4.23}$$

where F_r is the central force originated from the optical lattice and $\mathbf{a}_r$ is the second derivative of r with respect to z, the independent-propagation coordinate, that is

$$a_r = \frac{d^2r}{dz^2}. \tag{4.24}$$

Going back to the mathematical model it is found that the profile corresponding to the lattice is

$$u(r) = J_m^2(k_t r), \tag{4.25}$$

where $J_m(x)$ is a first kind Bessel function of order m and k_t is the lattice longitudinal wave number. As a model proposed, it is assumed that the profile $u(r)$ acts as a conservative potential that generates a force F_r in the fashion

$$F_r = -\frac{du}{dr}. \tag{4.26}$$

Equating derivatives and inserting terms in the original equation the model ends up with

$$\frac{d^2r}{dz^2} \propto -2J_m(k_t r)\Big(k_t J_{m+1}(k_t r) + \frac{m}{r}J_m(k_t r)\Big), \tag{4.27}$$

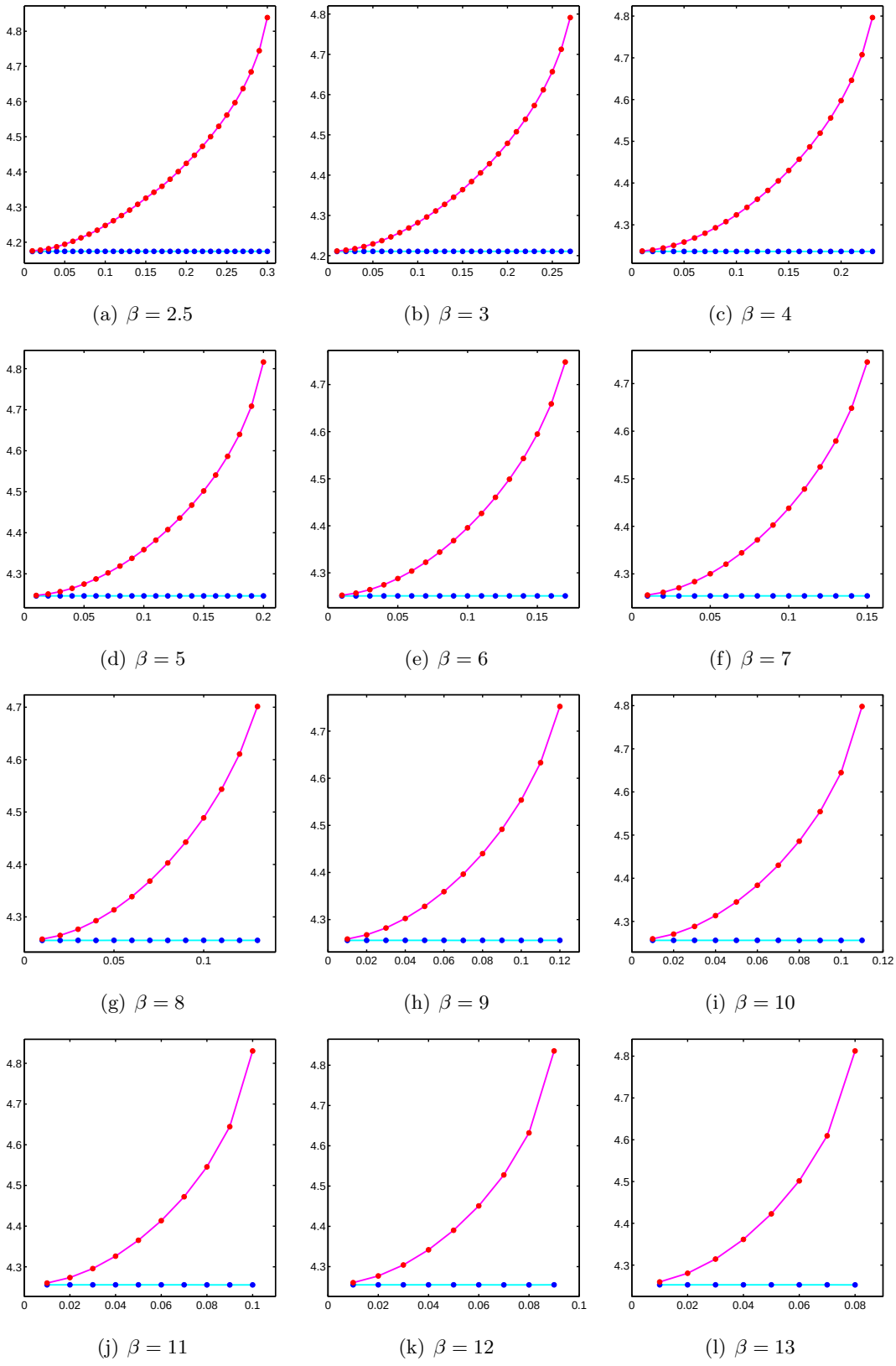

(a) $\beta = 2.5$ (b) $\beta = 3$ (c) $\beta = 4$

(d) $\beta = 5$ (e) $\beta = 6$ (f) $\beta = 7$

(g) $\beta = 8$ (h) $\beta = 9$ (i) $\beta = 10$

(j) $\beta = 11$ (k) $\beta = 12$ (l) $\beta = 13$

Figure 4.20: Each window fixes the value of β for all scatter curves, where the x axis stands for a initial tilt value p_θ, and the y axis represents a certain value of the r coordinate. For the case of blue points, it points the minimum value of $r(z)$ for each propagation, and red dot point maximum values of $r(z)$. It can be seen how the minimum values are constant for fixed z, while maxima values increase in an exponential fashion.

where the term m was removed since it is not the intention for this work to define an equivalence for mass m. Rather than that, it is sufficient to reach a proportionality relation. Thus, a nonlinear second order differential equation has been reached for the function $r(z)$. Rather than solving it, the next step is testing its accuracy. Plots of F_r against a_r are show in figures 4.21-4.23.

A linear behavior is found approximately for low values of β, where the expected straight lines widens resulting in a multiple valued function. Still, linearity appears in a mild fashion for central values of the initial tilt p_θ. Still. as β increases, linearity appears in a more precise way, and the model fits perfectly for a wide region in the parametric space. Nevertheless, for high values of p_θ the relations turns nonlinear for relatively high radius, but still maintaining a one to one correspondence. Meaning that even though behavior lacks linearity in one end of the curve, it can be somehow approximated by other functions, and showing two that both quantities are still related.

It has been demonstrated how the relationships seems to work in a more quantitative way by calculating the correlation coefficients for points in the parametric space and plotting the results in figure 4.24. Results seem to indicate the linear model fits well for lots of combinations.

4.6 Rotation rate variation

It is turn now to explore the dynamics of the soliton's motion as one after treating separately the functions $r(z)$ and $\theta(z)$. It has been proven how $\theta(z)$ is a linear function of propagation and how $r(z)$ exhibits a more elaborate behavior inside a particular region of the parametric $\beta - p_\theta$ space. Furthermore, the variations of $r(z)$ are not random nor follow numerical round off errors, thus the complete dynamic for the soliton can be explained using both models. This produces an explanation for bounces inside the light ring, and furthermore and perhaps most important, gives support and an explanation to the varying rotation rate around a light ring with null azimuthal modulation.

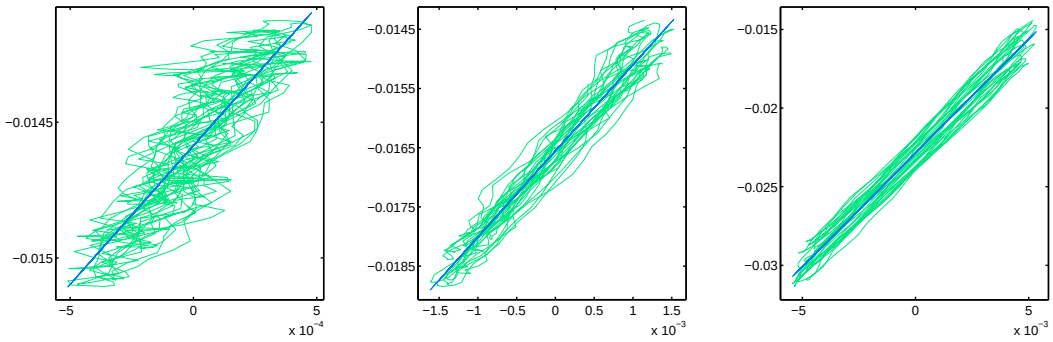

(a) $\beta = 2.5, p_\theta = 0.010$ (b) $\beta = 2.5, p_\theta = 0.030$ (c) $\beta = 2.5, p_\theta = 0.060$

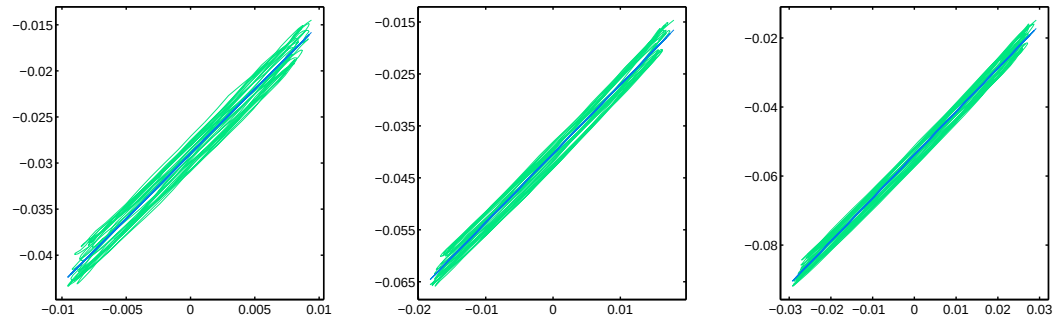

(d) $\beta = 2.5, p_\theta = 0.080$ (e) $\beta = 2.5, p_\theta = 0.110$ (f) $\beta = 2.5, p_\theta = 0.140$

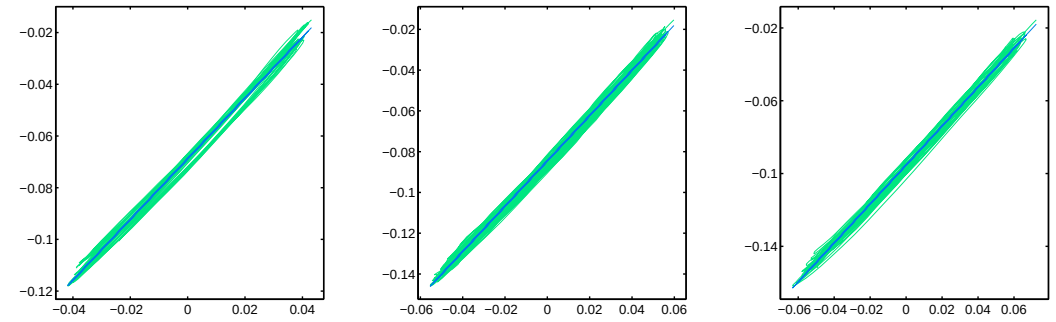

(g) $\beta = 2.5, p_\theta = 0.170$ (h) $\beta = 2.5, p_\theta = 0.200$ (i) $\beta = 2.5, p_\theta = 0.220$

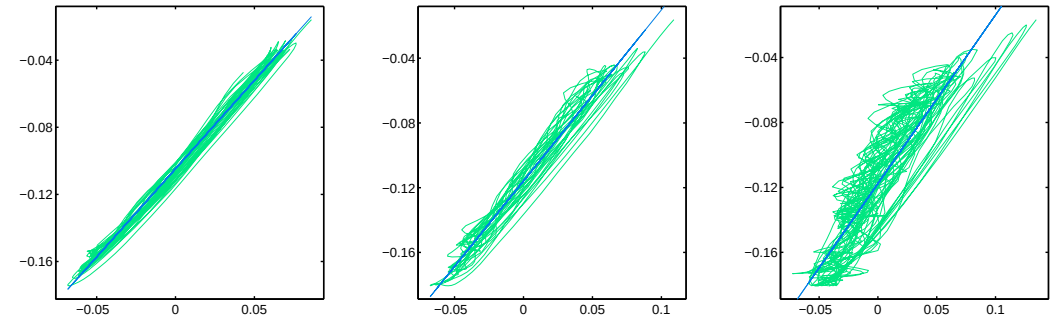

(j) $\beta = 2.5, p_\theta = 0.240$ (k) $\beta = 2.5, p_\theta = 0.270$ (l) $\beta = 2.5, p_\theta = 0.300$

Figure 4.21: Each window fixes β and p_θ, where the x axis corresponds to the radial acceleration, the second derivative of $r(z)$; and the y axis stands for the generalized radial force originating from the Bessel lattice profile. The straight line stands for the linear regression of the set of points originating from the quantifiers. The linear approximation is moderately valid for mild values of p_θ.

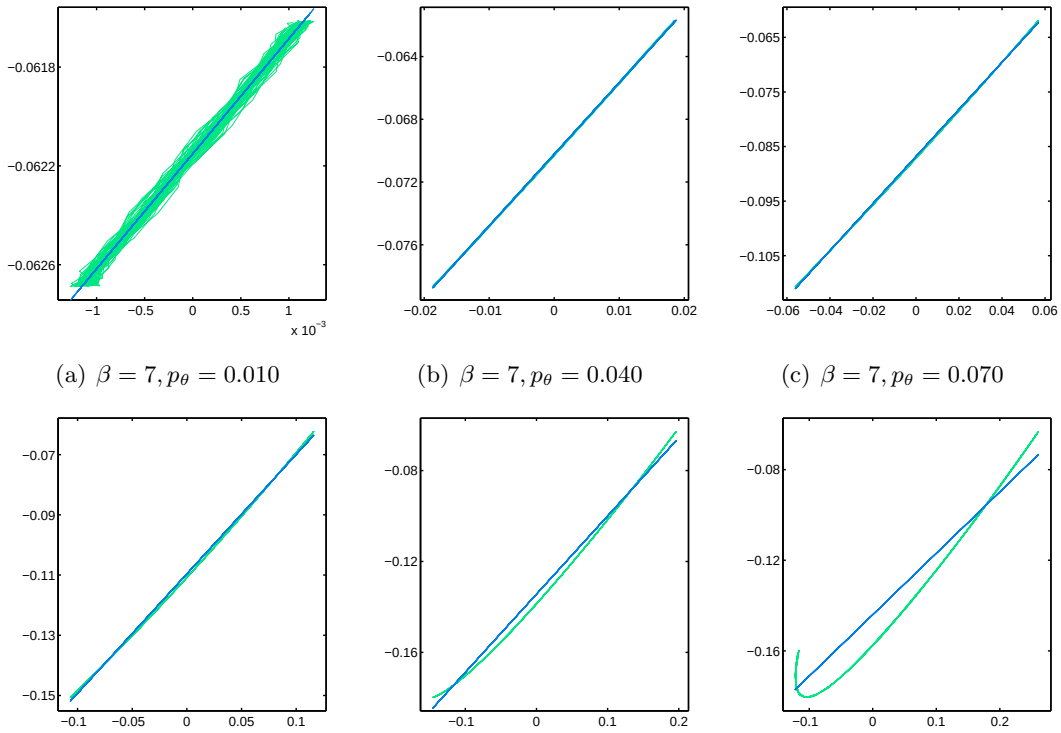

(a) $\beta = 7, p_\theta = 0.010$ (b) $\beta = 7, p_\theta = 0.040$ (c) $\beta = 7, p_\theta = 0.070$

(d) $\beta = 7, p_\theta = 0.100$ (e) $\beta = 7, p_\theta = 0.130$ (f) $\beta = 7, p_\theta = 0.150$

Figure 4.22: Each window fixes β and p_θ, where the x axis corresponds to the radial acceleration, the second derivative of $r(z)$; and the y axis stands for the generalized radial force originating from the Bessel lattice profile. The straight line stands for the linear regression of the set of points originating from the quantifiers. The linear approximation fits perfectly for a wide range of p_θ.

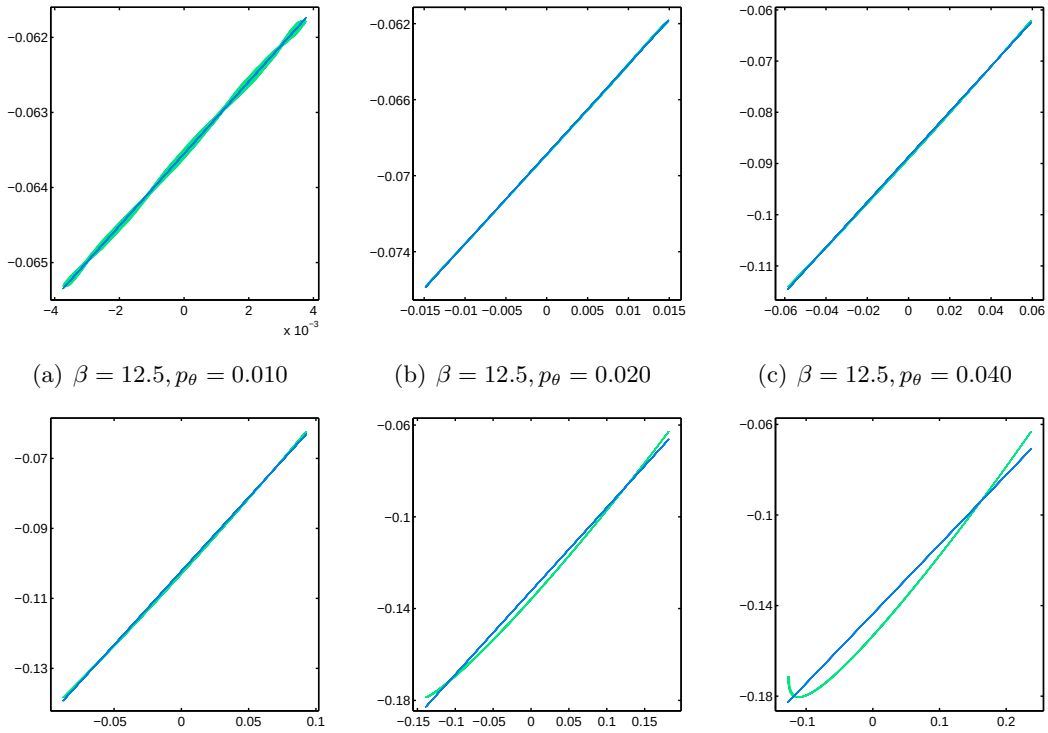

(a) $\beta = 12.5, p_\theta = 0.010$ (b) $\beta = 12.5, p_\theta = 0.020$ (c) $\beta = 12.5, p_\theta = 0.040$

(d) $\beta = 12.5, p_\theta = 0.050$ (e) $\beta = 12.5, p_\theta = 0.070$ (f) $\beta = 12.5, p_\theta = 0.080$

Figure 4.23: Each window fixes β and p_θ, where the x axis corresponds to the radial acceleration, the second derivative of $r(z)$; and the y axis stands for the generalized radial force originating from the Bessel lattice profile. The straight line stands for the linear regression of the set of points originating from the quantifiers. The linear approximation fits perfectly for a wide range of p_θ.

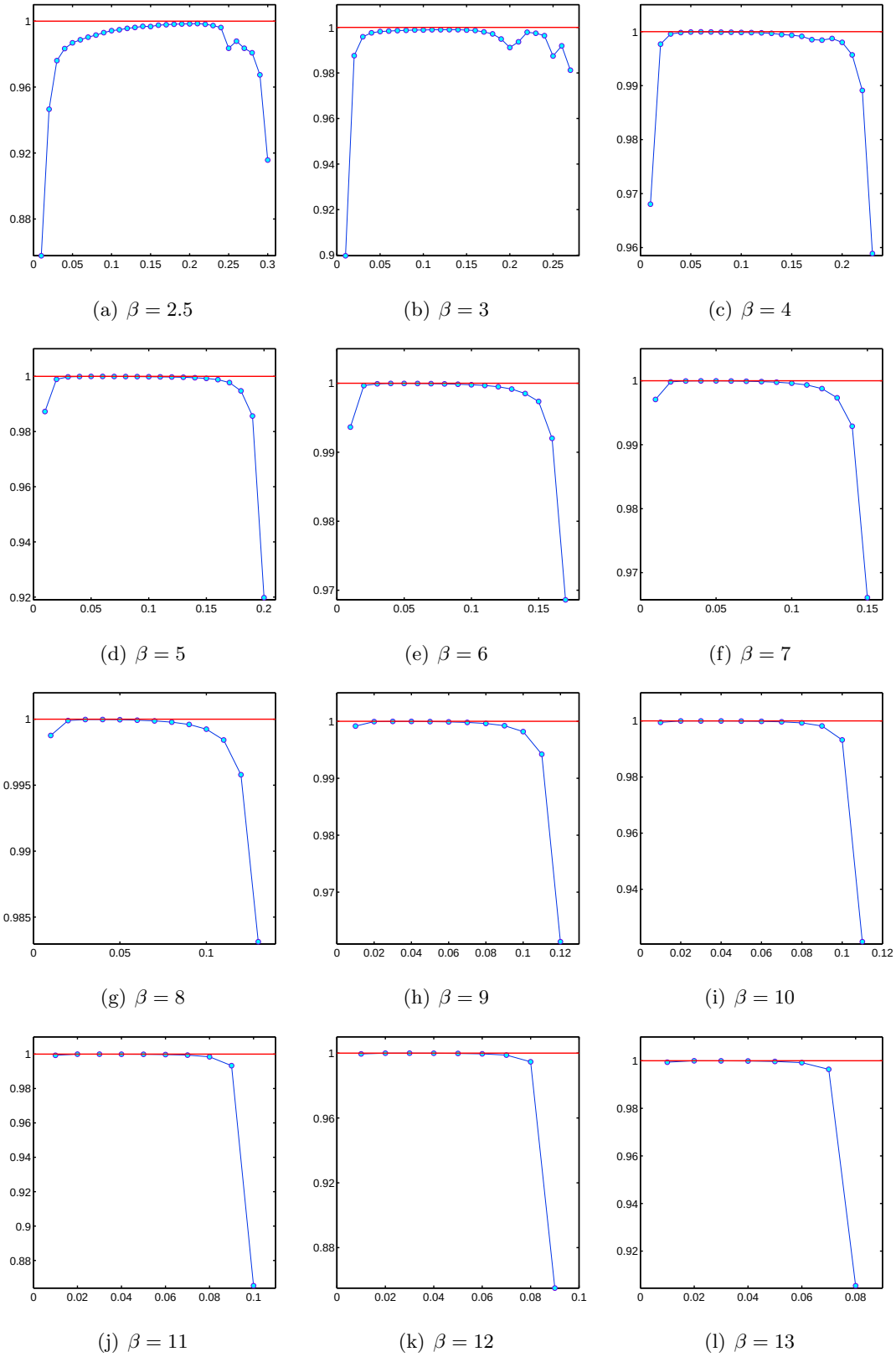

(a) $\beta = 2.5$ (b) $\beta = 3$ (c) $\beta = 4$

(d) $\beta = 5$ (e) $\beta = 6$ (f) $\beta = 7$

(g) $\beta = 8$ (h) $\beta = 9$ (i) $\beta = 10$

(j) $\beta = 11$ (k) $\beta = 12$ (l) $\beta = 13$

Figure 4.24: The correlation coefficient is plotted for a wide range of β and p_θ values. It is practicably equal to unity, meaning a perfect linear relation, for a high percentage of the plotted values. The values distort and turn nonlinear at low and high values of p_θ.

First, to give a clear insight of the problem, plots of the rotation rate γ are show for various points in the parametric space in fig. 4.25, where as noted before, γ is defined as

$$\gamma = \frac{|\Delta \mathbf{r}_t|}{\Delta z}, \tag{4.28}$$

where it describes how the position of the soliton chances with propagation steps, and again as usual, γ is taken with respect to the soliton's intensity centroid. In order to elucidate variations of γ, several scatter plots are exhibited in fig. 4.26, where points correspond to three different quantifiers of each curve: its maximum, minimum and mean value. The triad of values exhibit an incremental behavior as p_θ increases. This is due to the soliton's penetration on the light ring outer wall, which as seen before, increases as p_θ increases to. Thus, offering a bigger variation on the observed potential and a wider range for the values of γ. Furthermore, to exhibit such increments, plots on the standard deviation σ_γ are shown in fig 4.27.

More over, both models

$$\theta(z) = Qz, \tag{4.29}$$

and

$$\frac{d^2 r}{dz^2} \propto -2J_m(k_t r)\Big(k_t J_{m+1}(k_t r) + \frac{m}{r} J_m(k_t r)\Big), \tag{4.30}$$

seem to fit quite well inside a certain region in the parametric space. Therefore, it seams plausible to explain out of this facts how γ has a non zero variation. That is, hot the rotation rate is not constant along propagation in a lattice with no azimuthal modulation. So, for the conclusion of this section, it can be pointed how the transverse rotation rate γ is not constant along propagation, even though the soliton travels around circular light rings with null azimuthal modulation.

4.7 Soliton transverse motion and classic dynamic billiards

This work has demonstrated how solitons exhibit a decomposition on its dynamics of motion even though they are intrinsic nonlinear phenomena. Furthermore, the motion trajectory as a whole can be view as describing a billiards type dynamics in a moderate approximation.

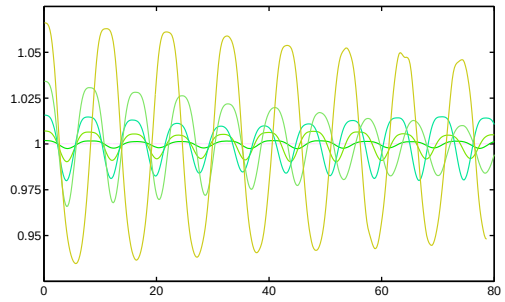

(a) $\beta = 3, p_\theta = \{0.05, 0.10, 0.15, 0.21, 0.27\}$

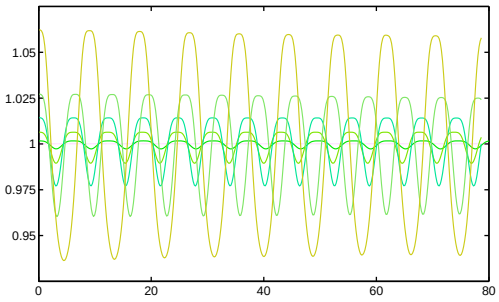

(b) $\beta = 5, p_\theta = \{0.04, 0.08, 0.12, 0.16, 0.20\}$

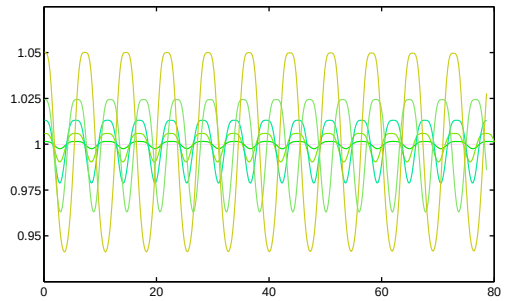

(c) $\beta = 7, p_\theta = \{0.03, 0.06, 0.09, 0.12, 0.15\}$

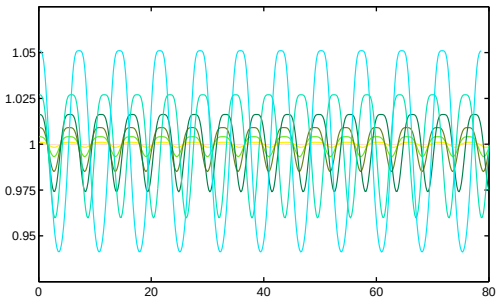

(d) $\beta = 9, p_\theta = \{0.02, 0.04, 0.06, 0.08, 0.10, 0.12\}$

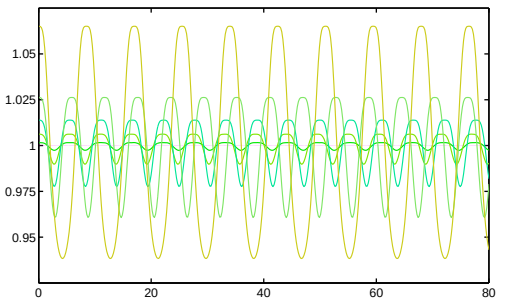

(e) $\beta = 11, p_\theta = \{0.02, 0.04, 0.06, 0.08, 0.10\}$

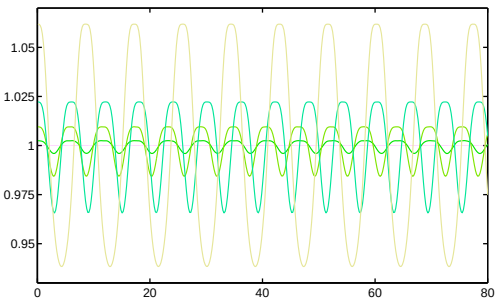

(f) $\beta = 13, p_\theta = \{0.02, 0.04, 0.06, 0.08\}$

Figure 4.25: Plots of the normalized transverse rotation rate $\gamma(z)$, against z. In order to normalize $\gamma(z)$, an integer number of periods was taken to avoid skewness to either low or high values.All single figures fixes β to a value, where each different curve corresponds to a value of p_θ.

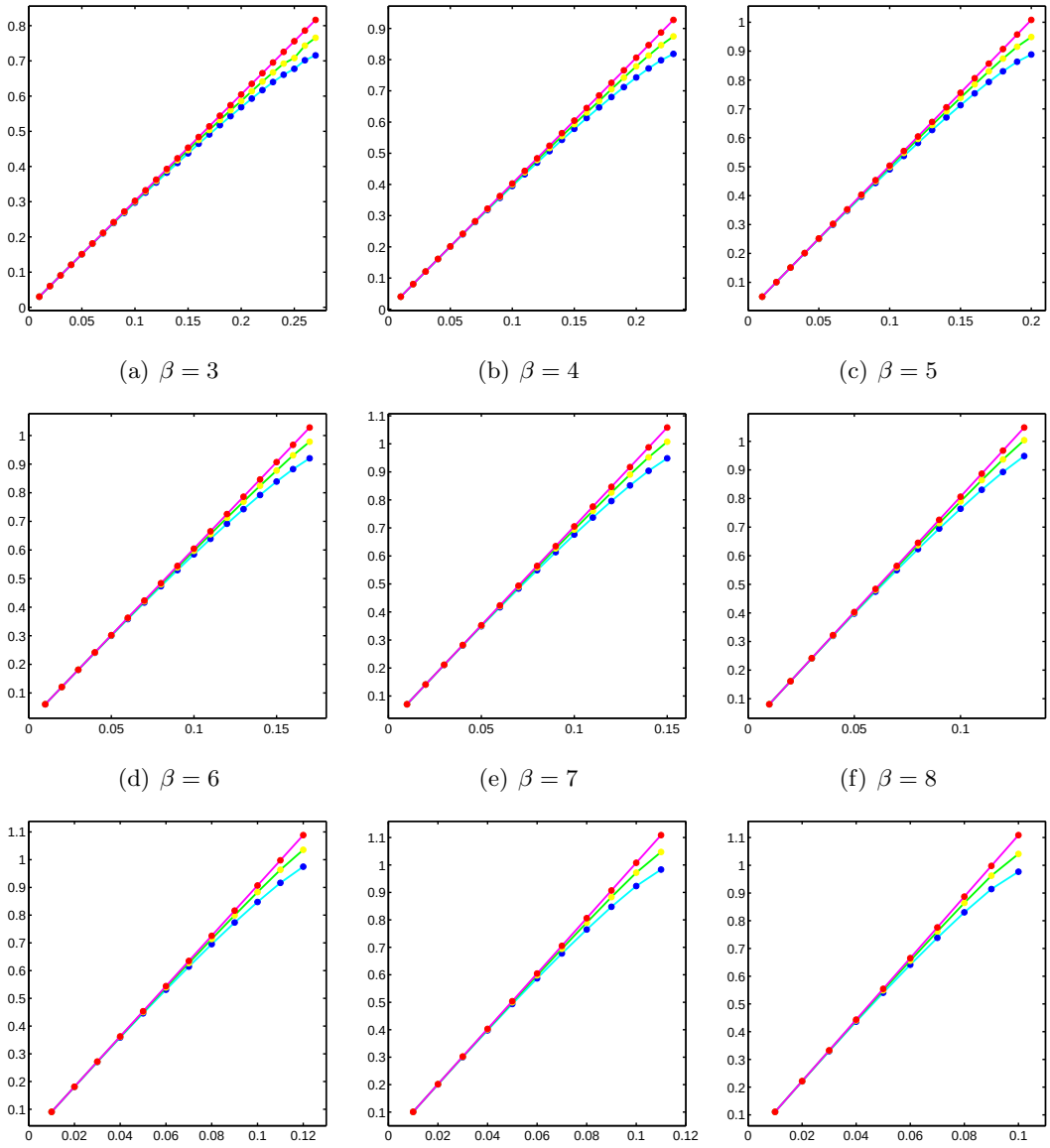

(a) $\beta = 3$ (b) $\beta = 4$ (c) $\beta = 5$

(d) $\beta = 6$ (e) $\beta = 7$ (f) $\beta = 8$

(g) $\beta = 9$ (h) $\beta = 10$ (i) $\beta = 11$

Figure 4.26: Plots of quantifiers of the transverse rotation rate $\gamma(z)$ against p_θ. In order to normalize $\gamma(z)$, an integer number of periods was taken to avoid skewness to either low or high values.All single figures fixes β to a value, where each different point corresponds to a value of p_θ. Upper, middle and lower (red, yellow and blue in color) points correspond to maximum, mean and minimum values respectively. It is appreciated how as p_θ increases, the triad of quantifiers increase in their single values. More over, the difference between minimum and maximum values increase to, elucidating the growing variation of $\gamma(z)$ as p_θ increases.

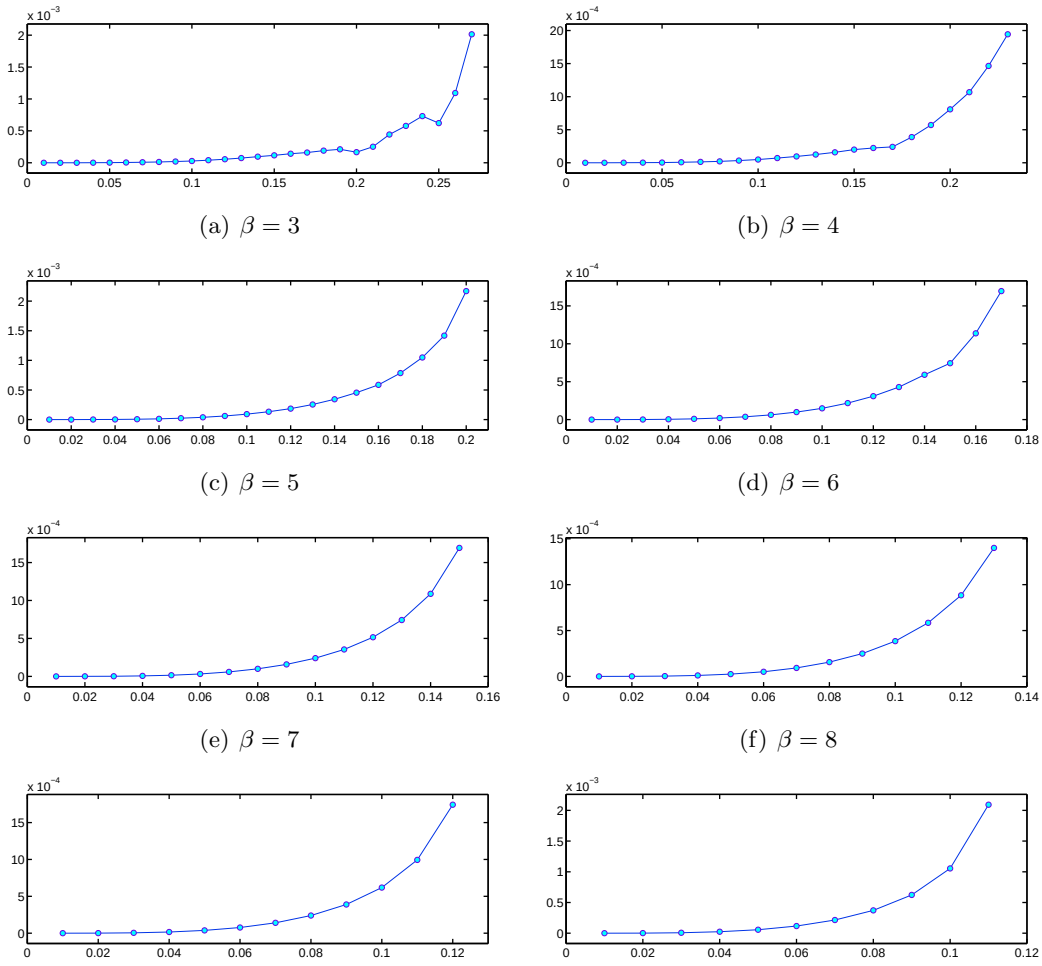

(a) $\beta = 3$ (b) $\beta = 4$

(c) $\beta = 5$ (d) $\beta = 6$

(e) $\beta = 7$ (f) $\beta = 8$

(g) $\beta = 9$ (h) $\beta = 10$

Figure 4.27: Plots of the standard deviation of $\gamma(z)$, against z. In order to normalize $\gamma(z)$, an integer number of periods was taken to avoid skewness to either low or high values.All single figures fixes β to a value, where each different point corresponds to a value of p_θ. As p_θ increases, so does the standard deviation σ_γ.

This follows the bounces of the soliton inside the light ring, where the last can be viewed as acting as a elastic wall for the particle like soliton, all this said inspired by a slight analogy. This section is an attempt to establishing an analogy and confection between billiards systems an a soliton transverse motion inside the a light ring of the non modulated Bessel lattice.

It is said solitons bounce back and forth inside the inner and outer walls of the light ring since the radial coordinate r starts from a minimum value, increases until it reaches a peak maximum value and starts decreasing until going back to the original initial r value, the minimum value for r. This is a process done repeatedly by the soliton, in such a continuous and smooth way following the dynamics of the r coordinate. Furthermore, it has been exhibited how this peak value for each cycle remains constant for a large region of the parametric space. This behavior of the radial coordinate constitutes the fundamentals to attempt stabilizing an analogy between the soliton motion studied in this section and dynamical billiards.

The first detail to exhibit is the orientation of the soliton, that is, its angle of transverse propagation. In the classical dynamics ideal case, a point particle maintains a constant orientation until it strikes with a wall, where it bounces by changing the orientation only of its momentum in a direction perpendicular to the wall. This is done ideally instantly, so the plot of its orientation angle can be viewed as a train of box car functions with different amplitudes, like stairs.

Another important detail to consider is the linear momentum associated with each bounce. A particle orientation is ruled by the ratio of its speed components, being in two dimension related to the inverse tangent function. That is, if ϕ is the orientation angle, v_x and v_y the speed components corresponding to the x and y directions respectively, then the orientation angle can be defined as

$$\phi = \tan^{-1}\left(\frac{vy}{vx}\right). \tag{4.31}$$

The instant orientation of the particle is perfectly defined by this quantity ϕ, where if the unit vector pointing in the direction of the particle is $\hat{u}$ it follows that

$$\hat{u} = \cos(\phi)\hat{x} + \sin(\phi)\hat{y}. \tag{4.32}$$

Now, momentum is a vector quantity having the same direction of the instant direction of the particle. So, if p is the particle momentum magnitude, then

$$\overrightarrow{p} = p\Big[\cos(\phi)\hat{x} + \sin(\phi)\hat{y}\Big]. \tag{4.33}$$

The momentum a body carries acts directly with the net force exerted on it via Newton's second law. In the case of a particle bouncing inside the walls of a confinement potential, as in the case of dynamic billiards, what determines if the particle crosses the wall or bounces back is the momentum directed in the force acting for it to recoil. In this case with circular symmetry, when a particle recoils the force exerted on it is directed radially inwards into the center of the potential, the origin $r = 0$. So, the momentum to be considered in each bounce must be projected along this radial line. That is, the effective momentum involved in the recoil process is

$$p_{ch} = \overrightarrow{p} \cdot \hat{r} = p\hat{u} \cdot \hat{r} = p\Big(\cos(\phi)\hat{x} + \sin(\phi)\hat{y}\Big) \cdot \Big(\frac{x}{r}\hat{x} + \frac{y}{r}\hat{y}\Big), \tag{4.34}$$

$$p_{ch} = \frac{p}{r}\Big(x\cos(\phi) + y\sin(\phi)\Big). \tag{4.35}$$

This is a quantifier that characterizes the outcome of the recoil. If it crosses a critical value depending on the structure of the body subject to the recoil and the force exerted. As it happens for the ideal particle case, this quantifier is a constant of motion for each recoil. That is, has exactly the same value right before crashing into the billiard walls. Since this is a function of the initial momentum magnitude p, it can be normalized, so just to kept track of the position of the particle and account for variations on it. That defines

$$p_u = \frac{1}{r}\Big(x\cos(\phi) + y\sin(\phi)\Big), \tag{4.36}$$

which will be a quantifier to treat.

Furthermore, this momentum projection over the line of action can be seen as a function of radius, since in the end both quantifiers are functions of propagation and can be put together in a phase diagram. Fig. 4.25 summarizes and exhibits this propagation quantifiers for an ideal classical billiard.

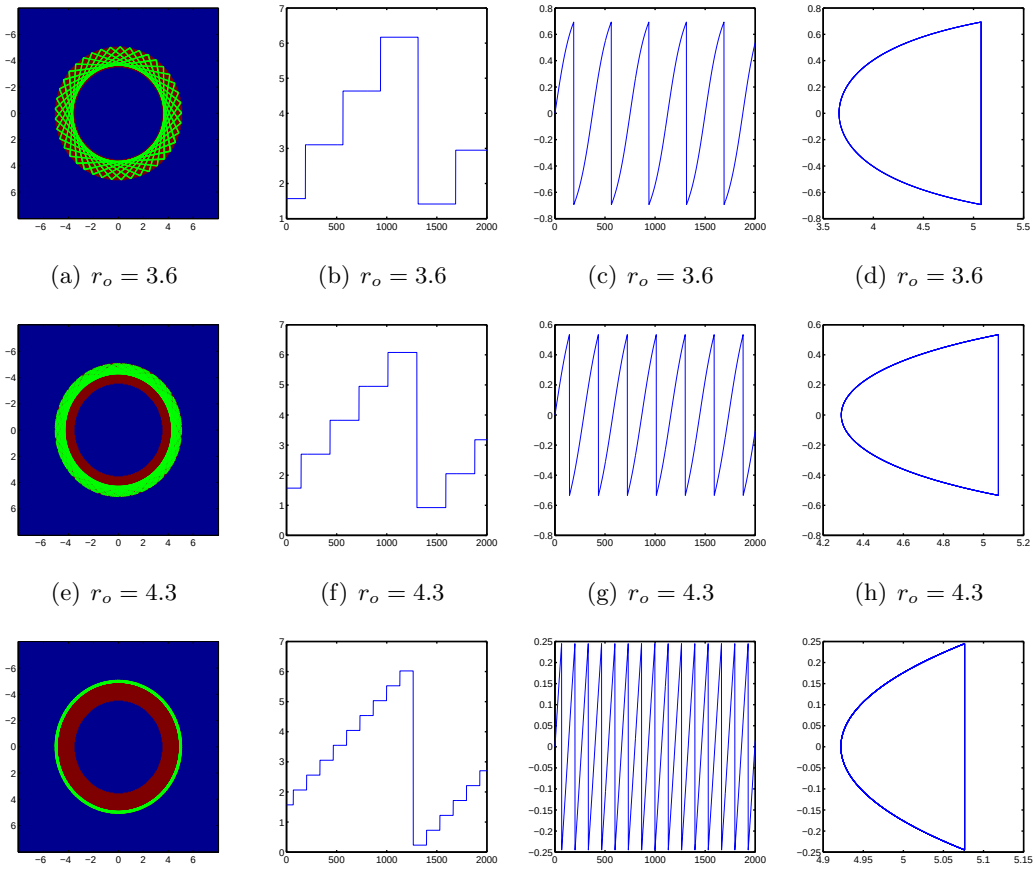

(a) $r_o = 3.6$ (b) $r_o = 3.6$ (c) $r_o = 3.6$ (d) $r_o = 3.6$

(e) $r_o = 4.3$ (f) $r_o = 4.3$ (g) $r_o = 4.3$ (h) $r_o = 4.3$

(i) $r_o = 4.9$ (j) $r_o = 4.9$ (k) $r_o = 4.9$ (l) $r_o = 4.9$

Figure 4.28: Dynamics of a point particle classical billiards assuming elastic collisions with an infinite potential wall. Each row consists of a different case, where the initial radius is set as the control variable. In all three cases the particle is launch azimuthally with respect to the orientation of the lattice. The first column resembles the billiard where the particle is confined, marked in red, and the particle it takes, colored in bright green. In all three cases, and as a general case for this system, the minimum radius along the whole trajectory is fixed for each bounce, and is equal to the initial radius. The second column corresponds to plots of the soliton orientation with respect to the x axis, where it can be seen how it is constant and changes abruptly at each recoil. The third column corresponds to the projection of the momentum along the line of collision, being it the effective momentum in each recoil process. Finally, the fourth column is a plot of the momentum projection against the radius.

For the case of solitons, the ideal behavior of the orientation angle ϕ is lost since the recoil is not instantaneous. It is rather described as fuzzy, since the potential fills the light ring containing the soliton, so the soliton is constantly being reoriented. Still, the soliton orientation follows a similar behavior, but with smoother and continues jumps. This is shown figures 4.29-4.32.

Nevertheless, nonlinear effects and diffraction conspire together to recreate an important detail from classical dynamic billiards. In such case, if the initial launch angle is such that the particle direction is initially azimuthal, for example $\frac{\pi}{2}$ when initially located at the x axis, the initial radius is kept as the minimum radius for the dynamic. That is, the point particle bounces of the wall and is reoriented in a way such as to respect the minimum radius limit equal to the initial value. Surprisingly, this fact is also present in soliton transverse dynamics, as shown in previous sections.

In the case of solitons p_u resembles the behavior as seen in classical billiards for non low values of β. That is, at $\beta = 3$ the function is periodic but with a modulated amplitude. Still, it can be appreciated how it changes form minimum to maximum in the same interval of z. But at higher values of β this anomalous behavior disappears and p_u behaves as in classical billiards, all this shown in figures 4.33-4.35.

When plotting the phase diagram of p_u and r at low values of β an anomalous and fuzzy behavior appears again, deviating completely from the classical one. Still, as β increases, the curve forms what appears to be an ellipse, meaning there is a close and compact relation between both variables, as in the classical case, except for the fact that in the classical case the particle recoils instantaneously, leaving half of the ellipse only. Since the soliton crosses the wall and recoil smoothly, this transition is rather slow and continuous, causing for the complete ellipse to take shape. This close relation is found in figures 4.36-4.38. A proper technique to quantify this relation is to calculate the derivative of one quantifier and plot it against the other. If there is a clear, constant dephasing between both quantities, this operation would result in plotting a straight line, which again, does not hold for low

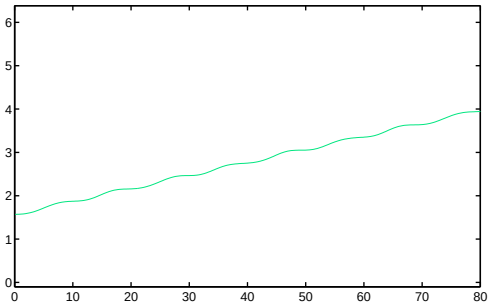

(a) $\beta = 2.5, p_\theta = 0.050$

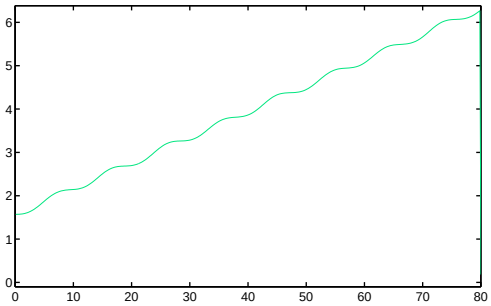

(b) $\beta = 2.5, p_\theta = 0.100$

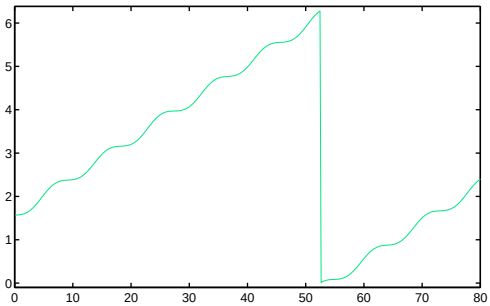

(c) $\beta = 2.5, p_\theta = 0.150$

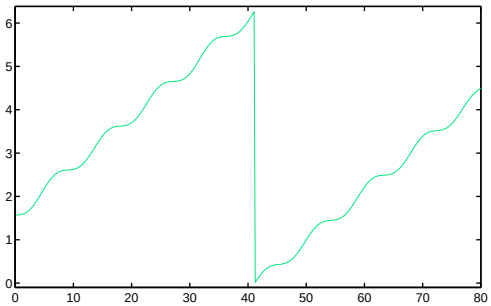

(d) $\beta = 2.5, p_\theta = 0.200$

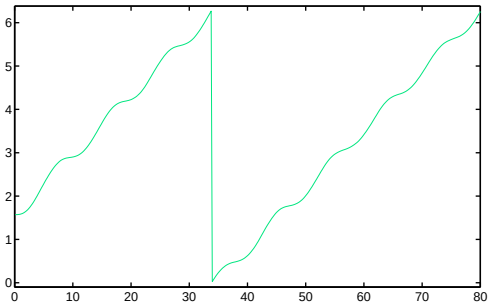

(e) $\beta = 2.5, p_\theta = 0.250$

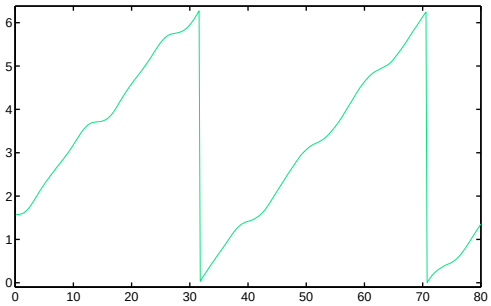

(f) $\beta = 2.5, p_\theta = 0.300$

Figure 4.29: Plots of the soliton angle orientation ϕ against propagation distance z. This behavior resembles that of the ideal classical billiard, but with transitions between collisions done in a rather smooth way. As the initial tilt t_θ reaches higher values, collisions start making more abrupt transitions.

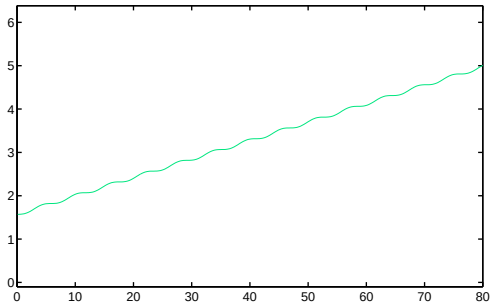

(a) $\beta = 6, p_\theta = 0.030$

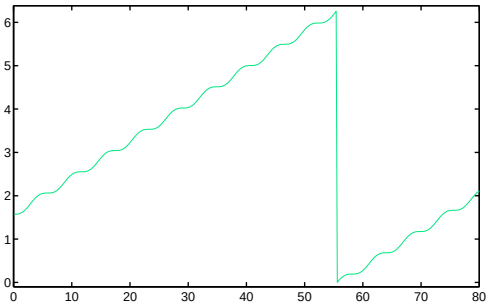

(b) $\beta = 6, p_\theta = 0.060$

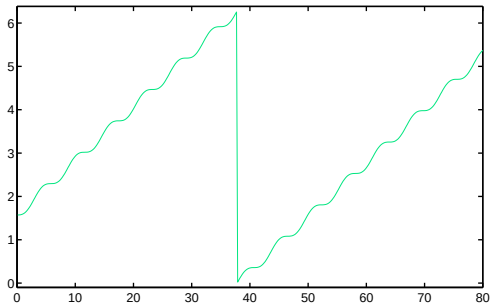

(c) $\beta = 6, p_\theta = 0.090$

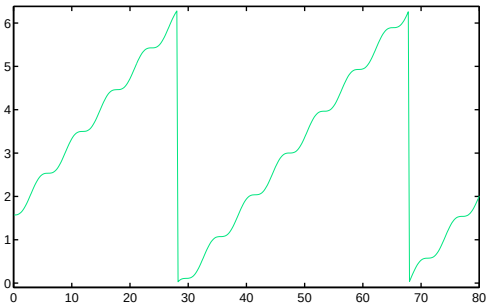

(d) $\beta = 6, p_\theta = 0.120$

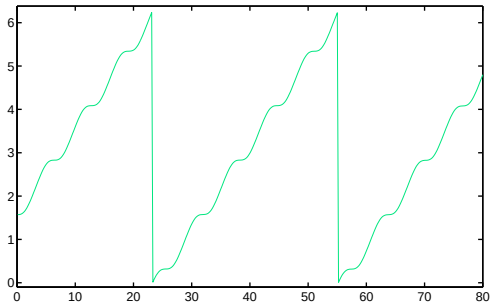

(e) $\beta = 6, p_\theta = 0.150$

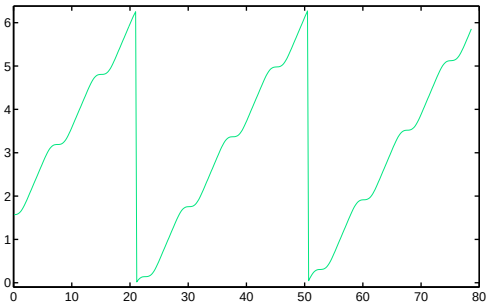

(f) $\beta = 6, p_\theta = 0.170$

Figure 4.30: Plots of the soliton angle orientation ϕ against propagation distance z. This behavior resembles that of the ideal classical billiard, but with transitions between collisions done in a rather smooth way. As the initial tilt t_θ reaches higher values, collisions start making more abrupt transitions.

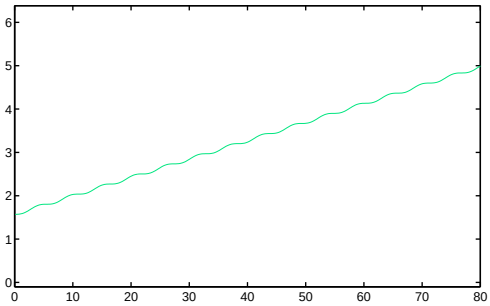

(a) $\beta = 9, p_\theta = 0.020$

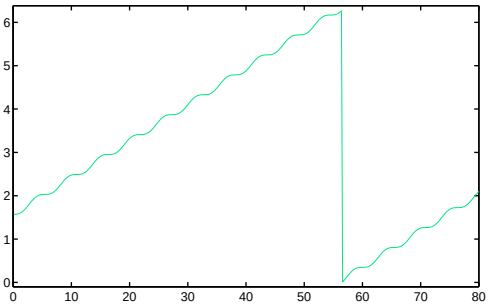

(b) $\beta = 9, p_\theta = 0.040$

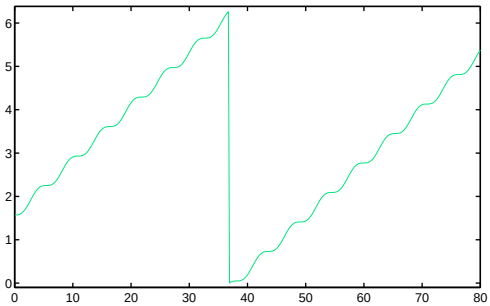

(c) $\beta = 9, p_\theta = 0.060$

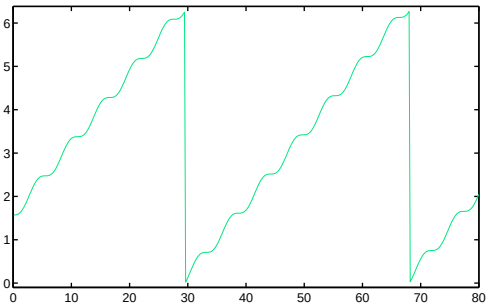

(d) $\beta = 9, p_\theta = 0.080$

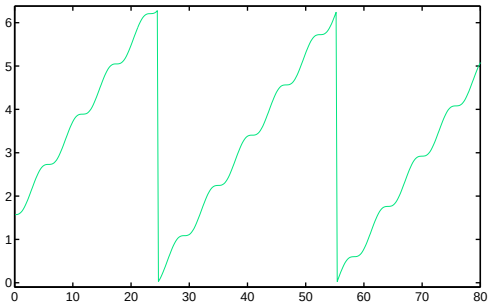

(e) $\beta = 9, p_\theta = 0.100$

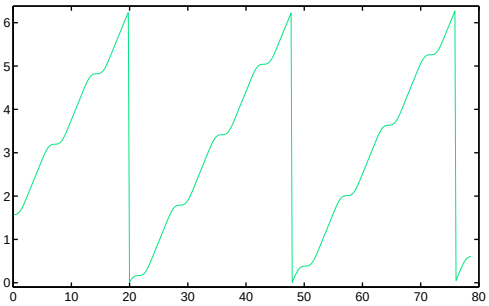

(f) $\beta = 9, p_\theta = 0.120$

Figure 4.31: Plots of the soliton angle orientation ϕ against propagation distance z. This behavior resembles that of the ideal classical billiard, but with transitions between collisions done in a rather smooth way. As the initial tilt t_θ reaches higher values, collisions start making more abrupt transitions.

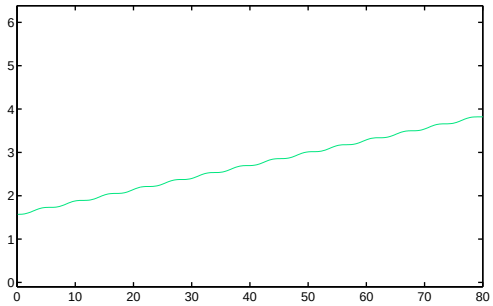

(a) $\beta = 12, p_\theta = 0.010$

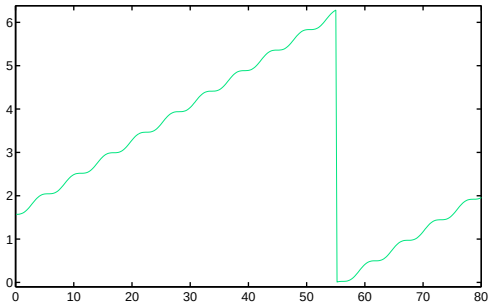

(b) $\beta = 12, p_\theta = 0.030$

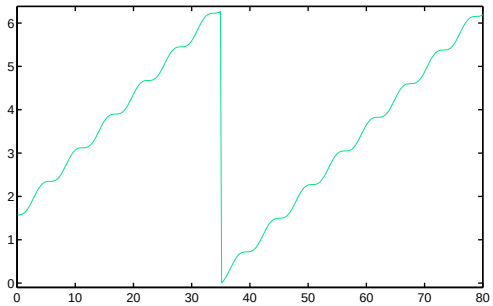

(c) $\beta = 12, p_\theta = 0.050$

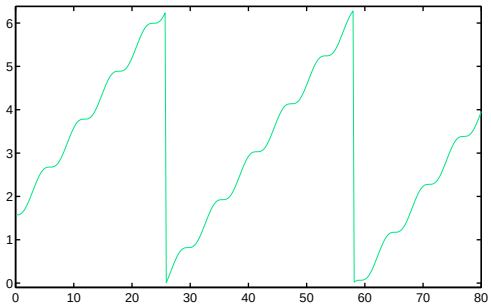

(d) $\beta = 12, p_\theta = 0.070$

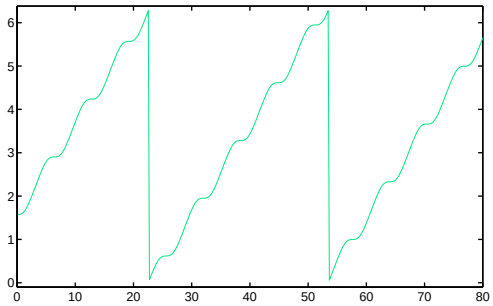

(e) $\beta = 12, p_\theta = 0.080$

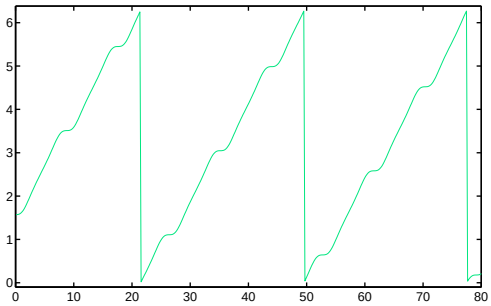

(f) $\beta = 12, p_\theta = 0.090$

Figure 4.32: Plots of the soliton angle orientation ϕ against propagation distance z. This behavior resembles that of the ideal classical billiard, but with transitions between collisions done in a rather smooth way. As the initial tilt t_θ reaches higher values, collisions start making more abrupt transitions.

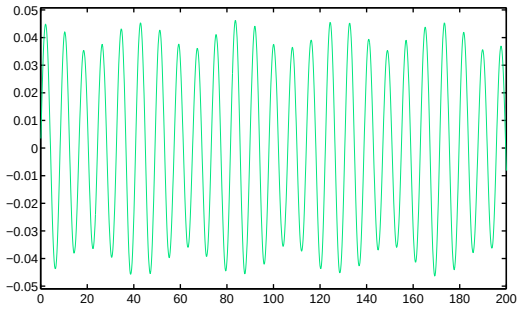

(a) $\beta = 3, p_\theta = 0.050$

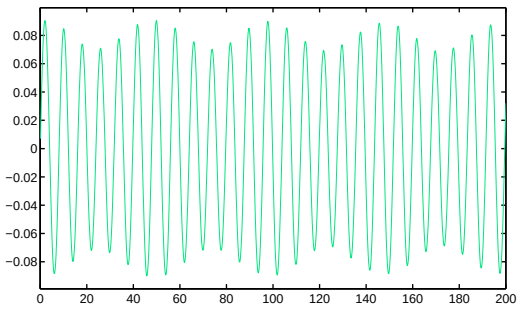

(b) $\beta = 3, p_\theta = 0.100$

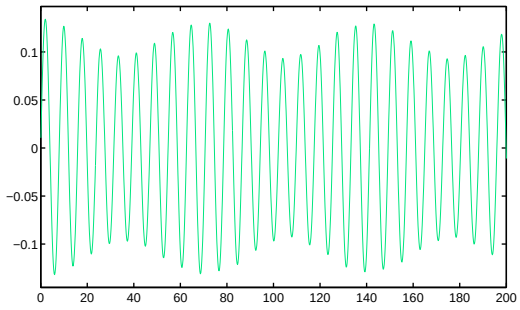

(c) $\beta = 3, p_\theta = 0.150$

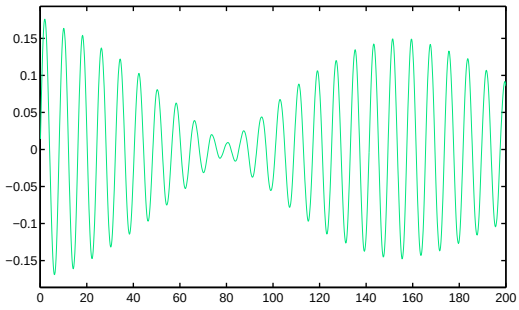

(d) $\beta = 3, p_\theta = 0.200$

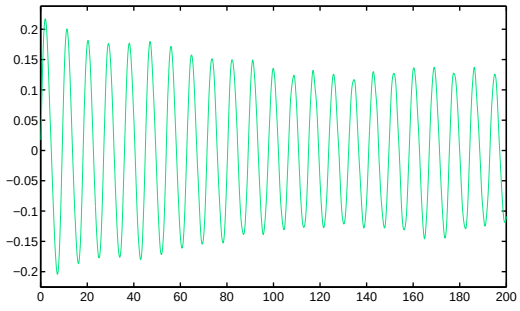

(e) $\beta = 3, p_\theta = 0.250$

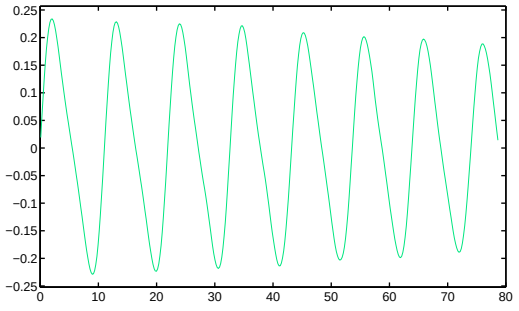

(f) $\beta = 3, p_\theta = 0.270$

Figure 4.33: Plots of the soliton normalized momentum projection p_u over the radial wall potential. Maxima corresponds to instants right before recoil completely takes place, that is, changing direction. For $\beta = 2.5$, p_r exhibits an anomalous yet periodic behavior, as it's amplitude is modulated.

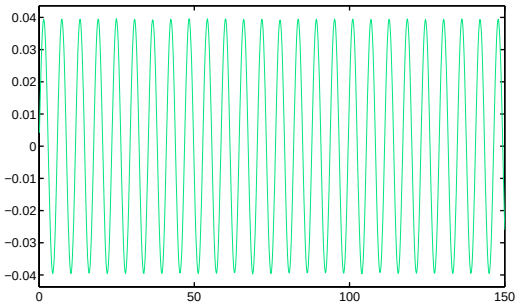

(a) $\beta = 6, p_\theta = 0.030$

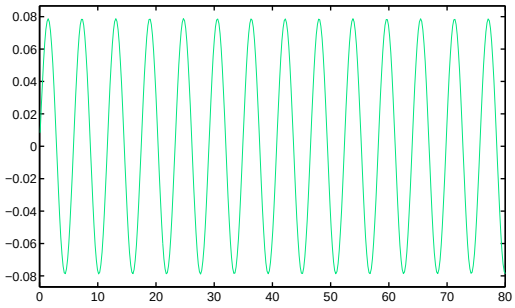

(b) $\beta = 6, p_\theta = 0.060$

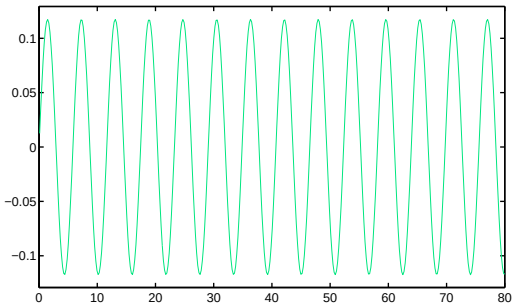

(c) $\beta = 6, p_\theta = 0.090$

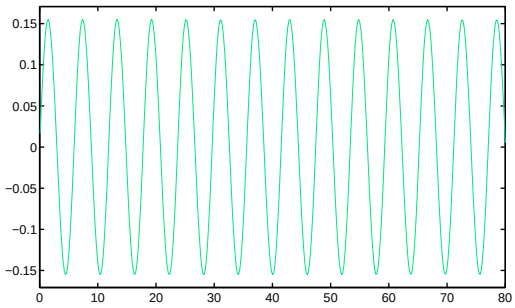

(d) $\beta = 6, p_\theta = 0.120$

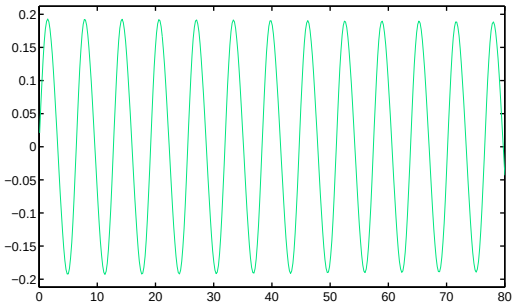

(e) $\beta = 6, p_\theta = 0.150$

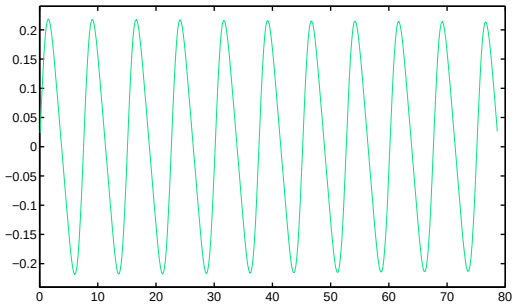

(f) $\beta = 6, p_\theta = 0.170$

Figure 4.34: Plots of the soliton normalized momentum projection p_u over the radial wall potential. Maxima corresponds to instants right before recoil completely takes place, that is, changing direction. For $\beta = 6$, the function is completely periodic.

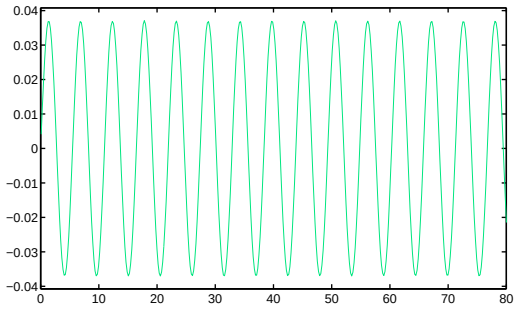

(a) $\beta = 9, p_\theta = 0.020$

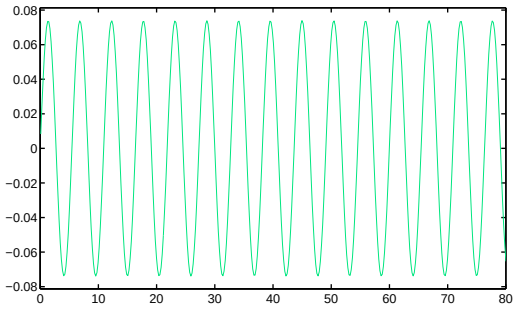

(b) $\beta = 9, p_\theta = 0.040$

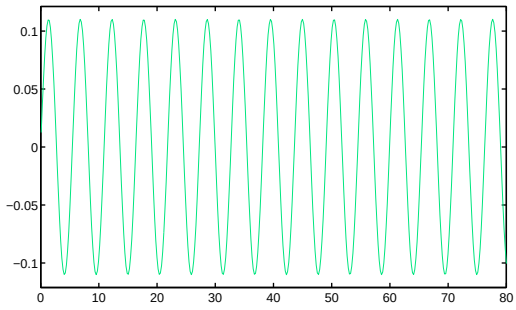

(c) $\beta = 9, p_\theta = 0.060$

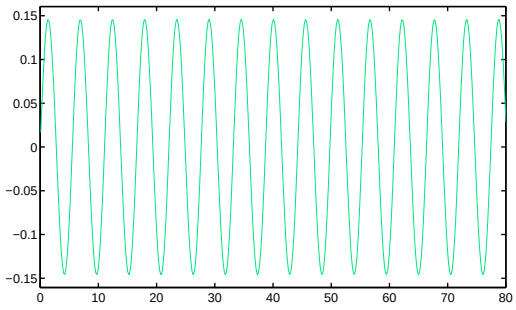

(d) $\beta = 9, p_\theta = 0.080$

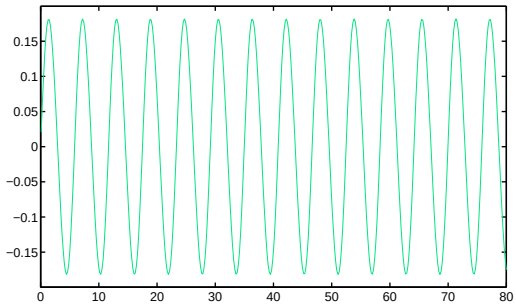

(e) $\beta = 9, p_\theta = 0.100$

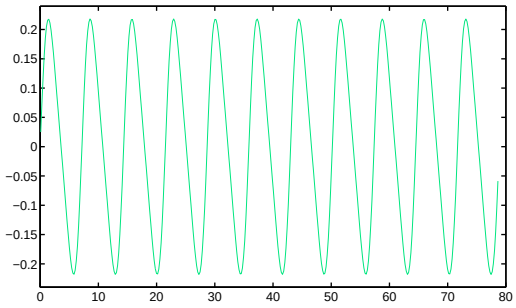

(f) $\beta = 9, p_\theta = 0.120$

Figure 4.35: Plots of the soliton normalized momentum projection p_u over the radial wall potential. Maxima corresponds to instants right before recoil completely takes place, that is, changing direction. For $\beta = 9$, the function is completely periodic.

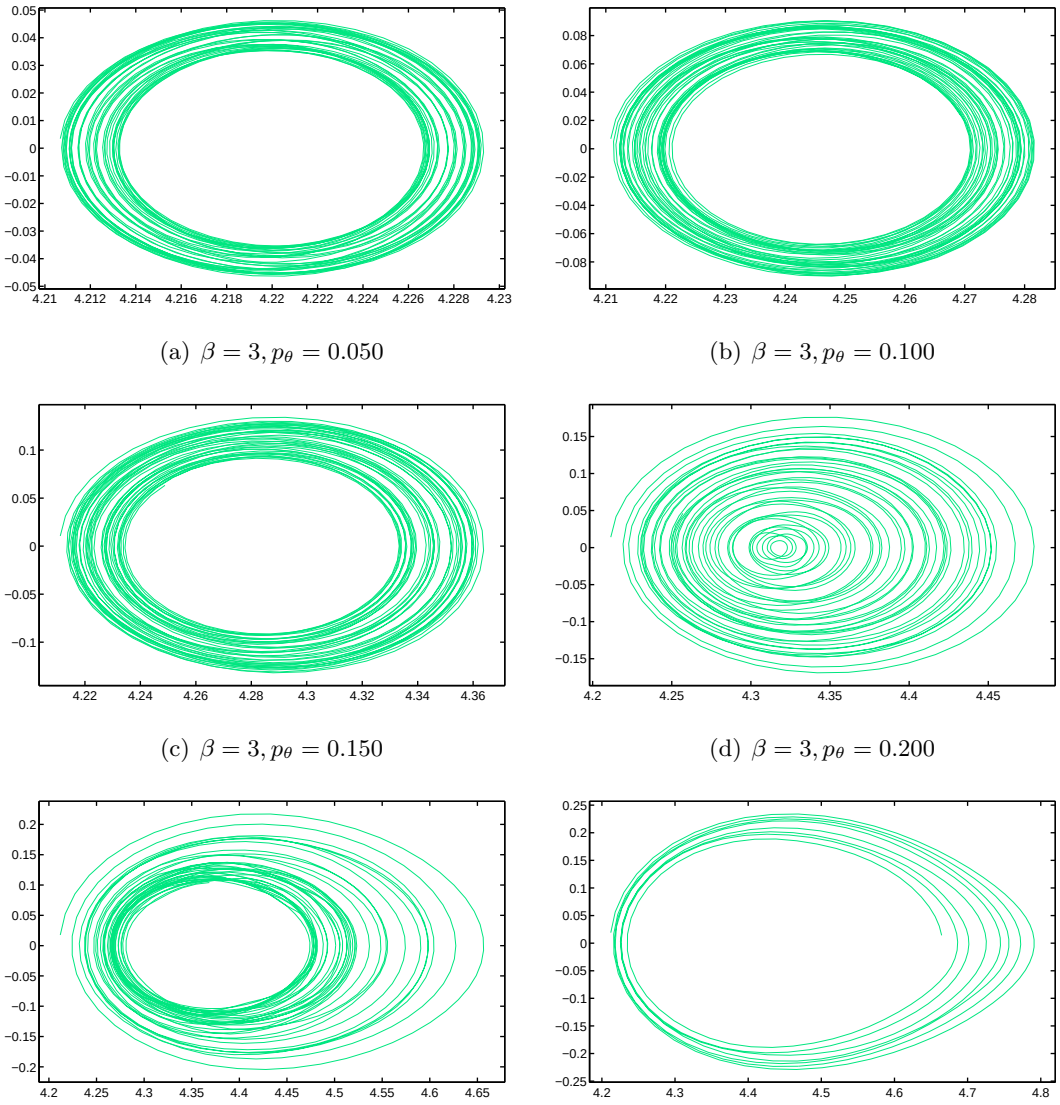

(a) $\beta = 3, p_\theta = 0.050$

(b) $\beta = 3, p_\theta = 0.100$

(c) $\beta = 3, p_\theta = 0.150$

(d) $\beta = 3, p_\theta = 0.200$

(e) $\beta = 3, p_\theta = 0.250$

(f) $\beta = 3, p_\theta = 0.270$

Figure 4.36: Phase diagrams of p_r against r for several values of p_θ. Anomalous behavior is exhibited at $\beta = 3$, as it can be appreciated in this figure.

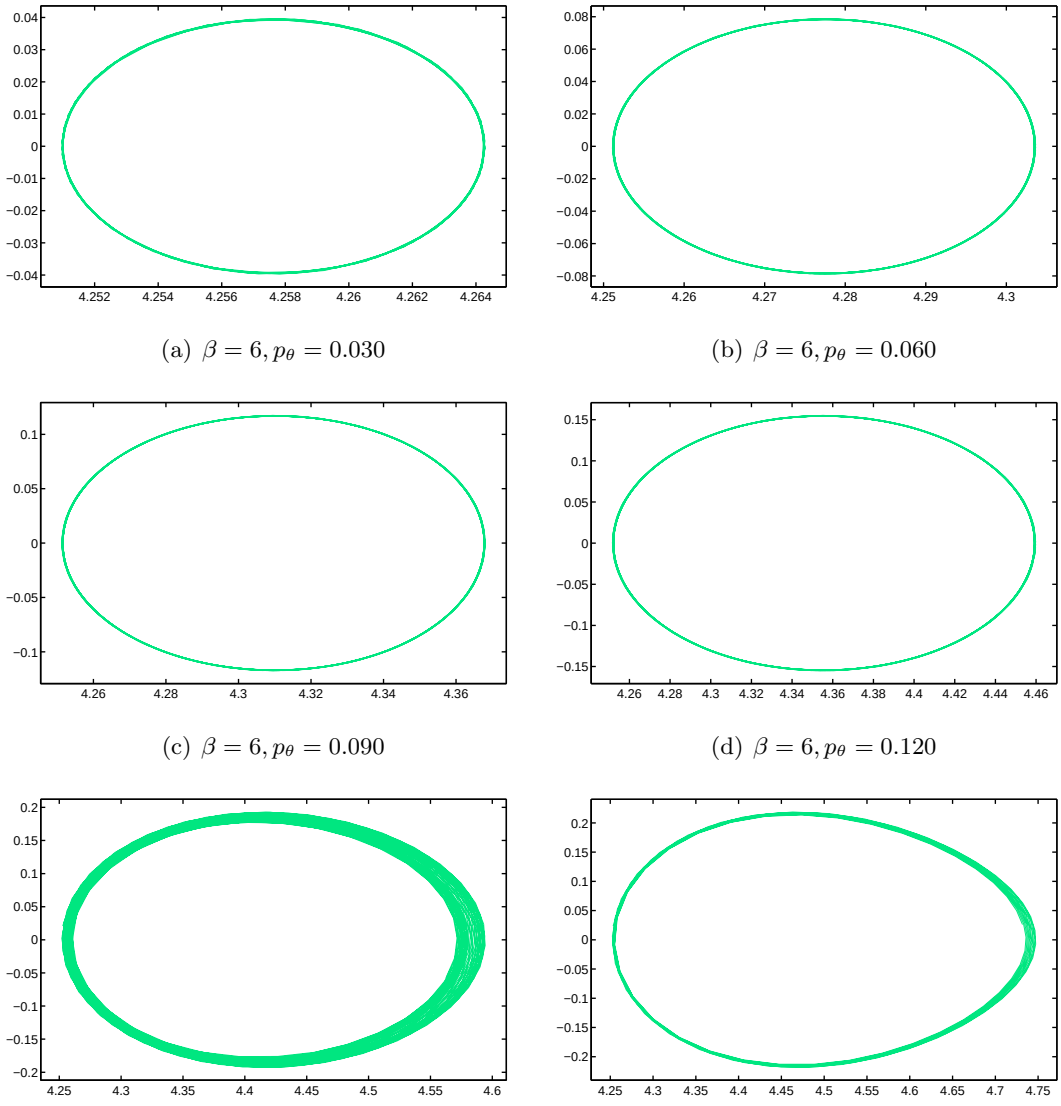

(a) $\beta = 6, p_\theta = 0.030$

(b) $\beta = 6, p_\theta = 0.060$

(c) $\beta = 6, p_\theta = 0.090$

(d) $\beta = 6, p_\theta = 0.120$

(e) $\beta = 6, p_\theta = 0.150$

(f) $\beta = 6, p_\theta = 0.170$

Figure 4.37: Phase diagrams of p_r against r for several values of p_θ. The functions seem closely related for non-high values of p_θ, as for high values the mapping becomes fuzzy.

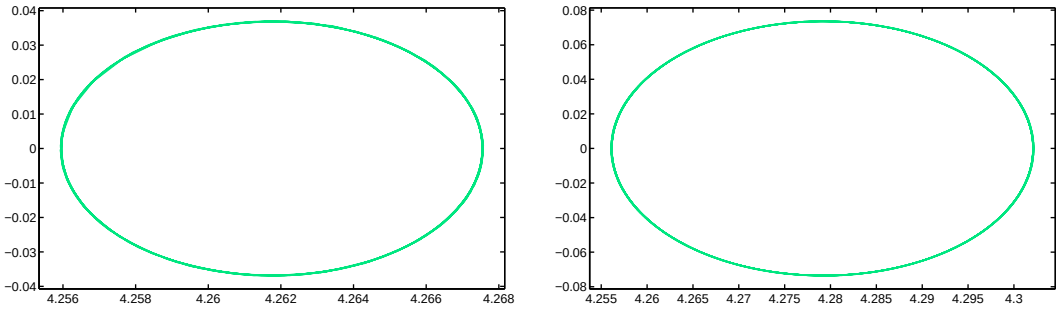

(a) $\beta = 9, p_\theta = 0.020$

(b) $\beta = 9, p_\theta = 0.040$

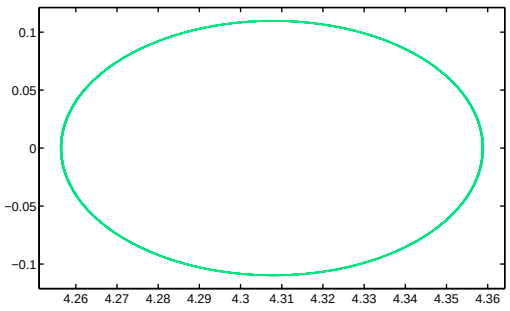

(c) $\beta = 9, p_\theta = 0.060$

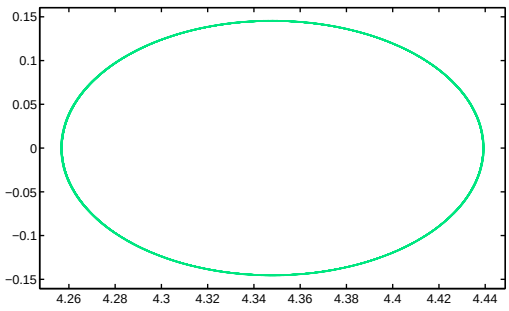

(d) $\beta = 9, p_\theta = 0.080$

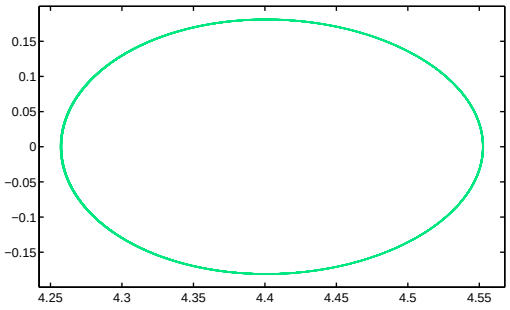

(e) $\beta = 9, p_\theta = 0.100$

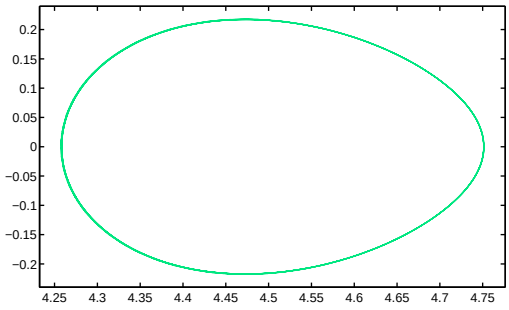

(f) $\beta = 9, p_\theta = 0.120$

Figure 4.38: Phase diagrams of p_r against r for several values of p_θ. The functions seem closely related for all values of p_θ.

values of β, but after overcoming a certain threshold holds exactly. Still, there is a small deviation from linearity at boundary values of the radius, as experimented in the relationship between the radial acceleration and its generalized force. This shown in figures 4.39-4.41.

Finally, to quantify this relationship, the correlation coefficient was plotted for the parametric space, where a value equal to -1 represents an exact linear relationship, which holds for a region in the parametric space. This shown in figure 4.42.

All this results help visualizing how periodic the motion is inside a light ring for a certain region of the parametric space, this leading to the explanation of why rotatory motion takes place. Since motion appears to be periodic, then if the soliton recoils in the first collision, it will do so indefinitely. This helping constructing the idea there are only two regimes of motion for the soliton. Furthermore, this helps strengthening the concept of soliton billiards, which would be solitons transverse motion describing billiards like systems.

4.8 Concluding remarks for the balanced Bessel lattice case

This chapter leaves interesting results concerning soliton propagation through balanced Bessel lattices. Still, more work is yet to be done, as there seems to be a strong connection with classical dynamic billiards. Moreover, this analysis must be applied to the general modulated Bessel lattice, where an azimuthal modulation is present.

The following points summarize the results from this chapter:
-There are two regimes of motion for solitons rotating around a light ring: rotatory and escaping
-Low values of β tend to present irregularities in its propagation quantifiers and most of the following results do not apply or apply approximately for this region.
-The width of the soliton is modulated via the radial potential function of the lattice
-The angular coordinate position is a linear function of z
-The radial coordinate motion can be derived from a second Newton law like approach.
-The minimum radius of propagation is maintained constant along propagation and equal to the initial radius

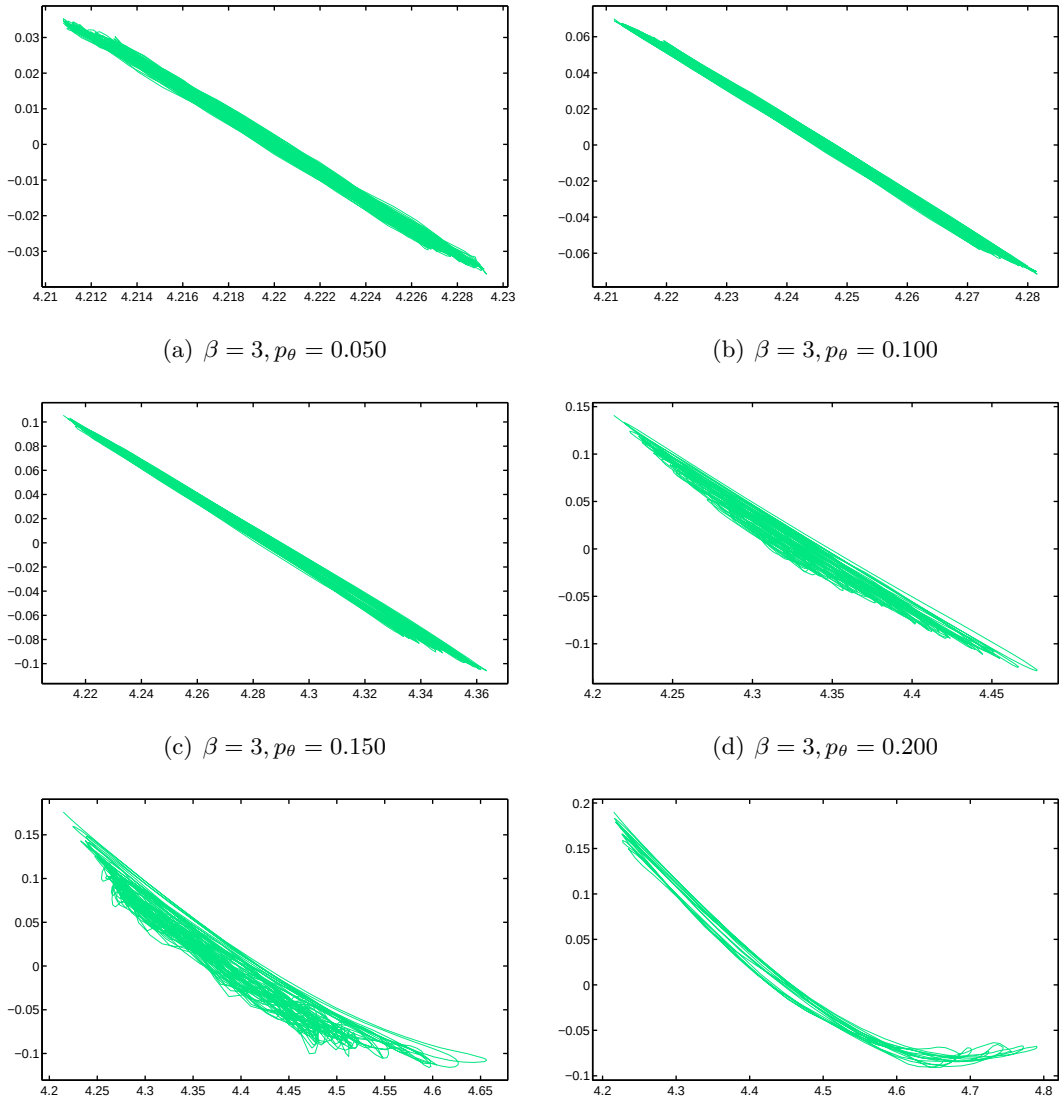

(a) $\beta = 3, p_\theta = 0.050$

(b) $\beta = 3, p_\theta = 0.100$

(c) $\beta = 3, p_\theta = 0.150$

(d) $\beta = 3, p_\theta = 0.200$

(e) $\beta = 3, p_\theta = 0.250$

(f) $\beta = 3, p_\theta = 0.270$

Figure 4.39: Phase diagrams of p_r first derivative against r for several values of p_θ. The behavior exhibited can be approximated to be semi-linear.

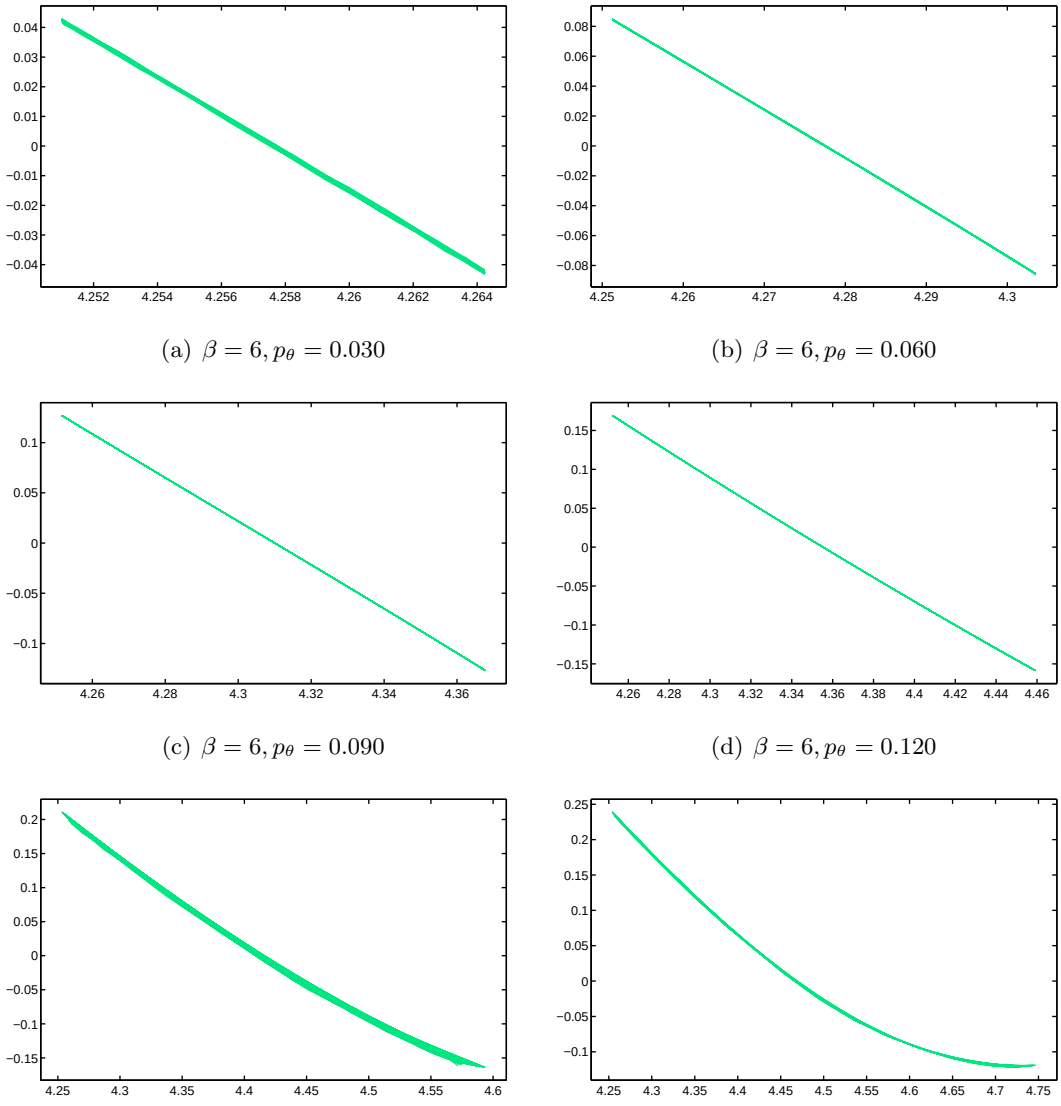

(a) $\beta = 6, p_\theta = 0.030$

(b) $\beta = 6, p_\theta = 0.060$

(c) $\beta = 6, p_\theta = 0.090$

(d) $\beta = 6, p_\theta = 0.120$

(e) $\beta = 6, p_\theta = 0.150$

(f) $\beta = 6, p_\theta = 0.170$

Figure 4.40: Phase diagrams of p_r first derivative against r for several values of p_θ. The behavior exhibited can be approximated as linear, but breaks at high radius and values of p_θ.

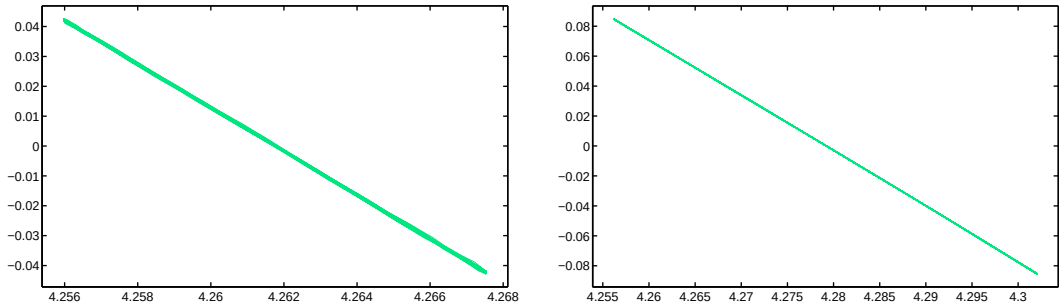

(a) $\beta = 9, p_\theta = 0.020$

(b) $\beta = 9, p_\theta = 0.040$

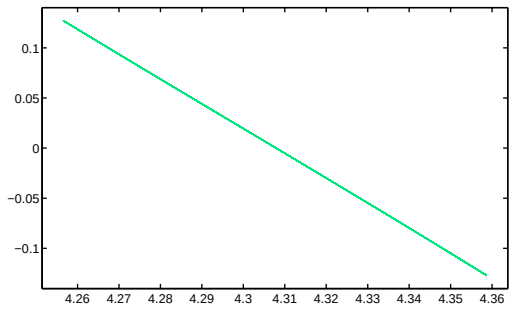

(c) $\beta = 9, p_\theta = 0.060$

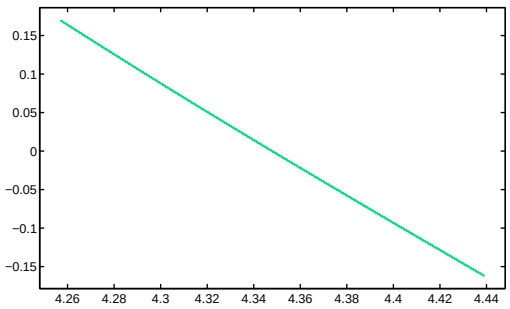

(d) $\beta = 9, p_\theta = 0.080$

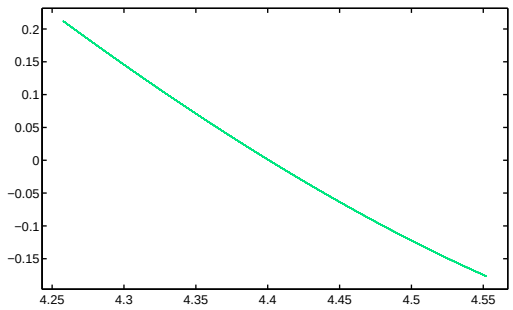

(e) $\beta = 9, p_\theta = 0.100$

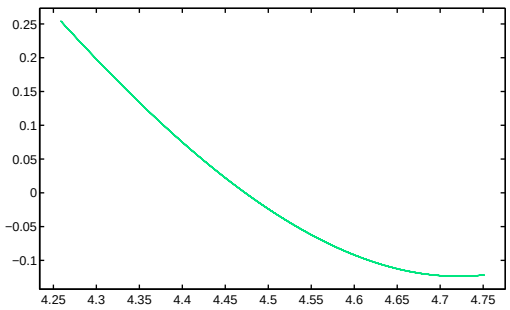

(f) $\beta = 9, p_\theta = 0.120$

Figure 4.41: Phase diagrams of p_r first derivative against r for several values of p_θ. The behavior exhibited can be approximated as linear, but breaks at high radius and values of p_θ.

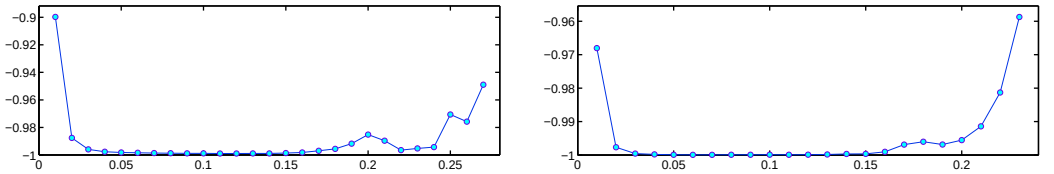

(a) $\beta = 3$

(b) $\beta = 4$

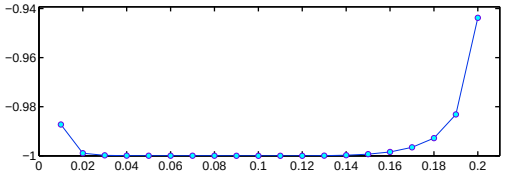

(c) $\beta = 5$

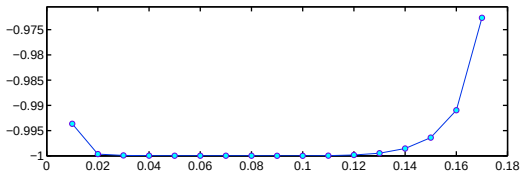

(d) $\beta = 6$

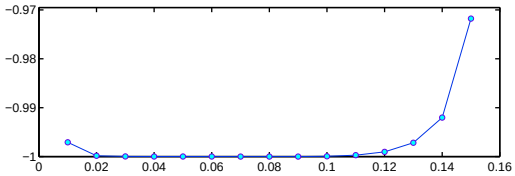

(e) $\beta = 7$

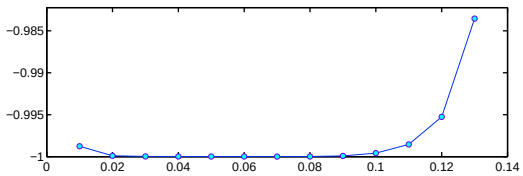

(f) $\beta = 8$

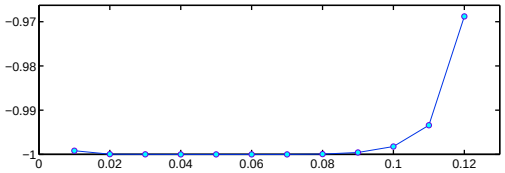

(g) $\beta = 9$

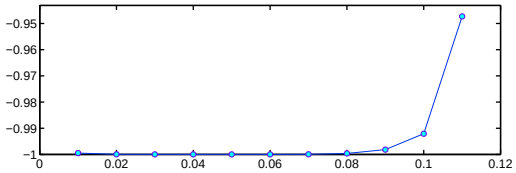

(h) $\beta = 10$

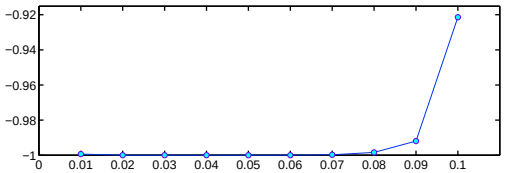

(i) $\beta = 11$

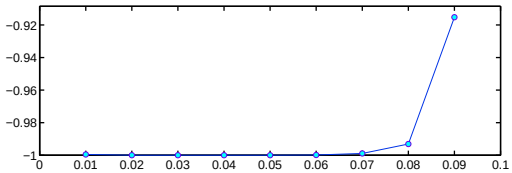

(j) $\beta = 12$

Figure 4.42: Correlation coefficient between the first derivative of p_u and r. The relationship holds linearly for a great amount of points in the parametric space.

-The maximum radius augments as the initial tilt does so

-The rotation rate has a non zero variation even though there is no azimuthal modulation

-Transverse motion is closely related to dynamic billiards system, which help explains why there are only two different regimes of motion

Chapter 5

Concluding remarks

Nonlinear effects can trigger interesting phenomena in nature, which analysis is often neglected due to numerical complications. Nonlinearity has been historically left behind simpler models due to the lack of computational power in the midst and creation of physics. Still, the advent of powerful systems for carrying highly complex operations has given nonlinearity a second chance in the physical and scientific world.

This work is devoted to the study of optical spatial solitons, or solitons for short in this thesis, which is a fundamental unit of propagation in nonlinear optics. Different possibilities have been explored, and amongst those remarkable results have emerged. Nevertheless, this research is just a small step in the understanding of nonlinear phenomena, and contributes nothing but few and subject details to what the whole theory and fields entitles. The results obtained from this research represent my small contribution to a continually growing field, and my first steps in what I sincerely hope fruitful career will be.

5.1 Summary of results

This work contributions deal with optical spatial solitons propagating through optical latices, a routing potential which can control the soliton motion. First, the effects of imposing an elliptically symmetry on the lattice where studied. This optical latice was described by a superposition of Mathieu nondiffracting beams, and the latice family itself was baptized as elliptical photonic latices. Stable propagation was observed for the soliton in the regime of longitudinal-transverse stationary propagation. Furthermore, transverse motion parallel to the longitudinal propagation was imposed on the soliton by imprinting an initial tilt on the

input beam in the form of a phase spatial dependent factor. Different regimes of transverse motion where observed while longitudinal propagation was stable, which constitutes the fundamental result of such part of the thesis. This because the elliptic photonic latice posses an nonzero azimuthal modulation which is not ignored by the soliton. Instead, the soliton slowly and continually transform itself to the new surrounding potential. This was an interesting fact, due to it had not been observed before. This part of the work has already been published in the scientific journal Optics Letters, where the corresponding paper can be found as [28].

Results continue as the research posses on a different kind of optical latice, the modulated Bessel latice. This family of latices consists of superpositions of even'ćosine and odd'śine Bessel beams. By an appropriate choice of coefficients this family of latice has been proved to conserve the power contained in the beam, this being a subtle but convenient fact for practical and experimental implementations. Still, this work is completely theoretical, as the results offered for this section constitute an introductory step in creating a model for transverse motion of a soliton in a Bessel circular light ring. For this research the modulation parameter introduced in the coefficients of the beam were chosen as to nullify modulation along circular light rings, thus providing an azimuthally symmetric potential for propagation. Still, it was proved how variations in dynamic quantifiers takes place and account for physical process. Furthermore, it still lays as a task to complete, but an attempt was started to make an analogy between these transverse motion dynamics and classical particle billiards. This results are currently being organized in order to publish them in an international optics journal.

5.2 Future work

Work and research on this subject is currently in progress, as the modulated light ring cases for the Bessel beams lays a challenge still. Furthermore, it appears an attractive idea to conceive this case as a more general theory correctly describing the null modulation light ring case explored in this work.

There also exists interest in working and researching on vortex type solitons, since all this work entitles to propagation of fundamental type solitons. The problem of vortex type solitons is a much more difficult one, due to the numerical requirements imposed by this profiles

and the instability they naturally posses.

Furthermore, a project on beam shaping for soliton propagation has been left on halt due to time restrictions. It deals with a superpositions of different order Bessel beams aspiring to form a controllable azimuthal modulation on a circular light ring. That is, not limiting work on the simple harmonic modulation imposed naturally by Bessel beams.

As research lays now, interesting opportunities are yet to be taken. The problem is now to conform a future agenda for working in the pending problems. Future will answer how well time was employed.

Bibliography

[1] Drazin and Johnson "Solitons: An Introduction" (1989) p. 15

[2] J. Scott Russell. Report on waves, Fourteenth meeting of the British Association for the Advancement of Science, 1844.

[3] Korteweg, D.J.; de Vries, G. (1895), "On the Change of Form of Long Waves advancing in a Rectangular Canal and on a New Type of Long Stationary Waves", Philosophical Magazine **39**: 422443

[4] N. J. Zabusky and M. D. Kruskal (1965). Interaction of 'Solitons' in a Collisionless Plasma and the Recurrence of Initial States. Phys Rev Lett **15**, 240

[5] M. Ablowitz, H. Segur, Solitons and the Inverse Scattering Transform, SIAM, Philadelphia, 1981.

[6] Lax, P. (1968), "Integrals of nonlinear equations of evolution and solitary waves", Comm. Pure Applied Math. **21**: 467490,

[7] "Monsters of the deep – Huge, freak waves may not be as rare as once thought". Economist Magazine. September 17th 2009. Retrieved 2009-10-04.

[8] Paul B. Umbanhowar, Francisco Melo and Harry L. Swinney (1996). "Localized excitations in a vertically vibrated granular layer". Nature **382** (29 August 1996): 793796.

[9] Boussinesq, J. (1877), Essai sur la theorie des eaux courantes, Memoires presentes par divers savants lAcad. des Sci. Inst. Nat. France, XXIII, pp. 1680

[10] A. Barone, F. Esposito, C. J. Magee, and A. C. Scott, "Theory and applications of the sine-Gordon equation," Riv. Nuovo Cimento **1** (1971) 227.

[11] F. Dalfovo, S. Giorgini, L. P. Pitaevskii, and S. Stringari, "Theory of Bose-Einstein condensation in trapped gasses," Rev. Mod Phys. **71**, 463 (1999)

[12] Kittel, Charles (1996) [1953]. "Chapter 1". Introduction to Solid State Physics (Seventh ed.). New York: John Wiley and Sons. pp. 10

[13] Y. Kartashov, V. Vyslouk, L. Torner, "Progress in Optics" vol 52.

[14] Z. Bouchal, Nondiffracting optical beams: physical properties, experiments, and applications," Czech J. Phys. **53**, 537 (2003)

[15] J. Durnin, Exact solutions for nondiffracting beams. I. The scalar theory," J. Opt. Soc. Am. A **4**, 651-654 (1987)

[16] J. C. Gutierrez-Vega, M. D. Iturbe-Castillo, and S. Chavez-Cerda, Alternative formulation for invariant optical fields: Mathieu beams," Opt. Lett. **25**, 1493-1495 (2000)

[17] M. A. Bandres, J. C. Gutierrez-Vega, and S. Chavez-Cerda, Parabolic nondiffracting optical wave fields," Opt. Lett. **29**, 44-46 (2004)

[18] A. V. Burvak, Y. S. Kivshar, and S. Trillo, Phys. Rev. Lett. **77**, 5210 (1996).

[19] D. E. Pelinovsky and Yu. A. Stepanyants, SIAM (Soc. Ind. Appl. Math.) J. Numer. Anal. **42**, 1110 (2004).

[20] Nye, J. F.; and M. V. Berry (1974). "Dislocations in wave trains" (PDF). Proceedings of the Royal Society of London, Series A 336

[21] Agrawal, Govind P. (2001). Nonlinear Fiber Optics (3rd ed.). San Diego, CA, USA: Academic Press. ISBN 0-12-045143-3

[22] Oliver Rbenknig, The Finite Difference Method (FDM) - An introduction, (2006)

[23] Sreenivasa Rao Jammalamadaka. The American Statistician. February 1, 2003, 57(1)

[24] T. Kariya, H. Kurata, Generalized Least Squares, Wiley, 2004

[25] Fieller, E.C. et al (1957) Tests for rank correlation coefficients :I. Biometrika **44**, 470481

[26] R. A. Fisher (1925). Statistical Methods for Research Workers, Edinburgh: Oliver and Boyd, 1925, p.43.

[27] N. W. McLachlan, "Theory and application of Mathieu functions" Dover. New York, 1962

[28] A. Ruelas, S. Lopez-Aguayo, and J. C. Gutirrez-Vega, "Stable solitons in elliptical photonic lattices," Opt. Lett. **33**, 2785-2787 (2008)